NOTICE

The quality of this microform is heavily dependent upon the quality of the original thesis submitted for microfilming. Every effort has been made to ensure the highest quality of reproduction possible.

If pages are missing, contact the university which granted the degree.

Some pages may have indistinct print especially if the original pages were typed with a poor typewriter ribbon or if the university sent us an inferior photocopy.

Reproduction in full or in part of this microform is governed by the Canadian Copyright Act, R.S.C. 1970, c. C-30, and subsequent amendments.

AVIS

La qualité de cette microforme dépend grandement de la qualité de la thèse soumise au microfilmage. Nous avons tout fait pour assurer une qualité supérieure de reproduction.

S'il manque des pages, veuillez communiquer avec l'université qui a conféré le grade.

La qualité d'impression de certaines pages peut laisser à désirer, surtout si les pages originales ont été dactylographiées à l'aide d'un ruban usé ou si l'université nous a fait parvenir une photocopie de qualité inférieure.

La reproduction, même partielle, de cette microforme est soumise à la Loi canadienne sur le droit d'auteur, SRC 1970, c. C-30, et ses amendements subséquents.

Canada

Performance Evaluation of Filament Wound Tubes After Long Term Exposure to Aggressive Environments

Nigel David Dudley

A Thesis

in

The Department

of

Mechanical Engineering

Presented in Partial Fulfillment of the Requirements
For the Degree of Master of Engineering
Concordia University
Montreal, Quebec, Canada

March 1995

ISBN 0-612-01342-1

Canada

ABSTRACT

Performance Evaluation of Filament Wound Tubes After Long Term Exposure to Aggressive Environments

Nigel David Dudley

Filament wound fiberglass/vinyl ester tubes with a winding angle of ±55°, incorporating either glass veil or PVC corrosion liners were exposed to 21°C water, 80°C water, 21°C hydrochloric acid (35%), 50°C HCl (35%), 21°C sulfuric acid (98%) or 21°C air for up to three years. Performance evaluation, starting at six months of exposure and repeated at six month intervals, was assessed by visual examination, testing to failure under a tensile axial load, testing to weepage using internal pressure to create hoop stress and internal pressure tests. The best performance was shown by the air exposed veil lined tubes and the sulfuric acid exposed PVC lined tubes. Both types of tubes showed a slight performance reduction when exposed to 21°C water and HCl, and a significant performance reduction with exposure to 80°C water and 50°C HCl. The performance reduction was seen after six months of exposure and remained constant thereafter. Veil lined tubes exposed to sulfuric acid suffered severe and rapid deterioration. Visual observations showed a correlation between environment and appearance changes. Laminate theory was used to predict stress-strain behavior and to calculate failure envelopes for virgin tubes. Comparison of theoretical and experimental results showed that while stress-strain behavior could be predicted, the quadratic interaction failure criterion cannot be used to predict failure by weepage or fracture.

Acknowledgements

I would like to thank the following people and organizations who have all contributed to this thesis:

Dr. Suong V. Hoa, who first allowed me to work as an assistant on the project while I was an undergraduate, and then allowed me to complete the project and pursue a M. Eng. Degree. I would also like to thank him for his guidance and patience.

The people at CPF Dualam Limited, who produced the test specimens and provided materials and space.

Natural Sciences and Engineering Research Council of Canada (NSERC), for their funding and allowing the use of the project results for this thesis.

Kathryn Arcudi, who after knowing me for just a few hours agreed to loan me her computer for a few weeks, that was several years ago. Now as my wife, I would like to thank her for her support and patience as I was completing this thesis.

Gregor Rohrauer, whose efforts made the project a reality.

Bob, Karen and Ron, who decided a thesis needs a Birthday once a year.

Chantal Chickalo, who produced the best colour prints I have ever seen.

Mario D'Orazio, for letting me use his laser printer. I sure hope it has some serviceable life left.

And a dozen other people who all helped me in one way or another.

Table of Contents

List of Tables

List of Tables (continued)

List of Tables (continued)

List of Tables (continued)

List of Figures

List of Figures (continued)

List of Figures (continued)

List of Figures (continued)

List of Figures (continued)

List of Figures (continued)

List of Figures (continued)

List of Figures (continued)

List of Figures (continued)

Nomenclature

A_{ij}, B_{ij}, D_{ij} = Stiffness of symmetric or unsymetric laminates; units vary

a_{ij} = In-plane compliance of a symetric laminate, in $N^{-1}m$; $i,j = 1,2,6$

a = Inner radii

b = Outer radii

d_i = Inside diameter

E = Strain

E_i = Engineering constants ; $i = x,y,s$

F_{ij}, F_i = Strength parameters, for stress components

G_{ij}, G_i = Strength parameters, for strain components

h = Total thickness of laminate, in m

k_i = Curvature, in m^{-1}; $i = 1,2,6$

L = Load

M_i = Moment, in Nm^{-1}; $i = 1,2,6$

m = Cos ϕ

N_i = Stress resultant, in Nm^{-1}; $i = 1,2,6$

n = Sin ϕ

P = Pressure

P_i = Uniform internal pressure

Q_{ij} = Components of stiffness; $i,j = x,y,s$ or $1,2,6$

R = Strength ratio

S = Longitudinal-traverse shear strength

S_{ij} = Components of compliance; $i,j = x,y,s$ or $1,2,6$

t = Wall thickness, m

U_i	= Linear combinations of on-axis stiffness and compliance in the multiple-angle formulation. Same notation but different combinations are used for stiffness and compliance; i = 1 to 5
X	= Longitudinal compressive strength
X'	= Longitudinal tensile strength
Y	= Transverse compressive strength
Y'	= Transverse tensile strength
σ_i	= Components of stress, on-axis i = x,y,s; off-axis i = 1,2,6
$\bar{\sigma}_i$	= Average stress across thickness of a laminate
ε_i	= On-axis components of strain, i = x,y,s; off-axis i = 1,2,6
ε_i^o	= In-plane strain, i = 1,2,6
ν_{ij}	= ν_{12} Longitudinal Poisson's ratio (axial loading); ν_{21} Hoop Poisson's ratio (hoop and biaxial loading)
ϕ	= Ply orientation, degrees

Subscripts

x	= Normal component along x axis
y	= Normal component along y axis
s	= Shear component in x-y plane
1	= Normal component along tube's longitudinal axis
2	= Normal component along tube's hoop axis
6	= Shear component in the 1-2 plane

CHAPTER 1. INTRODUCTION

Composites contain two or more components that are combined into a unified material [1,2].* The components retain their physical and chemical identities, thus it is possible to design the unified material to take advantage of the special properties of the contributing materials [2,3].

A combination of glass fibers and polymers form a group of composites known as fiber reinforced plastics (FRP) [4,5]. FRP's advantages of light weight, cost effectiveness, flexibility in construction, and high corrosion resistance [6,7] make it ideal for the construction of chemical processing equipment, replacing conventional metallic materials [6].

Corrosion resistant filament wound pipe is constructed from two distinct laminates. There is a resin-rich laminate in contact with the structure's contents which acts as a corrosion barrier, and a high fiber content filament wound laminate that provides structural support [8,9]. For those cases in which the containment of more aggressive chemicals or higher process temperatures is required, a thermoplastic, such as PVC, is substituted for the resin rich corrosion barrier [9].

[*] Numbers in brackets refer to references at the end of thesis

CPF Dualam Limited, located in Montreal, Quebec, produces chemical processing equipment for the North American market. Their patented "dual laminate" design uses a thermoplastic corrosion barrier in their FRP products [10].

Due to the nature of FRP, manufacturers must test their products under actual or simulated use conditions in order to determine suitability for use in a given environment. CPF Dualam Limited, NSERC and Concordia University's Composite Research Laboratory cooperated to create a project that was designed to evaluate and compare the corrosion resistance of two different FRP designs, CPF Dualam's dual laminate design and the more common veil corrosion barrier design, after long term exposure to certain aggressive environments.

Filament wound fiberglass/vinyl ester tubes with a winding angle of $\pm 55^{\circ}$ incorporating a C-veil or PVC corrosion barrier were filled with one of six liquid environments: room temperature water, $80^{\circ}C$ water, room temperature hydrochloric acid (35%), $50^{\circ}C$ HCl (35%), room temperature sulfuric acid (98%) and room temperature air. Evaluation of specimens began after six months of exposure and was repeated at six month intervals. The maximum exposure time was three years. Corrosion resistance was assessed by visual inspection, tensile axial tests, internal pressure to create hoop stress, and internal pressure tests.

Overall, Chapter 2 serves to introduce the reader to FRP and present some key points about FRP behavior. Chapter 3 gives a detailed description of the project. Chapter 4 uses laminate theory to produce theoretical predictions of the tube's stress-strain behavior under loading and ply stress for a given load. Failure envelopes in stress and strain space are calculated using the quadratic interaction failure criterion. Chapters 5 and 6 are devoted to presenting the results of the project. Chapter 7 is an analysis of the test results. And finally, chapter 8 presents conclusions that can be drawn from the project results.

CHAPTER 2. FRP: A Review

In order to understand the behavior of filament wound FRP structures, it is necessary to have some background on the subject.

2.1 Construction Materials

2.1.1 Vinyl Ester Resins

Vinyl ester resins are well suited for use in the production of chemically resistant FRP equipment and for use in the filament winding process.

Vinyl ester resins exhibit better than average resistance to chemical attack due to their unique structure, including built in steric protection of ester groups [11]. Another unique property of a vinyl ester molecule is that it contains a number of OH (hydroxyl) groups along its length. These OH groups can form physical bonds with similar groups on a glass fiber surface resulting in excellent wet-out and good adhesion properties [12]. Good fiber wet-out is essential for reducing voids in a filament wound part [13]. Vinyl ester resins also have the correct viscosity, 300 to 2000 cps, for use in the filament winding process [8].

Cured vinyl ester resin is more flexible and has higher fracture toughness than a cured polyester resin and it has excellent chemical resistance and tensile strength like epoxy resins [14]. One drawback of vinyl ester resins is the shrinkage that takes place during cure [14,15].

2.1.2 Glass Fibers

Glass fibers are the most common of all reinforcing fibers used in FRP construction. The principle advantage of glass fibers are low cost, high tensile strength, and high chemical resistance [16].

There are three types of glass fibers used in FRP construction, E glass, S glass, and C glass. E glass has the lowest cost of all commercially available reinforcing fibers, which is why it is in widespread use in the FRP industry [17]. C glass is used in chemical applications requiring greater corrosion resistance to acid than is provide by E glass [17].

Glass fibers in the form of veil, chopped strand mat [8] and long, untwisted parallel strands known as roving are used in the construction of filament wound tubes [8,17].

A problem with glass fibers is that they lose strength during handling [18]. Therefore, it is difficult to know what strength the fibers have retained after manufacturing has been completed.

2.1.3 Thermoplastics

Thermoplastics can have a wide range of mechanical and corrosion resistance properties due to the ability of manufacturers to modify the composition of these materials [19].

By itself, rigid polyvinyl chloride pipe is acceptable for use in corrosive environments [20]. It has excellent chemical resistance [20,21] to a wide range of corrosive fluids, particularly inorganic materials such as hydrochloric acid [20]. However, its range of application by itself is limited due to low impact strength, poor dimensional stability and low thermal distortion temperature [21].

2.2 Filament Wound Tube Construction

The wall of an FRP laminate for use in corrosive environments has two main layers: a corrosion liner and a structural layer.

2.2.1 Corrosion liner

Fabrication of an FRP laminate usually begins with the corrosion liner [22]. The corrosion liners can be one of two types, a resin rich laminate which is often referred to as a veil liner or a thermoplastic liner.

With the veil type corrosion liner the first layer is a surfacing veil saturated with catalyzed resin. This is covered with two layers of chopped strand mat, which are also saturated in catalyzed resin, to complete the corrosion liner [22]. The veil liner uses the corrosion resistance of the resin to protect the rest of the structure.

The surfacing veil is used to control the thickness of a resin rich layer and to give strength to the most crucial part of the corrosion barrier [12,22]. This layer is normally 0.25 to 0.50 mm thick and contains about 90% resin and 10% veil material [22,23]. The surfacing veil also prevents the mat from protruding to the surface and becoming wicking points for the corrosive environment to penetrate the laminate [23]. Monofilament glass or polyester filaments are commonly used as surfacing veil materials [22]. This resin-rich layer also serves as an impermeable liner to contain fluid or gas [24].

Chopped strand mat reinforcement consists of a felted matrix of chopped strand "E" or "ECR" glass fibers, 1.3 to 4.5 cm long and loosely held together by a styrene-soluble resin binder. The two mat layers form a layer about 2 mm thick and consist of about 70% resin and 30% glass [22]. The short fiber bundles and high resin content help produce laminates with good strength and excellent chemical resistance [22].

The use of a corrosion liner consisting of a layer of "C" (chemical) glass surfacing veil followed by plies of type E chopped strand mat was first proposed by Harvey Atkinson in 1962. Atkinson based his recommendation on his observation that the loss of strength of exposed laminates was rapid when the glass reinforcement exceeded about 30% [23]. Today, it is the typical universally accepted construction required for chemical resistant equipment [11] and, for a majority of environments, it is quite adequate and inexpensive [25].

The veil type corrosion barrier does have drawbacks. One is that defects such as voids are possible. Another is that it cannot be used at fiber stress levels of more than 10% of the structural fiber's ultimate strength [24]. Above this stress level the corrosion barrier can craze or crack allowing fluid into the laminate [24] so its use is limited to low pressure filament wound structures [6]. Also, it is more brittle than a thermoplastic corrosion barrier [9] and a sharp bump can crack it [7,9].

For more aggressive environments and higher process temperatures, dual laminate structures have been developed where the veil corrosion liner is replaced with a thermoplastic liner [9]. The design of CPF Dualam's thermoplastic corrosion barrier is a layer of thermoplastic, a layer of glass veil and one or two layers of chopped strand mat. The use of a thermoplastic liner also ensures a smooth, void free inner surface [9].

Whatever the type of corrosion barrier, its importance cannot be overemphasized. Once the corrosion liner is breached it is only a matter of time before the structural laminate fails due to deterioration [25].

2.2.2 Structural Layer

The structural layer of an FRP structure is applied in layers and provides strength and form. For the construction of FRP tubes the filament winding process is often employed [8,26,27,28].

Filament winding (F.W.) is a process in which continuous rovings are wetted in a resin bath, then wound (usually in a helical pattern) onto a rotating mold, called a mandrel [8,26,29]. The ability to control the winding angle allows the designer to orientate the glass filaments to carry the applied loads [28,29].

2.3 Filament Winding Angle

Theoretically, the filament winding angle, measured from the tube's longitudinal direction, can vary from 0 to 90° [30]. A simple method of calculating the appropriate winding angle for a given stress state is netting analysis.

Netting analysis is based upon the assumption that all load is carried by the fibers of a structure and ignores the contribution of the resin [28]. For a given ratio of applied hoop stress to axial stress being S, the winding angle, ϕ, is given by the relation [28,31]

$$\mathrm{Tan}^2\phi = S$$

For example, a tube with closed ends and internally pressurized is subjected to a biaxial load with the hoop stress twice the axial stress. For this load the ideal winding angle is $54^\circ 44'$ [28,30,31] which tubes are often wound at [27,30]. This angle winds an optimized helix pattern that provides a two to one ratio of hoop to longitudinal strength needed for the above biaxial loading. It is not the optimum pattern, but rather a compromise that can be conveniently wound on a lathe type winder [30].

The ideal pattern would have two thirds of the reinforcement wound as close as possible to 90° and the remaining third of the reinforcement wound at 0°. Such a pattern would make for a stronger tube using the same amount of material, or allow less material to be used for the same strength. Since the reinforcement is oriented in line with the loads it is resisting, it resists the loads more efficiently, and is not compromised by carrying the loads off the fiber axis. This concept is the essence of composite design [30].

2.4 Areas of Special Consideration and Variation Between FRP and Conventional Materials

When dealing with FRP it is important to be aware of the inherent differences between FRP and conventional isotropic materials.

The lack of a central information source with comprehensive codes, ASTM standards and design guides [32], combined with the emergence of specialized fabricators as the market for FRP has increased [33], has resulted in fabricators developing and using their own design and quality control specifications [11,32,33] which are often based on case studies [11,32]. This results in variation of structural properties, hence reliability [27], of FRP structures built by different shops.

Even when FRP structures are built by the same fabricator, there can be a wide variation in reliability. There are three main reasons for this.

First, construction of FRP structures is done by hand and with simple tooling, and quality control is usually not as rigorous as with conventional materials [27].

Second, there are inherent variations in the materials used to build FRP structures. Glass fibers are known to lose much of their virgin strength after passing through processing equipment [16,18].

Vinyl ester resin must be prepared by the addition of promoters, accelerators and retarders and then mixed, usually in the drum, before use [34,35]. A measured amount of catalyst must be added to start the resin cure [35,36]. Since the amount of catalyst, promoters, accelerators and retarders that may be present can vary from batch to batch, so can the strength of the cured resin. Cure plays one of the most important parts in the chemical resistance developed by FRP materials [11].

Third, FRP structures are also subject to visible defects. Air bubbles, blisters, impact cracks, crazing, delamination, fisheye, dry spots, pimple, pit or pinhole, resin pocket, scratch, wormholes and wrinkles are visible defects [37]. These defects can severely degrade a structure's performance. Filament wound structures are also susceptible to jackstrawing. Jackstrawing is seen as white streaks (or fiber whitening) in the laminate, and occurs as a result of inadequate wet-out of the fiberglass strands [15]. While jackstrawing is an obvious aesthetic problem, its effect on mechanical properties is uncertain [15].

The resulting variations in materials and production result in the thickness and physical properties varying significantly throughout a piece of FRP equipment [7,27].

Along with the inherent variations of FRP properties there are several considerations that must also be taken into account.

One is the difficulty of accurately determining what are the normal physical properties of a particular composite for a basis of design or for inspection purposes [7]. This is in turn compounded by the relative fragileness of FRP compared to metals. Testing, especially on filament wound structures, can only measure 40% to 80% of the actual physical property and the test procedure itself is also a major contributor of random error in the test results [7].

Compared to steel, FRP is weaker, more flexible, more brittle, and has less resistant to creep [7,27]. Lack of ductility causes the most difficulty in design, since local overloading causes cracking rather than yielding [27]. In chemical processing equipment a crack in the veil corrosion liner critically compromises its function [9,25].

Designing structures built with conventional isotropic metallic materials is based on well established methods. Application of these methods to FRP structures can result in disaster [27]. In order to account for the anisotropy and ply to ply characteristic variations of the composite materials system, the appropriate stress-strain relations must be used [7]. The stress-strain relations can give accurate predictions of elastic behavior, but cannot be relied upon to predict fracture stresses [28]. There also exist various failure

criteria that can be applied, but these are often simplified due to the nature of anisotropic materials. Failure criteria do not explain the mechanisms of failure that may be present [38].

In service the FRP structure can be subject to complex loads involving biaxial or triaxial states of stress [28]. Stress can be either mechanical or nonmechanical in nature [39]. Mechanical stress is the result of an applied load such as internal pressure or wind load. Nonmechanical stress is the result of temperature change, absorption of moisture and residual fabrication stress [39].

2.5 Fluid Absorption Behavior of Vinyl Ester Laminates

Vinyl ester resins, along with all polymers used in composites, are subject to liquids diffusing into the resin [40]. The first essential stage of laminate degradation is always contact with, and ingress by, the penetrating fluid [41].

In one study by Marshall [40], the diffusion of water into vinyl ester resins and their glass reinforced laminate was examined. The resin used was Derakane™ 411-45. The laminate was four layers of 450 g/m^2 CSM, covered with one layer of 50 g/m^2 C-veil and a 0.5 mm unreinforced gel coat on the external surfaces, i.e. [gel coat/C-veil/4 layer CSM/C-veil/ gel coat]$_T$.

Unstressed and undamaged samples were exposed to water at ambient temperature (19 - 24°C).

One result of this study showed that undamaged and unstressed resin samples reached an equilibrium concentration of 0.8% (grams of water per gram of sample) after 1500 hours (62.5 days). Laminate samples were found to have an equilibrium content of 0.75%. Sorption data for vinyl ester resins and resin/glass laminates in water at 20°C is shown in Fig. 2-1 [40].

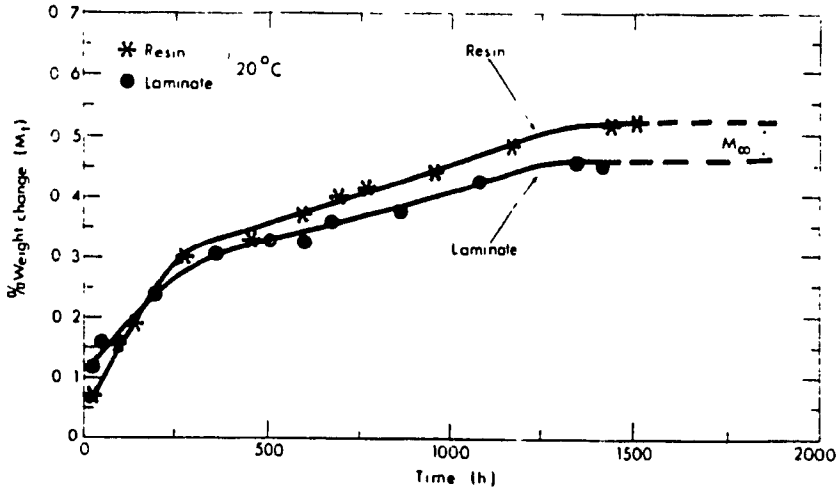

Fig. 2-1: Sorption data for vinyl ester resins and resin/glass laminates immersed in water at 20°C [40].

The diffusion behavior of hydrochloric acid (2 Molar) in unstressed, undamaged laminates has been found to be nearly identical to that of water [40].

Fluids can also diffuse into thermoplastics [40].

2.6 Mechanical Effects of Fluid Absorption

Absorption of liquid into the resin causes swelling [11,41,42,43]. Since most fibers used in composites are impermeable, deformation of a unidirectional composite is greatest in the transverse direction [44]. With multidirectional laminates the multidirectionality of the fibers prohibits free deformation resulting in residual stresses [44].

Another effect of liquid absorption is the degradation of mechanical properties of the resin [43,44]. The transverse and shear properties of unidirectional composites degrade, but the longitudinal properties change little due to the retention of mechanical properties by the fibers [45]. If the absorbed liquid attacks the fibers, the longitudinal properties will be degraded. The interlaminar shear strength of composite laminates is reduced by increasing the moisture absorption [46].

2.7 Chemical Effects of Fluid Absorption

The chemical resistance of FRP depends upon every component of the composite material and also every constituent of the aggressive fluid environment [41]. Due to the many variables involved, which can singly or jointly affect performance, corrosion resistance for a given situation can be difficult to judge [11]. The effect of an aggressive environment upon an FRP laminate can vary from negligible to complete deterioration [11].

There are three areas of chemical attack: chemical attack of the resin [11,46,47] which can be called resin attack, resin-glass interface attack [11,46], and chemical attack on the glass fibers [11,46] which can be called glass attack. The resin-glass interface is considered to be the most susceptible to degradation than either the resin or the glass reinforcement [48].

An increase in temperature will invariably increase the rate of attack, in some instances to the point where degradation is extremely rapid [11]. Since FRP is not homogeneous it does not react at predictable rates [11].

2.8 Visual Signs of Chemical Attack

Chemical resistance of FRP to a given environment can be judged in part by changes in appearance [47,49]. Experience has shown that a given class of chemical solution will give a characteristic type of appearance change in a laminate [49].

Blisters [11,47,49], opacity [49] and discolouration [11] are some of the visual signs used to judge corrosion resistance. Some key points of these visual signs are [49]:

Blisters: Defined as rounded elevations in the surface of the plastic with boundaries that may be more or less sharply defined, and be the results of chemical attack on the resin - glass interface. Type I blisters originate along the glass fiber of the C-veil. These blisters tend to be small with a radius of 1-3 mm and more numerous than type II. Type II blisters begin within the chopped strand mat. With continued exposure to the corrosive environment, this small blister can grow in diameter or combine with another small blister to form a much larger elevation at the surface.

Opacity: This property can be affected by changes in the specimen's surface, the resin, or by changes at the glass/resin interface.

Discoloration: Chemical medium absorbing into the resin can cause discolouration.

2.9 Aggressive Environments

"Aggressive" environments for reinforced plastic include oils, solvents, acids and even water [40]. Of particular interest for this project are water, hydrochloric acid and sulfuric acid.

Water is known for glass-resin interface attack and is usually seen as cloudiness or opaqueness of the laminate [47]. Hot water is known for glass attack [11].

Hydrochloric acid (37%) [11,23] and sulfuric acid (25%)[23] are also known for glass attack. Acids have been found to alter the physical properties of laminates far more than water, largely because they attack the glass [40].

Table 2-1 shows Dow Chemical's recommended maximum service temperature of Derakane™ 411 resin in certain chemical environments [50].

Table 2-1: Maximum service temperature of Derakane™ 411 resin in certain chemical environments [50].

Chemical Environment	Maximum recommended temperature °F/°C
Air (immersion)	210 / 99
Hydrochloric Acid 20%	180 / 82
" " 37%	150 / 65
Sulfuric Acid 93%	Not recommended
Water, distilled	180 / 82

2.10 Failure Patterns of F.W. Pipe

The failure pattern of filament wound pipe is dependent upon several factors: the manner of loading, the ratio of hoop to axial stress, angle of the F.W. layer and construction of the pipe.

Testing under hoop and biaxial stress is achieved by a combination of internal pressurization and an appropriate test fixture [28,31,51,52,53].

2.10.1 Internal Pressure Biaxial Stress Failure Pattern

Under internal pressure (biaxial load of $\sigma_H = 2\ \sigma_A$) the initial stress-strain response of filament wound glass fiber/polyester pipes with a winding angle of $\pm 55^\circ$ was linear. As loading continues, and at

very low strain, the stress strain response becomes non-linear [31,51]. A typical stress strain diagram for a pipe under the above biaxial loading is presented in Fig. 2-2 [31].

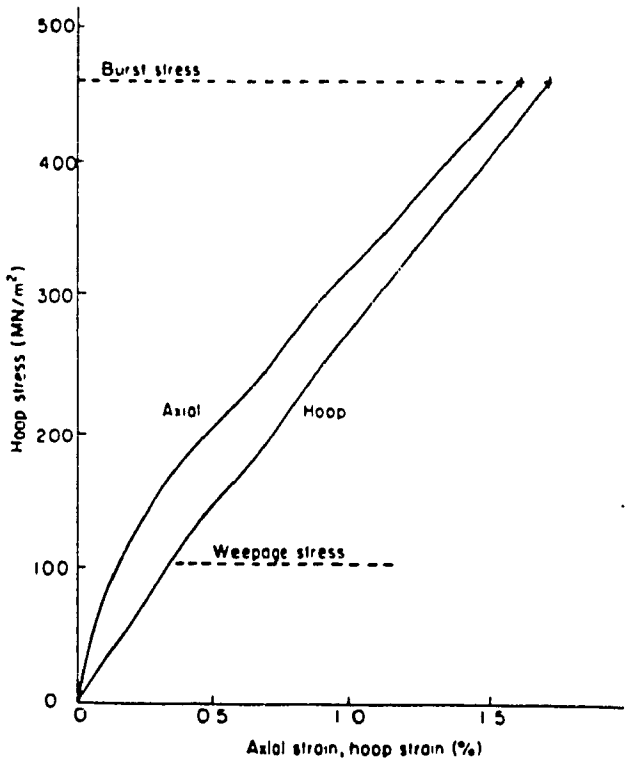

Fig. 2-2: Typical stress-strain behavior of a ± 55° filament wound E-glass/epoxy tube under biaxial stress [31].

In some composite systems, the onset of non-linearity has been attributed to both cohesive failure of the resin matrix and irreversible loosening of the fiber resin bond [51]. This resin failure means that the response of the tube tends to approach that predicted for a pipe with no resin [31,51]. The transition from linear to non-linear response is smooth in angle ply laminates [51].

The first visible sign of damage is the development of transverse cracks which are seen as thin white streaks parallel to the fibers [31,51]. As pressure is increased these streaks would grow and increase in number [31,51]. Next, interlaminar cracks associated with transverse cracks would develop and produce small, isolated opaque patches [51].

Without the benefit of an internal rubber liner, initial failure would generally be by weepage [28,31,51]. The first evidence of weepage is the development of droplets along lines parallel to the filament winding direction [31]. In some cases weepage occurs as a fine jet of test fluid [28,51]. In some cases failure may be by burst [28].

For weepage to take place there must be a continuous path through the pipe wall. This is possible when a transverse crack in the innermost layer is crossed at a point by a transverse crack in the second layer which is in turn crossed by a transverse crack in the third layer, etc. The occurrence of interlaminar cracking increases the probability

of a continuous crack path and hence weepage. Jet weepage is a sign that interlaminar cracking is present, at least along the outermost interlaminar plane. Weepage is not possible by interlaminar cracking alone as it does not result in a continuous path through the pipe wall [51].

Inspection of a cross-section of the pipe wall revealed transverse laminar cracks, interlaminar and oblique transverse cracks, and free edge delaminations from the tips of transverse cracks [51]. Transverse cracks are formed in response to strains normal to the fibers and interlaminar cracks in response to shear strains, oblique transverse cracks may be the result of both tensile and shear strains [51].

With a rubber liner, final failure of the pipe is by bursting [28,31]. At this stage the resin is not contributing to load bearing and when the tensile stress in the fibers reaches the limiting strength of the glass failure occurs [31].

Testing of 5 cm diameter, $\pm 54.75^{\circ}$ filament wound tubes constructed with vinyl ester resin under hydrostatic closed end loading showed that weep strength was controlled by the strength of the resin [52].

2.10.2 Internal Pressure Hoop Stress Failure Pattern

Under hoop loading ($\sigma_A = 0$) the stress strain response followed the same pattern of changing from linear to non-linear as loading increased [31,51]. Fig. 2-3 shows a typical stress strain diagram for a pipe under hoop loading [31].

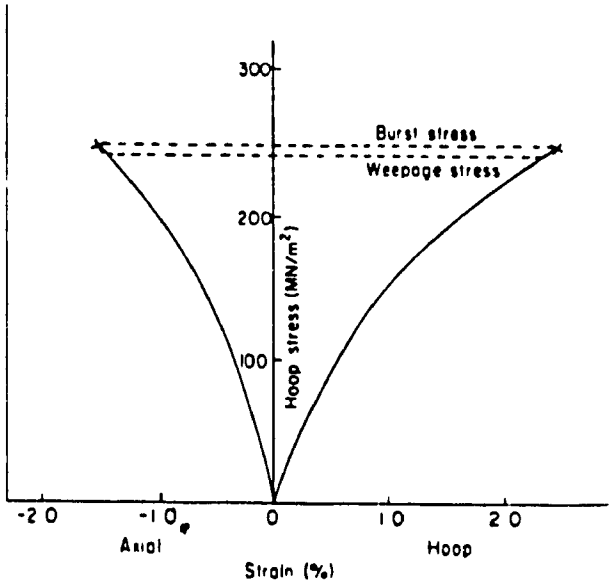

Fig. 2-3: Typical stress-strain response for a ±55° filament wound E-glass/epoxy tube under hoop stress [31].

Whitening also occurred but was of a different form. The main features were large opaque patches and fine striations parallel to the fibers which are due to delamination and fiber debonding [51].

Initial failure is by weepage [28,31,51]. One study found weepage was in the form of sudden jetting of the test fluid [31].

Final failure is associated with delamination between adjacent layers of fiber wound at different angles and appears as large patches of uniformly white regions in the pipe wall. Delamination is then associated with bending of the pipe and final catastrophic failure involves fiber breakage which appears to start in regions of delamination [31].

2.10.3 Tensile Axial Stress Failure Pattern

As the axial loading is done without fluid, initial failure by weepage is obviously not possible and final failure is by fracture. Figure 2-4 shows the appearance of a $\pm 55^{\circ}$ filament wound E-glass/epoxy after failure by fracture under a tensile axial load. Under tensile loading angle ply laminates exhibit two kinds of stress-strain nonlinearity. At a winding angle close to 0° a stiffening effect is observed so that the modulus increases with increasing load. At larger winding angles, a softening effect is observed so that the modulus decreases with increasing load. The stiffening effect is attributed to the longitudinal tensile stresses in various plies, whereas the softening effect is attributed to the shear stresses [53].

Fig. 2-4: Typical appearance of a ±55° filament wound E-glass/epoxy tube after final failure by fracture under tensile axial load [31].

CHAPTER 3. Project Description

As both the test specimens and test set-ups were unique, this chapter serves to describe how the project was set up.

3.1. Materials Used to Construct the Tubes

The resin used to construct the tubes was Derakane™ 411-45 manufactured by The Dow Chemical Company. It is a vinyl ester resin with a monomeric styrene content of 45% [54]. Table 3-1 shows the physical properties of this resin [4,55]

Table 3-1: Physical properties of Derakane™ 411-45 [4,55].

Tensile Strength	11,800 psi (81.36 MPa)
Tensile Modulus	4.9E5 psi (3.38 GPa)
Elongation	5%
Viscosity (@ 77°F)	400 cps

The resin was accelerated with 0.35% cobalt napthalate (6%) and 0.05% dimethylaniline. The catalyst was 1.5% DHD-9 (50% methyl ethyl ketone peroxide, 50% dibutyl pthalate) with 9% active oxygen.

A small number of veil lined tubes were constructed using 411-C-45 resin due to a temporary shortage of 411-45. This resin differs marginally in properties, with the "C" grade being slightly more corrosion resistant.

The other materials used for the construction of the tubes were [56]:

- Fiberglass Canada "process 30" 2200 Tex roving for the filament winding (F.W).
- Fiberglass Canada M753 chopped strand mat, 50 g/m^2 (mat).
- Regina Fiberglass Limited F2/30 C-glass veil (veil).
- Sixteen, 6.1 m lengths of Darvic™ polyvinyl chloride 108 mm O.D. pipe.

Some of the characteristics of Darvic PVC are given in Table 3-2 [57].

Table 3-2: Darvic PVC characteristics [57].

Tensile Strength	8000 psi (55.16 MPa)	
Modulus	4.9 E5 psi (3.38 GPa)	
Elongation	4%	
Maximum Temperature for Exposure to	35% HCl	< 60°C
	98% H_2SO_4	20°C
	Water	< 60°C

3.2 Tube Lay-up

The lay-ups of the test specimens for this project are:

- $[\text{Veil / 2 Mat / FW } [55/-55/55/-55]]_T$
- $[\text{PVC / Veil / Mat / FW } [55/-55/55/-55]]_T$

3.3 Tube Construction Details

Construction of the test specimens was performed by CPF Dualam using the methods they would normally employ to construct their commercial products.

3.3.1 Veil Lined Tube Construction

Construction of the veil lined tubes required that a removable mandrel be constructed. The mandrel to produce veil lined tubes with the same midplane radius as the PVC tubes was fabricated by tightly wrapping two layers of corrugated cardboard and a top layer of 0.0254 mm mylar release film around a steel mandrel. The mandrel could produce tubes up to 6.1 m long. Sixteen, 6.1 m tubes were produced with a winding angle $\pm 55^{\circ}$. These were numbered 1 to 16 and will be referred to as veil 55° or veil lined tubes.

3.3.2 PVC Lined Tube Construction

The first step was to sand the exterior surface of the PVC tube with a 24 grit sanding disk to improve bonding. Next, a layer of C-glass veil was hand laid around the tube. A layer of CSM was the next layer to be applied, again by hand. The final layer of the tube was two circuits of $\pm 55^{\circ}$ filament winding applied with a mechanical winder using the PVC tube as the winding mandrel. All the above layers were applied with resin. Sixteen, 6.1 m long PVC lined tubes were constructed. These tubes were numbered 19 to 34. These tubes will be referred to as PVC 55° or PVC lined tubes.

3.4 Preparation of Tubes for Aging

After the resin was cured, the ends of the tubes where the winding pattern reverses (about 20 cm) were cut off and discarded. The remainder of the tube was cut into five 115 cm lengths.

Next, one end of the tubes was sealed. For the PVC lined tubes a PVC disk was solvent welded in place, then covered with a hand lay-up. The veil lined tubes were sealed with just a layer of hand lay-up.

3.5 Labelling System

In order to keep track of the 155 tubes to be used in the projet, and the 465 test specimens scheduled for testing, a simple, two-part labeling system was used.

The first part of the label was marked on the 115 cm tube when it was cut from the parent tube. The label is composed of the parent tube number and a letter. The letter indicates the position on the parent tube from which the 115 cm segment was cut. "A" is an end piece. Traveling toward the other original end, "B" is the next segment, "C" is the center piece and "E" is the other end piece. The family line of the 155 115 cm specimens created is shown in Table 3-3.

The second part of the label, on the right hand side of the hyphen separating the two parts, is composed of one number and one letter. The number indicates the test used on the tube: "1" for the hoop test, "2" for the biaxial test and "3" for the axial test. The letter indicates the test point for which the tube was tested for. "A" and "B" are for test point one, "C" and "D" are for test point two, etc. This pattern was continued for the remaining four test points.

For example 15C-2J is a veil lined tube that was the center segment of the parent tube #15. It was tested under biaxial loading for test point five.

Table 3-3: The family line of the 155 115 cm specimens.

Parent pipe #	Original length	Lay-up & resin	Segments cut	Length of segments	Label given
1 to 11	All 6.1 m	V/2M/2±55°†/ 411	5	All 115 cm	1A → 1E to 11A → 11E
12 to 15		V/2M/2±55°/ 411-C	5		12A → 12E to 15A → 15E
16		V/2M/2±55°/ 411	5		16A → 16E
19 to 34		PVC/V/M/ 2±55°/411	5		19A → 19E to 34A → 34E

† The ±55°, indicates the filament winding angle

3.6 Tube Dimensions

Prior to environmental aging the inside and outside diameters of the test specimens were measured. From these results the means of these dimensions were calculated. The results are shown in Table 3-4.

Table 3-4: The average tube dimensions.

	Liner	
	Veil	PVC
I.D.	105.54 mm	103.06 mm
O.D.	115.54 mm	116.36 mm
t	5.5 mm	6.65 mm

3.7 Environmental Exposure

Exposure to working environments was simulated by filling the tubes with different liquids.

The tubes were filled with room temperature water, H_2SO_4 (98%), HCl (35%), water at 80°C or HCl (35%) at 50°C. The elevated temperatures were achieved by placing the filled tubes in custom made heating tanks. Both types of tubes had specimens that were exposed to room temperature air. Due to the text limitations of the graphing programs used, room temperature HCl and water will also be referred to as cold HCl and cold water respectively. Also, hot HCl and hot water will refer to the respective elevated temperature environment.

The veil lined tubes exposed to sulfuric acid were found to deteriorate rapidly and were dropped from the project.

3.8 Specimen Testing

Testing of the tubes was to be done as a series of six test points over a period of three years. Target exposure time for the first test point was to be six months, with subsequent test points at six month intervals. At each test point, two exposed PVC lined and veil lined tubes from each environment were selected and drained of the liquid they contained. Tubes that had been exposed to acid were flushed with a solution of water and calcium carbonate. From this point the tubes were left exposed to room temperature air until they were tested.

Each tube was cut into three, 38 cm long sections. This yielded two test specimens from each liner/environment for the three tests.

One major problem faced by this project was to develop reliable tests. Ideas were tried on aged test specimens. As a result, there were some tests in which the test set-up failed, not the tube. This problem was especially acute with the biaxial test, as roughly 40% of the tests performed were deemed to be failed tests. All tests were designed so that the applied stress could be controlled easily.

3.8.1 Hoop Test

The objective of the hoop test was to use internal pressure and induce a hoop stress in the tube while the axial stress remained zero. To achieve this a jig that would seal the ends yet allow the tube to move axially was required. The jig used is shown in Fig. 3-1. Designed to fit inside the tube, it consists of a stainless steel rod with an aluminum disk bolted to each end. Sealing between the inner surface of the tube and outer diameter of the disk was accomplished with O-rings. A hole in the disk was tapped to accept pipe fittings.

Producing and maintaining the seal between the disks and the tube was the main problem with this test. Sealing required the minimum gap possible between the disk and the tube without binding. For the veil tubes, four disks with an outer diameter of 102.28 mm, 102.31 mm, 102.36 mm and 102.41 mm were made. This was necessary as the inner diameter of the veil lined tubes varied slightly.

Occasionally, even with the largest disk possible in place, the O-ring either would not seal, or if it did the gap at spots would allow the O-ring to be forced out of position during the test. This problem was solved by using automotive body filler. Using a disk as a guide, the minimum of filler was used to fill in the gaps between the disk and tube to provide a surface that would produce a good seal and produce the minimum gap between disk and tube.

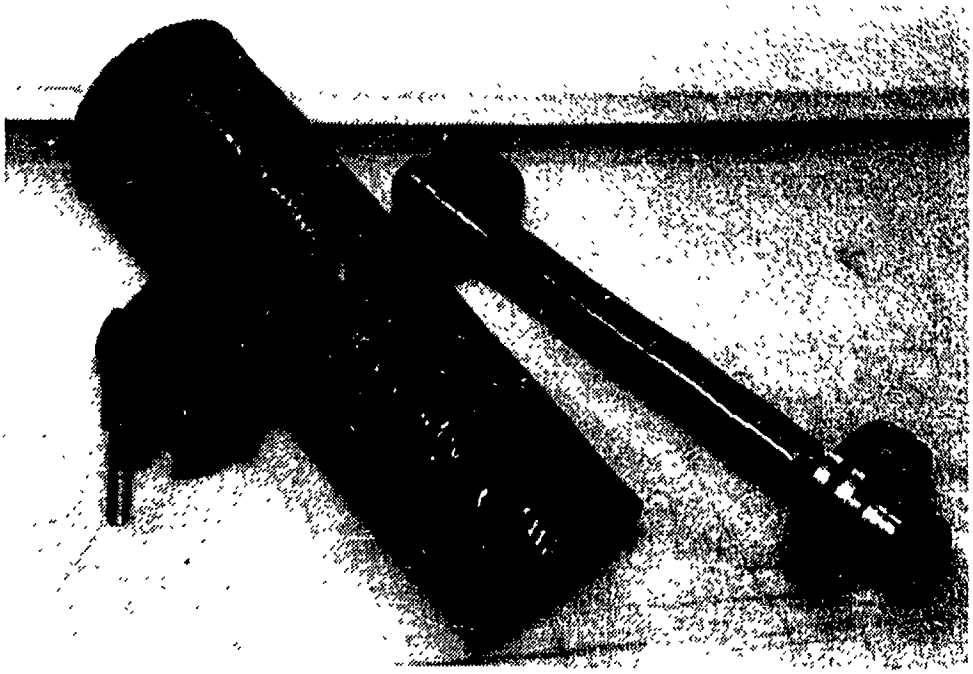

Fig. 3-1: Hoop test jig.

As the inner wall of all the thermoplastic lined tubes was smooth and had a constant inner diameter, the aforementioned problem with the veil tubes was avoided. However, the loss of the O-ring seal due to extrusion of the O-ring between the tube and disk during the test was a problem. This problem became evident as pressure applied to the tubes exceeded 17 MPa. This problem was solved by producing a pair of disks with two O-ring seals each.

Prior to testing the tubes were inspected. Those with the best inner walls were selected for the hoop test. The four main steps in tube preparation were: filing a radius on the inside diameter at each end,

attaching hoop and axial strain gages at the tube's center (if required), labelling, and then taking a before-test photograph. A thin layer of white grease was then applied to the seal area to reduce seal friction and then the test jig was assembled inside the tube. Due to seal drag and Poisson's effect there will be an axial tension present [58], however this will be ignored and perfect hoop loading will be assumed.

The tubes were tested standing vertically in a containment enclosure. The enclosure had a plexiglass side allowing for observation and a video recording to be made during the test. The test fluid used for the first three test points was a water and water soluble oil mix. This was changed to just water for the final three test points. Fluid pressure was supplied by an air powered intensifier capable of producing 410 MPa. Control of the intensifier was achieved by throttling the air exiting the intensifier's exhaust and regulating the air supply pressure well below normal working values. Loading was generally 7 MPa/min. A calibrated pressure transducer measured the applied pressure.

Pressure was gradually increased until failure occurred. In general, failure of internally pressurized unlined filament wound tubes is by weepage [18,31,51], so the results from this test set-up were the weepage pressure of the veil lined tubes. The performance of the PVC lined tubes would depend upon the ability of the PVC liner to retain its integrity.

3.8.2 Biaxial Test

The objective of the biaxial (internal pressure) test was to apply hoop and axial stress at a ratio of 2:1 to the tube using internal pressure. While it seemed simple to seal the ends of the tubes to produce the desired biaxial stresses, in practice it was quite difficult.

The first method tried was to seal the tube ends with a hand lay-up layer. After a number of tests this method was found to be inadequate. Sealing the ends with steel caps glued in place with epoxy was the next method tried. This method was more reliable. A tube with a set of steel caps glued in position is shown in Fig. 3-2. 10 end caps were manufactured with a range of inside diameters to accommodate the range of O.D. of the test specimens.

Pressurization was produced with the same setup as for the hoop test. The pressure was to be increased until failure occurred. Like the hoop test, failure of the veil lined tubes should be by weepage and failure of the PVC lined tubes would depend upon the performance of the PVC liner.

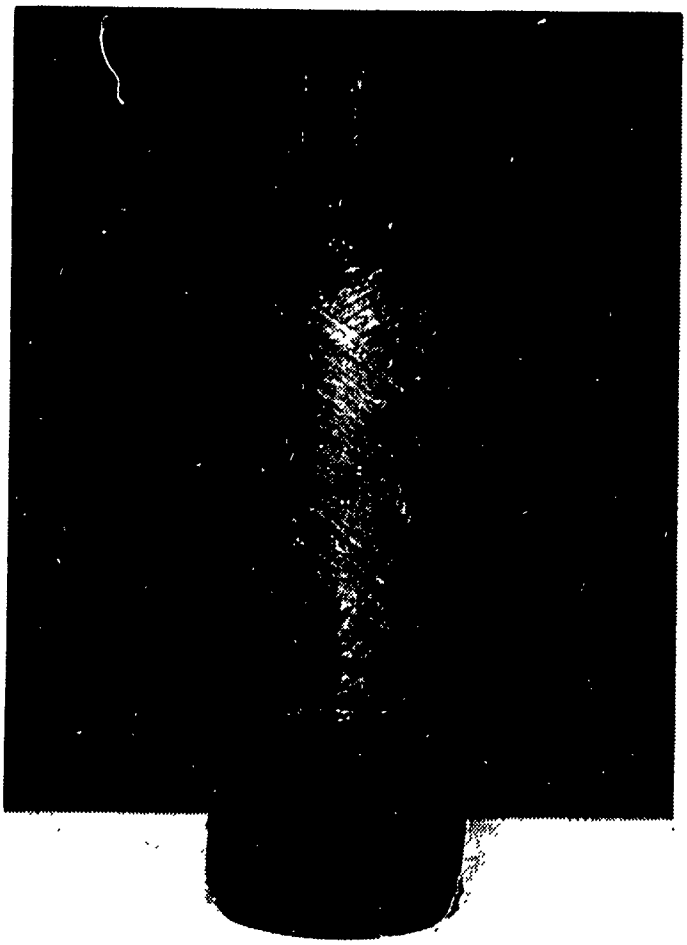

Fig. 3-2: A tube with a set of end caps glued in place.

Preparation for the biaxial test consisted of lightly grinding an 8 cm wide path around both ends of the tube and the select fitting of end caps to match the O.D. of the tube. The end cap was then glued to the tube using Ciba Giegy ambient cure Araldite epoxy (100 parts AW 106 resin to 80 parts HV 953U hardener by weight). Once the end caps were in place the tube was gaged (if required), labelled, and photographed. The test specimens were tested in the vertical position in the same manner as the hoop test.

3.8.3 Axial Test

The axial test was designed to place the test specimen under a tensile axial stress in a controlled manner until failure occurred. The failure load was deemed to be the load at which the first failure occurred. After this point, loading would continue until the tube could no longer sustain any applied load.

A custom made axial test jig, shown in Fig. 3-3, was used for testing. The tube is held at its ends between circular grips. The grips run on inclined surfaces to provide increasing gripping force as the load was increased. Loading was achieved by the use of a 1.3 MN capacity Tinius Olson hydraulic press. A tube about to undergo the axial test is shown in Fig. 3-4.

Fig. 3-3: Axial test jig.

Preparation for the axial test started with lightly grinding a 7 cm wide patch around each end of the tube. This was then covered with a hand lay-up of two layers of chopped strand mat and resin. When cured, these tabs were lightly grounded to be concentric with the tube. The tube was then gaged (if required), labelled for test and photographed.

One concern of this test was whether the test jig was pulling evenly on the tube. A test was run with strain gages placed 120° apart at the center of the tube. No evidence of bending prior to failure was indicated in the results.

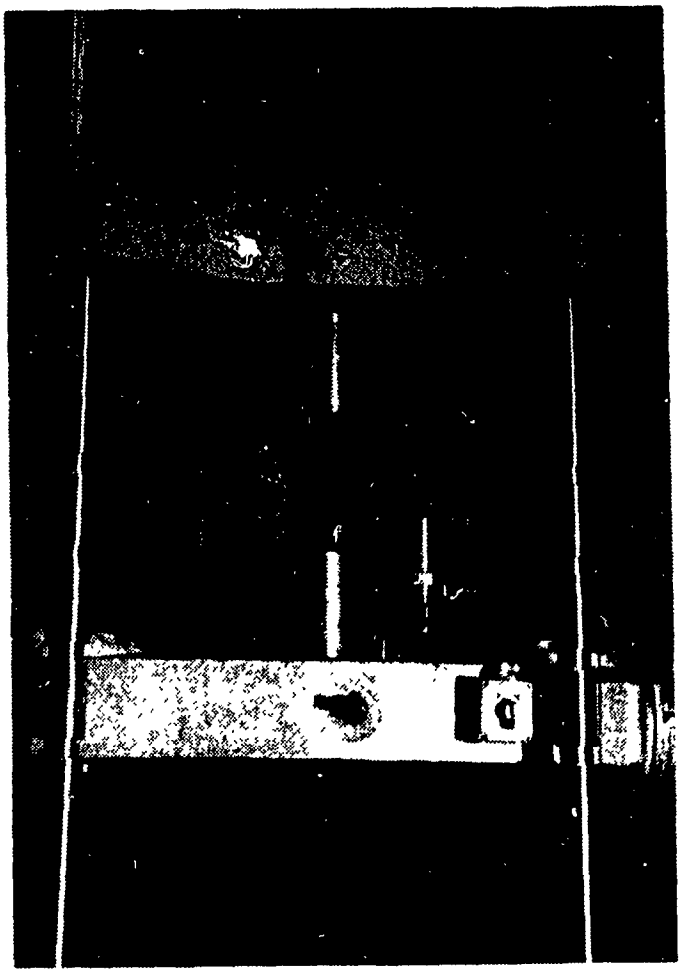

Fig. 3-4: A tube in the axial test jig ready for testing.

3.9 Data Acquisition

For each test a file was kept. Each tube had a before-test and an after-test photograph taken. Each test was recorded on video tape. During testing, a voltmeter was in the video frame and displayed the applied pressure or load. During most of test point one, data was recorded manually. Later it was accomplished with a Fluke 2280A data acquisition system.

For the hoop and biaxial tests, pressure was measured by a pressure transducer/amplifier set-up which sent an analog signal to the voltmeter and Fluke. This system was calibrated in psi. During testing of a tube with strain gages applied, the Fluke Data Logger was set to run continuously, recording the applied pressure, surface strains ε_1 (axial strain) and ε_2 (hoop strain), and the apparent Poisson's ratio, ν_{21}, every five seconds or so.

For the axial test, a signal from a load cell on the upper grip was processed and amplified and the analog voltage output displayed on the voltmeter. Another load cell provided a signal for the Fluke data logger. This system was calibrated in lbs x 1000. For thcse tubes with strain gages the applied load, surface strains ε_1 (axial strain) and ε_2 (hoop strain), and the apparent Poisson's ratio, ν_{12}, were recorded. For the axial test, the Fluke was manually triggered at every 4.448 kN (1000 lbs) increase in load except near failure, when it was triggered at the operator's discretion.

CHAPTER 4. Laminate Analysis

Laminate analysis of the lay-ups used in this project follows the methods found in reference 39. The sign conventions for stress, strain and angle of transformation are shown in Fig. 4-1.

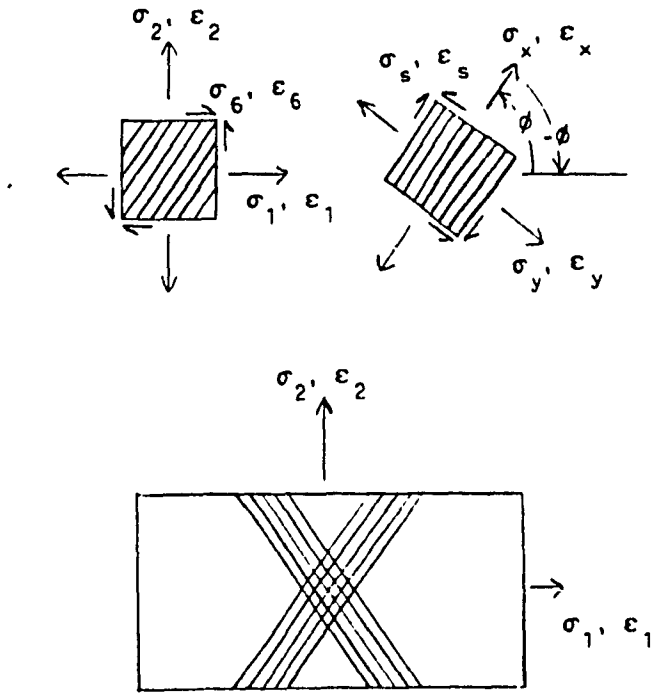

Fig. 4-1: Sign conventions for stress, strain and angle of transformation.

The subscript 6 is used to designate the shear component in the 1-2 plane. This is because the subscript 3 may designate the 3rd normal stress component in 3 dimensional problems and can be a source of confusion if used to designate the 1-2 plane shear component.

4.1 Stress-Strain Relationships for the Tubes

Table 4-1 shows the matrix multiplication table for the generalized stress-strain relations in terms of stiffness modulus for laminates.

Table 4-1: Generalized stress-strain relations in terms of stiffness modulus.

	E	**k**
N	**A**	**B**
M	**B**	**D**

The matrix quantities above are row, column, and square matrices as follows:

$$\mathbf{N} = N_i = \begin{Bmatrix} N_1 \\ N_2 \\ N_6 \end{Bmatrix} \qquad \mathbf{M} = M_i = \begin{Bmatrix} M_1 \\ M_2 \\ M_6 \end{Bmatrix} \qquad (4\text{-}1)$$

$$\mathbf{E} = \varepsilon_i^o = \begin{Bmatrix} \varepsilon_1^o \\ \varepsilon_2^o \\ \varepsilon_6^o \end{Bmatrix} \qquad \mathbf{k} = k_i = \begin{Bmatrix} k_1 \\ k_2 \\ k_6 \end{Bmatrix} \qquad (4\text{-}2)$$

$$\mathbf{A} = A_{ij} = \begin{bmatrix} A_{11} & A_{12} & A_{16} \\ A_{21} & A_{22} & A_{26} \\ A_{61} & A_{62} & A_{66} \end{bmatrix} \qquad (4\text{-}3)$$

$$\mathbf{B} = B_{ij} = \begin{bmatrix} B_{11} & B_{12} & B_{16} \\ B_{21} & B_{22} & B_{26} \\ B_{61} & B_{62} & B_{66} \end{bmatrix} \qquad (4\text{-}4)$$

$$\mathbf{D} = D_{ij} = \begin{bmatrix} D_{11} & D_{12} & D_{16} \\ D_{21} & D_{22} & D_{26} \\ D_{61} & D_{62} & D_{66} \end{bmatrix} \qquad (4\text{-}5)$$

The matrix multiplication table may be written in matrix notation as

$$\mathbf{N} = \mathbf{AE} + \mathbf{Bk} \qquad (4\text{-}6)$$

$$\mathbf{M} = \mathbf{BE} + \mathbf{Dk} \qquad (4\text{-}7)$$

Multiplying Equation (4-6) by **a**, the inverse of **A** gives

$$\mathbf{aN} = \mathbf{aAE} + \mathbf{aBk} \qquad (4\text{-}8)$$

Since

$$\mathbf{aA} = \mathbf{I}, \text{ the identity matrix}$$

Equation (4-8) may be rewritten as

$$\mathbf{E} = \mathbf{aN} - \mathbf{aBk} \qquad (4\text{-}9)$$

Substituting this into Equation (4-7)

$$M = B(aN - aBk) + Dk \qquad (4\text{-}10)$$

$$= BaN - BaBk + Dk \qquad (4\text{-}11)$$

$$= BaN + (D - BaB)k \qquad (4\text{-}12)$$

In terms of a matrix multiplication table, the generalized stress-strain relation in terms of **N** and **k** and based on equations (4-9) and (4-12) is shown in Table 4-2.

Table 4-2: Generalized stress-strain relations in terms of **N** and **k**.

	N	**k**
E	**a**	**- aB**
M	**Ba**	**D - BaB**

These equations are useful for structures with a fixed cylindrical cross section such as the tubes tested in this project [59]. Since the curvature, **k**, will be assumed to be constant for a given tube during testing, the term **aBk** may also be considered to be a constant. Therefore strain may be calculated as

$$E = aN \qquad (4\text{-}13)$$

Table 4 3 shows the in-plane stress-strain relations for symmetric laminates in terms of compliance.

Table 4-3: In-plane stress-strain relation of symmetric laminates in terms of compliance.

	N_1	N_2	N_6
ε_1^o	a_{11}	a_{12}	a_{16}
ε_2^o	a_{21}	a_{22}	a_{26}
ε_6^o	a_{61}	a_{62}	a_{66}

Table 4-4 shows the in-plane stress-strain relations for symmetric laminates in terms of stiffness.

Table 4-4: In-plane stress-strain relation of symmetric laminates in terms of stiffness.

	ε_1^o	ε_2^o	ε_6^o
N_1	A_{11}	A_{12}	A_{16}
N_2	A_{21}	A_{22}	A_{26}
N_6	A_{61}	A_{62}	A_{66}

If the stiffness or compliance multiplication matrix is known the other may be found by inverting the matrix.

4.2 In-Plane Stiffness of Tubes

The engineering constants of the individual layers are listed in Table 4-5 [60].

Table 4-5 : Engineering constants of the individual layers used to construct the test specimens [60].

	MAT	FILAMENT WINDING	VEIL	PVC
E_x (GPa)	8.40	35.0	3.50	2.34
E_y (GPa)	8.40	10.4	3.50	2.34
ν_x	0.20	0.281	0.33	0.40
E_s (GPa)	3.50	3.20	1.32	0.84
t (mm)	1.40	0.54	0.33	3.30

All the tubes are asymmetric, balanced angle ply laminates. It is assumed that the strain is constant across the laminate thickness.

The following relations exist between engineering constants and the components of stiffness.

$$Q_{xx} = mE_x \qquad Q_{yy} = mE_y$$
$$Q_{yx} = m\nu_x E_y \qquad Q_{xy} = m\nu_y E_x \qquad (4\text{-}14)$$
$$Q_{ss} = E_s \qquad m = [1 - \nu_x \nu_y]^{-1}$$

The components of stiffness for each constituent layer of the laminates is shown in Table 4-6.

Table 4-6: Components of stiffness for each layer.

	MAT	FILAMENT WINDING	VEIL	PVC
Q_{xx}(GPa)	8.75	35.84	3.92	2.79
Q_{yy}(GPa)	8.75	10.65	3.92	2.79
Q_{xy}(GPa)	1.75	2.99	1.29	1.11
Q_{yx}(GPa)	1.75	2.99	1.29	1.11
Q_{ss}(GPa)	3.50	3.20	1.32	0.84
m	1.0417	1.0240	1.1222	1.1905

In order to calculate the off axis stiffness, the linear combinations of the on-axis stiffness must be calculated. The linear combinations are defined by

$$
\begin{aligned}
U_1 &= 0.125\ [\ 3Q_{xx} + 3Q_{yy} + 2Q_{xy} + 4Q_{ss}\ ] \\
U_2 &= 0.5\ [\ Q_{xx} - Q_{yy}\ ] \\
U_3 &= 0.125\ [\ Q_{xx} + Q_{yy} - 2Q_{xy} - 4Q_{ss}\ ] \\
U_4 &= 0.125\ [\ Q_{xx} + Q_{yy} + 6Q_{xy} - 4Q_{ss}\ ] \\
U_5 &= 0.125\ [\ Q_{xx} + Q_{yy} - 2Q_{xy} + 4Q_{ss}\ ]
\end{aligned}
\qquad (4\text{-}15)
$$

The results for the materials used in tube construction are given in Table 4-7.

Table 4-7: Linear combinations of on-axis stiffness of each layer.

	MAT	FILAMENT WINDING	VEIL	PVC
U_1 (GPa)	8.75	19.78	3.93	2.79
U_2 (GPa)	0.00	12.60	0.00	0.00
U_3 (GPa)	0.00	3.46	0.00	0.00
U_4 (GPa)	1.75	6.45	1.30	1.11
U_5 (GPa)	3.50	6.66	1.31	0.84

The formulas for the in-plane stiffness modulus for angle-ply laminates are given in Table 4-8. ϕ is the ply orientation.

Table 4-8: In plane stiffness modulus formulas for angle ply laminates.

	1	U_2	U_3
A_{11}/h	U_1	$\cos 2\phi$	$\cos 4\phi$
A_{22}/h	U_1	$-\cos 2\phi$	$\cos 4\phi$
A_{12}/h	U_4		$-\cos 4\phi$
A_{66}/h	U_5		$-\cos 4\phi$

$$A_{16} = A_{26} = 0$$

The above in-plane stiffness modulus formulas are only valid for a symmetric lay-up. In order to simplify the laminate analysis it will be assumed that our laminate is symmetric and $A_{16} = A_{26} = 0$ is valid.

The normalized in-plane stiffness for the filament winding layer as the winding angle varies from 0° to 90° is given in Table 4-9.

Table 4-9: Normalized in-plane stiffness of filament winding layer for 0° to 90° winding angle.

WINDING ANGLE (DEG)	A_{11}/h (GPa)	A_{22}/h (GPa)	A_{12}/h (GPa)	A_{66}/h (GPa)
0	35.84	10.65	2.99	3.20
5	35.43	10.63	3.20	3.40
10	34.27	10.59	3.80	4.08
15	32.42	10.60	4.72	4.93
20	30.03	10.73	5.85	6.06
25	27.27	11.08	7.05	7.26
30	24.34	11.75	8.18	8.39
35	21.43	12.82	9.10	9.31
40	18.71	14.33	9.71	9.91
45	16.31	16.31	9.92	10.12
50	14.33	18.71	9.71	9.91
55	12.82	21.44	9.11	9.32
60	11.75	24.34	8.18	8.39
65	11.08	27.27	7.05	7.26
70	10.73	30.03	5.85	6.06
75	10.60	32.42	4.72	4.93
80	10.59	34.27	3.80	4.08
85	10.63	35.43	3.20	3.40
90	10.65	35.84	2.99	3.20

The veil and chopped strand mat layers can be considered to be quasi-isotropic and the PVC layer is isotropic. As a result the in-plane modulus becomes

$$A_{11}/h = A_{22}/h = U_1$$
$$A_{12}/h = U_4 \qquad (4\text{-}16)$$
$$A_{66}/h = U_5$$

The normalized in-plane stiffness for the individual layers of the tubes are given in Table 4-10.

Table 4-10: Normalized in-plane stiffness of individual layers.

	COMPONENTS OF STIFFNESS (GPa)			
LAYER TYPE	A_{11}/h	A_{22}/h	A_{12}/h	A_{66}/h
PVC	2.79	2.79	1.11	0.84
VEIL	3.93	3.93	1.29	1.32
MAT	8.75	8.75	1.75	3.50
F.W. 55°	12.82	21.44	9.11	9.32

The stiffness modulus of a laminate is simply the arithmetic average of the stiffness of the constituent plies. The components of stiffness may be calculated as

$$A_{ij} = \Sigma A_{ijk} \frac{t_k}{h} \qquad (4\text{-}17)$$

where k = Veil, mat. F.W., or k = PVC, veil, mat, F.W., t = thickness of a given layer and h = total thickness of the particular laminate.

For the two tube types in this project the calculated normalized in-plane stiffness components are shown in Table 4-11 and the corresponding normalized in-plane compliance components are shown in Table 4-12.

Table 4-11: Normalized in-plane stiffness of both tube types.

	COMPONENTS OF STIFFNESS (GPa)			
TUBE TYPE	A_{11}/h	A_{22}/h	A_{12}/h	A_{66}/h
PVC 55°	7.02	9.61	3.65	3.93
VEIL 55°	10.11	13.63	4.73	5.74

Table 4-12: Normalized in-plane compliance of both tube types.

	COMPONENTS OF COMPLIANCE (TPa^{-1})			
TUBE TYPE	$a_{11}h$	$a_{22}h$	$a_{12}h$	$a_{66}h$
PVC 55°	177.50	129.66	-67.42	254.45
VEIL 55°	118.08	87.59	-40.98	174.21

4.3 Apparent Longitudinal Poisson's Ratio

For axial loading

$$\nu_{12} = -\frac{\varepsilon_2^o}{\varepsilon_1^o} = -\frac{a_{21}}{a_{11}} \qquad (4\text{-}18)$$

For biaxial loading

$$\nu_{12} = -\frac{\varepsilon_2^o}{\varepsilon_1^o} = -\frac{a_{21} + 2a_{22}}{a_{11} + 2a_{12}} \qquad (4\text{-}19)$$

For hoop loading

$$\nu_{12} = -\frac{\varepsilon_2^o}{\varepsilon_1^o} = -\frac{a_{22}}{a_{12}} \qquad (4\text{-}20)$$

The theoretical longitudinal poisson's ratio of each tube type under each loading applied are given in Table 4-13.

Table 4-13: The apparent longitudinal Poisson's ratio during testing for both tube types.

	APPARENT LONGITUDINAL POISSON'S RATIO, ν_{12}		
TUBE TYPE	AXIAL TEST	BIAXIAL TEST	HOOP TEST
PVC 55° VEIL 55°	0.380 0.347	-4.498 -3.715	1.923 2.137

4.4 Ply Stress Analysis

When an external stress is applied to a tube it responds with an equal and opposing stress. As the laminate acts as one unit it may be assumed that the in-plane strains are uniform. Since each layer of the laminate retains its own unique stress-strain properties it must have its own unique stress state.

For a given laminate

$$\varepsilon^{o}_{\text{laminate}} = \varepsilon_{\text{lamina A}} = \varepsilon_{\text{lamina B}} = \ldots = \varepsilon_{\text{lamina n}} \qquad (4\text{-}21)$$

$$\sum_{A}^{n} \bar{\sigma}_{\text{lamina}} = \bar{\sigma}_{\text{laminate}}$$

For a given stress the resulting total strains can be calculated using Table 4-14, and from the total strains the stress of each layer can be calculated using the stress-strain relations in Table 4-15. From these equations it is possible to calculate the amount of stress in each ply for a given applied stress.

Table 4-14: Average stress - In-plane strain relation of a symmetric laminate in terms of compliance.

	$\bar{\sigma}_1$	$\bar{\sigma}_2$	$\bar{\sigma}_6$
ε_1^o	$a_{11}h$	$a_{12}h$	$a_{16}h$
ε_2^o	$a_{21}h$	$a_{22}h$	$a_{26}h$
ε_6^o	$a_{61}h$	$a_{62}h$	$a_{66}h$

Table 4-15: Off-axis stress-strain relation in terms of stiffness.

	ε_1	ε_2	ε_6
σ_1	A_{11}/h	A_{12}/h	A_{16}/h
σ_2	A_{21}/h	A_{22}/h	A_{26}/h
σ_6	A_{61}/h	A_{62}/h	A_{66}/h

For the veil lined tubes under wall stresses of (0, 100,0), (50,100,0) and (100,0,0) MPa the laminate's theoretical hoop and axial strains and individual ply stresses are given in Table 4-16.

Table 4-16: Theoretical hoop and axial laminate strains and ply stresses for (0,100,0), (50,100,0) and (100,0,0) MPa wall stresses. Veil lined tubes.

	Wall Stress (MPa)		
	(0,100,0)	(50,100,0)	(100,0,0)
$\mu\varepsilon^{o}_{1}$	-4098	1806	11808
$\mu\varepsilon^{o}_{2}$	8759	6710	-4098
	Ply Stress (MPa)		
$\sigma_{veil,1}$	-4.81	15.75	41.11
$\sigma_{veil,2}$	29.13	28.70	-0.88
$\sigma_{mat,1}$	-20.52	27.54	96.14
$\sigma_{mat,2}$	69.46	61.87	-15.19
$\sigma_{F.W.,1}$	27.26	84.28	114.04
$\sigma_{F.W.,2}$	150.46	160.31	19.70

For the PVC lined tubes the theoretical laminate strains and ply stresses for wall stresses of (0, 100,0), (50, 100,0) and (100.0,0) MPa are given in Table 4-17.

Table 4-17: Theoretical hoop and axial laminate strains and ply stresses for(0, 100,0), (50, 100,0) and (100,0,0) MPa wall stresses. PVC lined tubes.

	Wall Stress (MPa)		
	(0, 100,0)	(50, 100,0)	(100, 0,0)
$\mu\varepsilon_1^o$	-6742	2133	17750
$\mu\varepsilon_2^o$	12966	9594	-6742
	Ply Stress (MPa)		
$\sigma_{PVC,1}$	-4.42	16.60	42.02
$\sigma_{PVC,2}$	28.69	29.13	0.89
$\sigma_{veil,1}$	-9.76	20.76	61.06
$\sigma_{veil,2}$	42.25	40.45	-3.59
$\sigma_{mat,1}$	-36.30	35.46	143.54
$\sigma_{mat,2}$	101.65	87.68	-27.93
$\sigma_{F.W.,1}$	31.68	114.75	166.13
$\sigma_{F.W.,2}$	216.57	225.15	17.15

4.5 Theoretical Stress-Strain Response

For a pipe under internal hydrostatic pressure, a pipe wall element may be considered as being subjected to a triaxial stress state. For a thin walled structure when $t/r < 0.10$, the stress state can be assumed to be reduced to a planar or biaxial stress state [61].

The average wall stresses can be calculated as:

$$\sigma_H = \frac{Pr}{t} \qquad (4\text{-}22)$$

and

$$\sigma_A = \frac{Pr}{2t} \qquad (4\text{-}23)$$

where P is the pressure, r is the radius and t is the thickness.

For the veil lined tubes $t/r = 0.105$ and for the PVC lined tubes $t/r = 0.129$. While these values are just slightly higher than the limit, the error in using equations 4-22 and 4-23 is minimal.

For a veil lined tube subjected to an internal pressure P (Psi) the average wall stresses in MPa are:

$$\sigma_H = 0.06552\ P\ (MPa) \qquad (4\text{-}24)$$

$$\sigma_A = 0.03276\ P\ (MPa) \qquad (4\text{-}25)$$

and for a PVC lined tube:

$$\sigma_H = 0.05343\ P\ (MPa) \qquad (4\text{-}26)$$

$$\sigma_A = 0.02672\ P\ (MPa) \qquad (4\text{-}27)$$

For the axial loading the average axial stress is load divided by the area of the tube wall across the thickness. For an applied load L (lbs) the average wall stress in MPa for a veil lined tube is calculated as:

$$\sigma_A = 0.00233\ L\ (MPa) \qquad (4\text{-}28)$$

and for a PVC lined tube:

$$\sigma_A = 0.00194\ L\ (MPa) \qquad (4\text{-}29)$$

From these equations and Table 4-14 the stress-strain graphs of the tubes under the three loading states can calculated. These are shown in Figures 4-2 to 4-7.

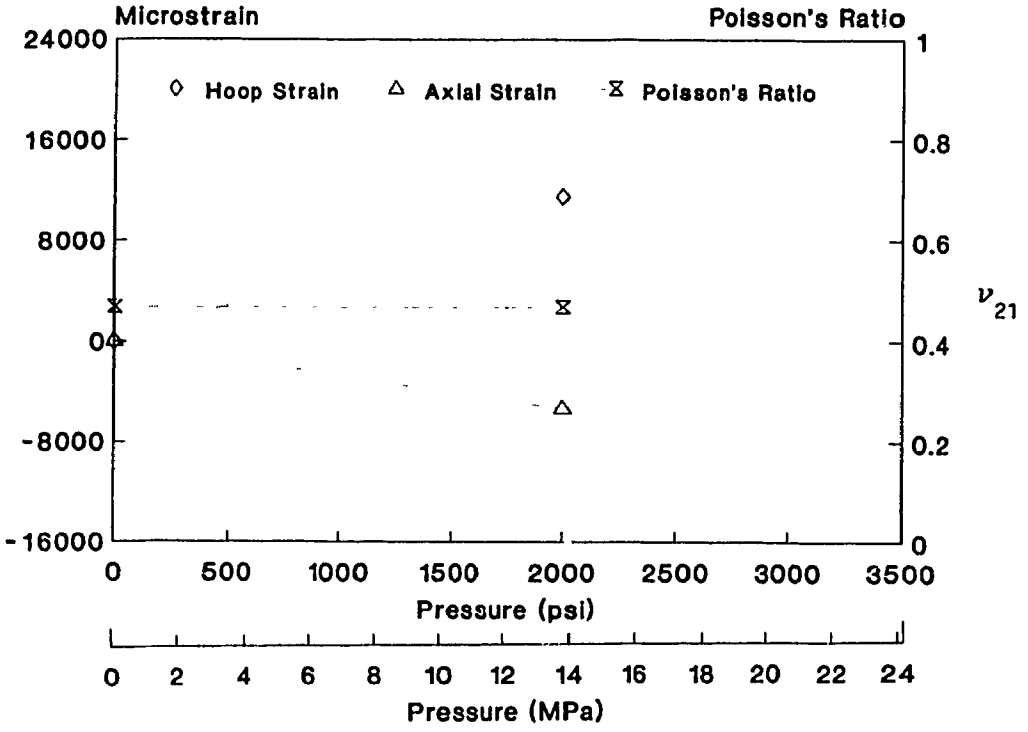

Fig. 4-2: Theoretical stress-strain graph.
Hoop test, veil lined tube.

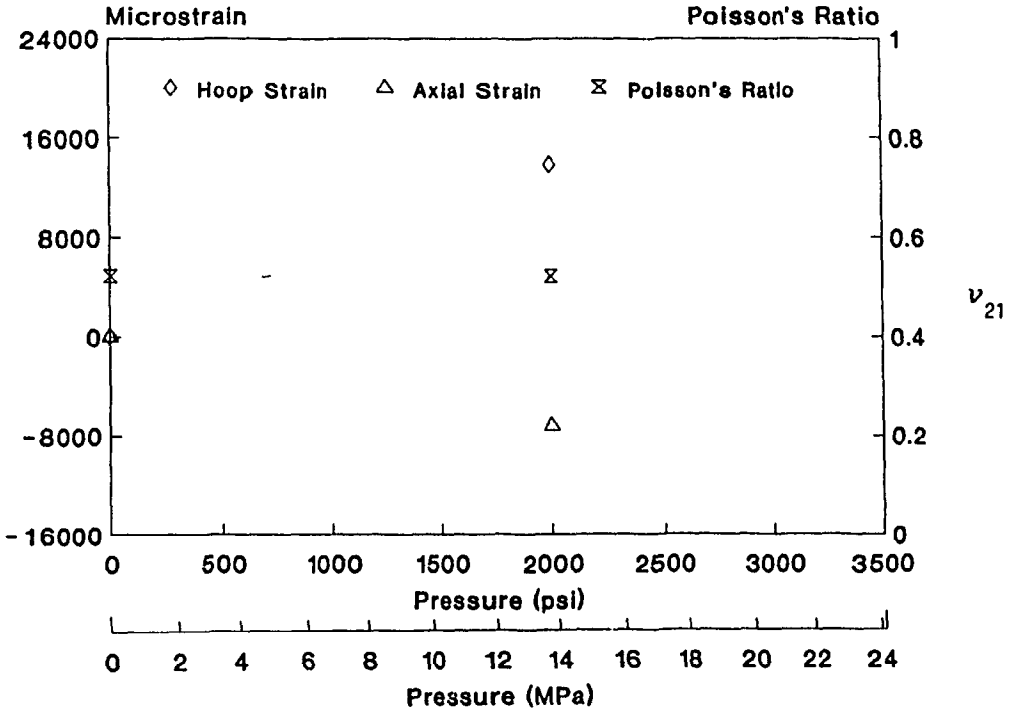

Fig. 4-3 Theoretical stress-strain graph.
Hoop test, PVC lined tube.

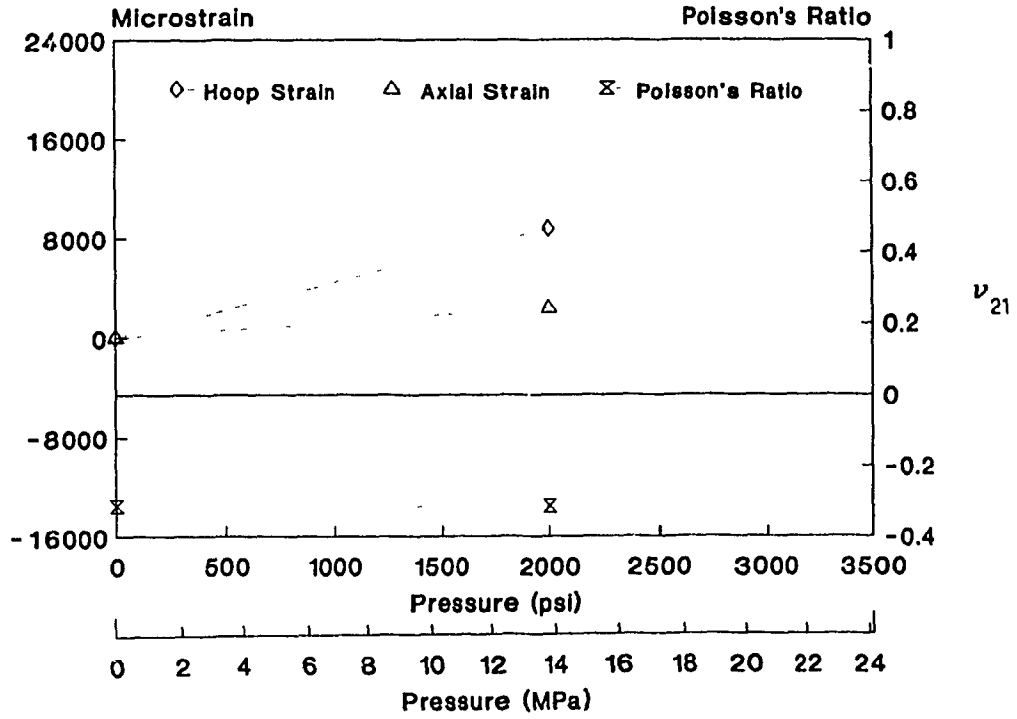

Fig. 4-4 Theoretical stress-strain graph.
Biaxial test, veil lined tube.

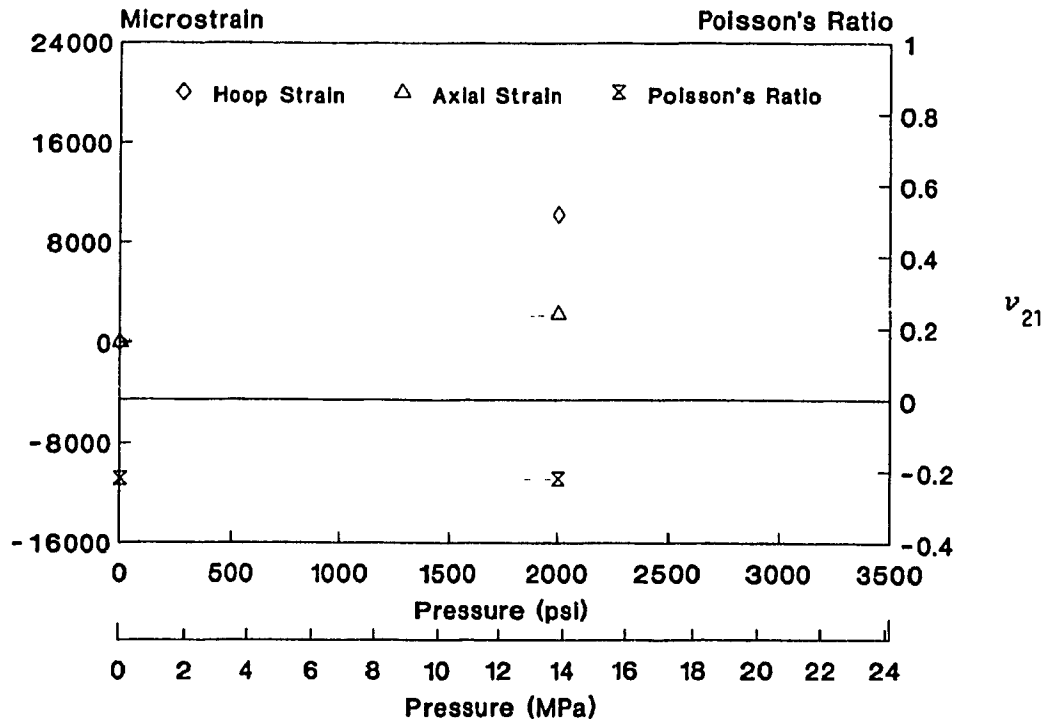

Fig. 4-5 Theoretical stress-strain graph.
Biaxial test, PVC lined tube.

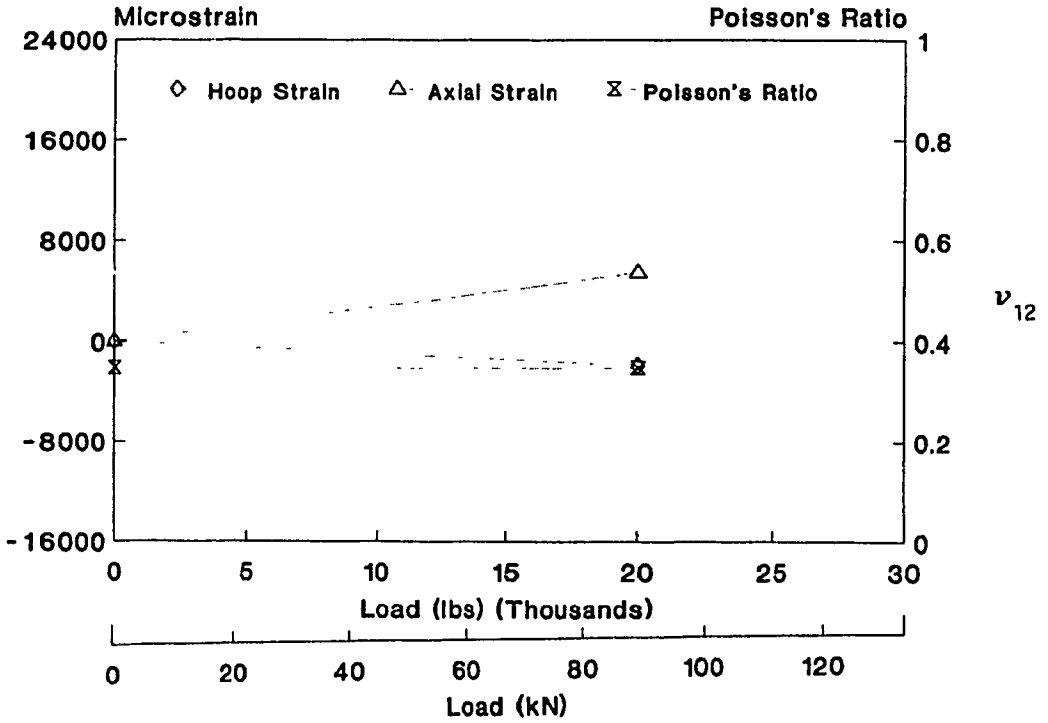

Fig. 4-6 Theoretical stress-strain graph.
Axial test, veil lined tube.

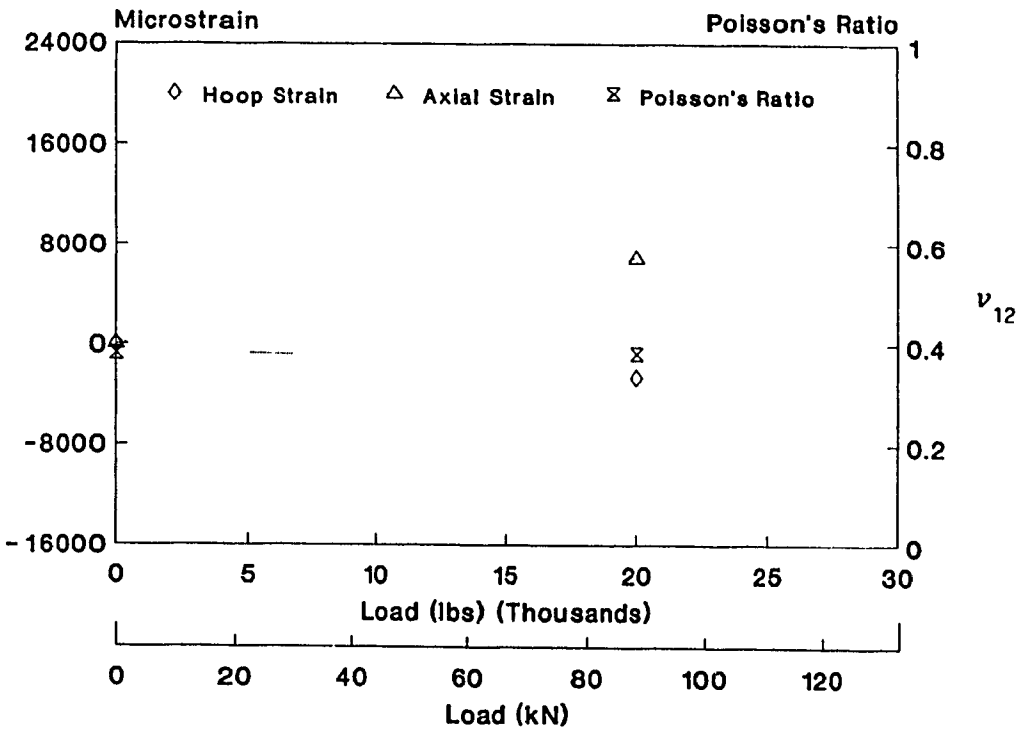

Fig. 4-7 Theoretical stress-strain graph.
Axial test, PVC lined tube.

4.6 Stress Space and Strain Space Failure Envelopes

The strength of a laminate is based upon the strength of the individual plies. As the load is increased there will be a first ply failure (FPF), followed by other ply failures until the last ply fails [62].

One popular approach for failure criteria is the quadratic interaction criterion:

$$F_{ij}\sigma_i\sigma_j + F_i\sigma_i = 1 \qquad (4\text{-}30)$$

This can be expressed in strain components.

$$G_{ij}\varepsilon_i\varepsilon_j + G_i\varepsilon_i = 1 \qquad (4\text{-}31)$$

where F's and G's are strength parameters. Failure occurs when either equation is met.

Equation 4-30 can be expanded for the case of two-dimensional stress (i, j = 1,2,6).

$$\begin{aligned} &F_{11}\sigma_1^2 + 2F_{12}\sigma_1\sigma_2 + F_{22}\sigma_2^2 + F_{66}\sigma_6^2 \\ &\quad + 2F_{16}\sigma_1\sigma_6 + 2F_{26}\sigma_2\sigma_6 \\ &\quad + F_1\sigma_1 + F_2\sigma_2 + F_6\sigma_6 = 1 \end{aligned} \qquad (4\text{-}32)$$

The strength of a uniaxial composite in its orthotropic axis should be unaffected by the direction of the shear stress component. Thus, all linear and first degree shear stress terms in Equation 4-32 may be deleted. With the removal of these terms Equation 4-32 may be simplified to.

$$\begin{aligned} &F_{xx}\sigma_x^2 + 2F_{xy}\sigma_x\sigma_y + F_{yy}\sigma_y^2 + F_{ss}\sigma_s^2 \\ &\quad + F_x\sigma_x + F_y\sigma_y = 1 \end{aligned} \qquad (4\text{-}33)$$

where i, j = x, y, s.

There are four quadratic strength parameters analogous to the four independent components of modulus. There are two linear strength parameters as a result of the difference in tensile and compressive strengths. Of the six strength parameters, F_{xx}, F_x, F_{yy}, F_y, and F_{ss} can be measured in simple tests. The sixth term, F_{xy}, is related to the interaction between the two normal stress components. It is assumed that the sixth term is a generalization of the von Mises criterion and equal to - 0.5.

If the typical strength of a unidirectional composite is known, the strength parameters in stress space may be calculated using the following equations:

$$\begin{aligned} F_{xx} &= \frac{1}{X\,X'}, \\ F_x &= \frac{1}{X} - \frac{1}{X'}, \\ F_{yy} &= \frac{1}{Y\,Y'}, \\ F_y &= \frac{1}{Y} - \frac{1}{Y'}, \\ F_s &= \frac{1}{S^2} \end{aligned} \qquad (4\text{-}34)$$

Typical strengths of unidirectional layers of the materials used in the test specimen construction are shown in Table 4-18 [60].

Equation 4-31 can be derived from equation 4-30 by substituting the stress components with strain components:

$$F_{ij}\,Q_{ik}\,Q_{if}\,\varepsilon_k\,\varepsilon_f + F_i\,Q_{ij}\,\varepsilon_j = 1 \qquad (4\text{-}35)$$

Table 4-18 : Longitudinal tensile (X), longitudinal compressive (X'), transverse tensile (Y), transverse compressive (Y'), and shear (S) strengths of unidirectional plies [60].

	MAT	FILAMENT WINDING	VEIL	PVC
X (MPa)	133	820	75	53
X'(MPa)	133	610	75	53
Y (MPa)	133	75	75	53
Y'(MPa)	133	133	75	53
S (MPa)	62.5	34.5	37.5	26.5

We can define

$$G_{kf} = F_{ij}\, Q_{ik}\, Q_{if}$$
$$G_{j} = F_{i}\, Q_{ij} \qquad (4\text{-}36)$$

So that the failure criterion in strain space is

$$G_{kj}\, \varepsilon_k\, \varepsilon_j + G_k\, \varepsilon_k = 1 \qquad (4\text{-}37)$$

Expanding and invoking symmetry results in

$$G_{xx}\, \varepsilon_x^2 + 2G_{yy}\, \varepsilon_x\, \varepsilon_y + G_{yy}\, \varepsilon_y^2 + G_{ss}\, \varepsilon_s^2 + G_x\, \varepsilon_x + G_y\, \varepsilon_y = 1 \qquad (4\text{-}38)$$

where

$$
\begin{aligned}
G_{xx} &= F_{xx} Q_{xx}^2 + 2F_{xy} Q_{xx} Q_{yy} + F_{yy} Q_{xy}^2 \\
G_{yy} &= F_{xx} Q_{xy}^2 + 2F_{xy} Q_{xy} Q_{yy} + F_{yy} Q_{yy}^2 \\
G_{xy} &= F_{xx} Q_{xx} Q_{xy} + F_{xy}[Q_{xx} Q_{yy} + Q_{xy}^2] + F_{yy} Q_{xy} Q_{yy} \qquad (4\text{-}39) \\
G_{ss} &= F_{ss} Q_{ss}^2 \\
G_{x} &= F_{x} Q_{xx} + F_{y} Q_{xy} \\
G_{y} &= F_{x} Q_{xy} + F_{y} Q_{yy}
\end{aligned}
$$

Transformation of the strength parameters in strain space is straight forward. The linear parameters transform like stress components; the quadratic parameters transform like the stiffness components. Transformation of linear strength parameters in strain space in power function is given in Table 4-19.

Table 4-19: Transformation of linear parameters in strain space in power functions.

	G_x	G_y
G_1	m^2	n^2
G_2	n^2	m^2
G_6	mn	$-mn$

$m = \cos \phi$
$n = \sin \phi$

ϕ = angle of rotation in degrees

The transformation of the quadratic strength parameters in strain space in multiple angle functions is given in Table 4-20.

Table 4-20: Transformation of quadratic strength parameters in stress space in multiple angle function.

	1	U_2	U_3
G_{11}	U_1	$\cos 2\phi$	$\cos 4\phi$
G_{22}	U_1	$-\cos 2\phi$	$\cos 4\phi$
G_{12}	U_4		$-\cos 4\phi$
G_{66}	U_5		$-\cos 4\phi$
G_{16}		$0.5 \sin 2\phi$	$\sin 4\phi$
G_{26}		$0.5 \sin 2\phi$	$-\sin 4\phi$

where the U's are defined as

$$
\begin{aligned}
U_1 &= 0.125 \left[3G_{xx} + 3G_{yy} + 2G_{xy} + 4G_{ss} \right] \\
U_2 &= 0.5 \left[G_{xx} - G_{yy} \right] \\
U_3 &= 0.125 \left[G_{xx} + G_{yy} - 2G_{xy} - 4G_{ss} \right] \\
U_4 &= 0.125 \left[G_{xx} + G_{yy} + 6G_{xy} - 4G_{ss} \right] \\
U_5 &= 0.125 \left[G_{xx} + G_{yy} - 2G_{xy} + 4G_{ss} \right]
\end{aligned}
\qquad (4\text{-}40)
$$

Equations 4-33 and 4-38 only give a go-or-no-go indication of failure. The information given by the failure criterion can be increased by using a different variable, strength ratio R:

$$
\sigma_{i(a)} = R\,\sigma_i \qquad \varepsilon_i^* = \varepsilon_{i(a)} = R\,\varepsilon_i \qquad (4\text{-}41)
$$

where stress or strain components without remarks are those applied or imposed; and subscript (a) or asterisk means the allowed or the ultimate stress or strain. Features of this ratio are

- When applied stress or strain is zero, R = infinity.
- When the stress or strain is safe, R > 1.
- When the allowable stress or strain is reached, R = 1.
- R cannot be less than unity which has no physical reality.

Modifying equations 4-30 and 4-31 by introducing the strength ratios yields,

$$[F_{ij}\sigma_i\sigma_j]R^2 + [F_i\sigma_i]R = 1$$
$$[G_{ij}\varepsilon_i\varepsilon_j]R^2 + [G_i\varepsilon_i]R = 1 \qquad (4\text{-}42)$$

these have the form

$$aR^2 + bR - 1 = 0 \qquad (4\text{-}43)$$

Thus it is possible to solve for the stress ratio. There are two conjugate roots, R and R', corresponding to the applied stress strain vector going in opposite directions.

The in-plane strength of laminates is found by finding the strength ratio for each layer subjected to a given state of load resultants. The layer with the lowest strength ratio will fail first. The relation between in-plane strain and the applied stress resultant is

$$\varepsilon_i^o = a_{ij} N_j \qquad (4\text{-}44)$$

Substituting this into Equation 4-42 for a layer with ϕ orientation:

$$[G_{ij}^{(\phi)} \varepsilon_i^o \varepsilon_j^o] R_{(\phi)}^2 + [G_i^{(\phi)} \varepsilon_i^o] R_{(\phi)} = 1 \qquad (4\text{-}45)$$

$$[G_{ij}^{(\phi)} a_{ik} a_{jf} N_k N_f] R_{(\phi)}^2 + [G_i^{(\phi)} a_{ij} N_j] R_{(\phi)} = 1 \qquad (4\text{-}46)$$

$$[H_{ij}^{(\phi)} N_k N_f] R_{(\phi)}^2 + [H_i^{(\phi)} N_j] R_{(\phi)} = 1 \qquad (4\text{-}47)$$

where

$$H_{ij}^{(\phi)} = G_{ij}^{(\phi)} a_{ik} a_{jf}, \qquad H_i^{(\phi)} = G_i^{(\phi)} a_{ij} \qquad (4\text{-}48)$$

The in-plane strength of a multi-directional laminate will have multiple strength ratios; one set (R and R') for each ply orientation. Two factors control the ply failures in the laminate. First, the in-plane compliance **a**. This is a function of the ply volume fractions and is non-linear. The second factor is the specific ply orientation. The H functions in Equation 4-48 are vector products of the the transformed strength parameters G's of the ply and the in-plane compliance of the laminate.

4.7. Calculation of Failure Envelopes in Stress and Strain Space.

Due to the large number of calculations required to produce the failure envelopes in stress and strain space a computer program was written to perform all the required calculations. It is presented in Appendix 1.

4.8 Failure Envelopes and Theoretical Loading Vectors in Stress Space

Calculation of the failure envelopes in stress space is accomplished with Equation 4-47. By normalizing the stress resultant, for each applied unit stress the strength ratios are equal to the ultimate strength. Each layer of the tubes has its own envelope. As the angle of the layer is changed, the failure envelope of the layer will change position. The straight lines on the graphs are the loading paths used in the tests. The loading paths are constant and independent of ply ratios.

4.8.1 PVC Lined Tubes

The failure envelopes of the plies of a PVC lined tube and the stress vectors applied during testing are shown in Fig. 4-8. The graph shows that FPF occurs with the filament winding layer for all loadings. The tube will be its strongest under biaxial loading but the optimum loading is with a slightly higher N_1/h. A more exact ratio is 1.1:2. Under biaxial loading the next layer to fail would be PVC followed closely by the veil layer. Under hoop or axial loading the veil layer is the second layer to fail followed by the PVC layer.

One question raised by this failure envelope is why does the filament winding layer fail first? The answer can be found by transforming the off-axis stress to on-axis stress. The on-axis filament winding stress for the wall stresses of (0,50,0), (25,50,0) and (50,0,0) MPa are given in Table 4-21.

Table 4-21: On-axis filament winding stresses for tube wall stresses of (0,50,0), (25,50.0) and (50,0,0) MPa. PVC lined tube.

	Wall Stress (MPa)		
	(0,50,0)	(25,50,0)	(50,0,0)
$\sigma_{F.W.,x}$	77.87	94.41	33.08
$\sigma_{F.W.,y}$	46.25	75.53	58.55
$\sigma_{F.W.,s}$	43.43	25.93	-34.99

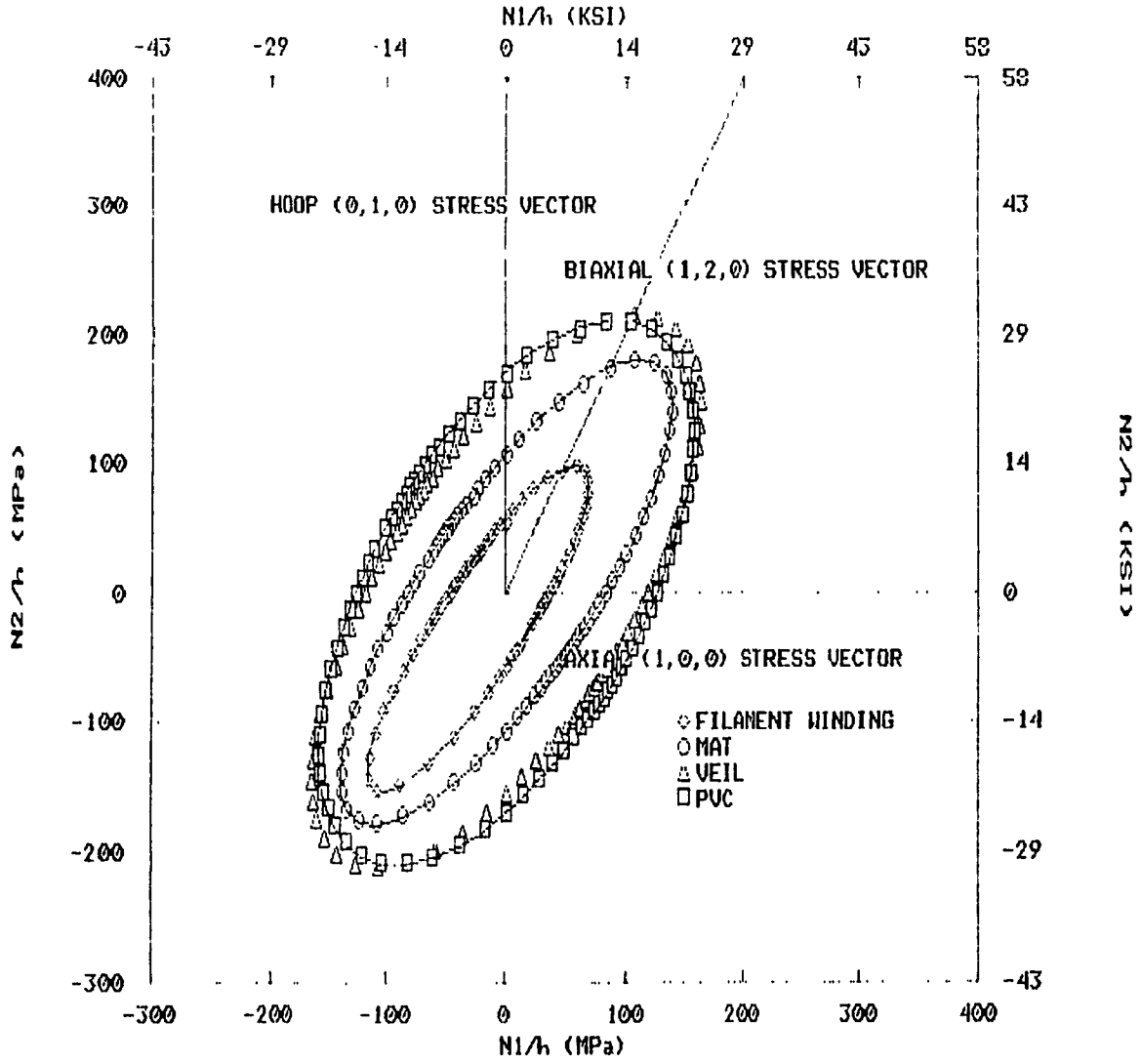

Fig. 4-8: Failure envelopes and stress vectors in stress space. PVC lined tube.

The values in Table 4-21 are for a positive angle of rotation. For a negative rotation, the values are the same except the shear stress changes sign.

Comparing these results to those in Table 4-18 it can be seen that the shear strength is exceeded under the hoop and axial stress conditions and the transverse tensile strength is exceeded under the biaxial loading. The hoop and biaxial stress states are for an internal pressure of 6.44 MPa and the axial stress state is for a load of 114.65 kN.

4.8.2 Veil Lined Tubes

The failure envelopes of the plies of the veil tubes and the stress vectors applied during testing are shown in Fig. 4-9. The graph shows that FPF occurs with the filament winding layer for all loadings. Again the tube is strongest under biaxial loading, but the optimum loading is with a slightly higher N_1/h. A more exact ratio is 1.1:2. The next layer to fail is the mat layer and the final layer to fail is the veil layer.

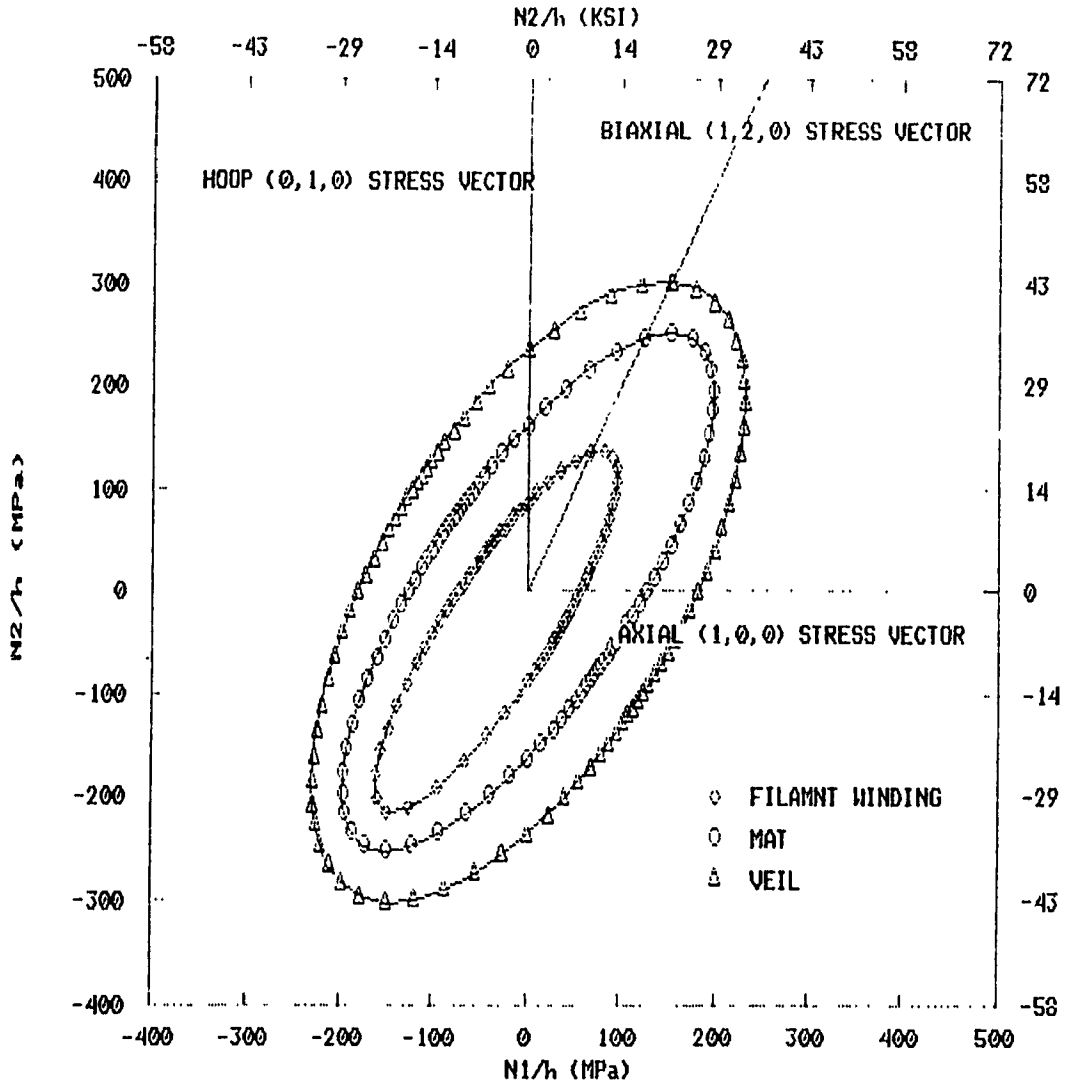

Fig. 4-9: Failure envelopes and stress vectors in stress space. Veil lined tube.

Again, the question raised by this failure envelope is why does the filament winding layer fail first? The answer can be found by transforming the off-axis stress to on-axis stress. The on-axis filament winding stresses for the wall stresses of (0,75,0), (37.5,75,0) and (80,0,0) MPa are given in Table 4-22.

Table 4-22: On-axis filament winding stresses for tube wall stresses of (0,75,0), (37.5,75,0) and (80,0,0) MPa. Veil lined tube.

	Wall Stress (MPa)		
	(0,75,0)	(37.5,75,0)	(80,0,0)
$\sigma_{F.W.,x}$	82.44	101.46	40.58
$\sigma_{F.W.,y}$	50.84	81.98	66.40
$\sigma_{F.W.,s}$	43.41	26.75	-35.85

The values in Table 4-22 are for a positive rotation. For a negative rotation, the values are the same except the shear stress changes sign. Again, comparing these results to those in Table 4-18, it can be seen that the transverse tensile strength is exceeded under biaxial loading, and under hoop and axial loading the shear strength is exceeded.

4.9 Failure Envelopes in Strain Space

Calculation of the failure envelopes in strain space is accomplished with Equation 4-44. One feature of failure envelopes in strain space is that they remain fixed for each ply orientation. Now when the lay up is changed, the loading path will change position in strain space. The loading paths in strain space have slopes with a run of one and a rise equal to the apparent Poisson's ratio of the lay-up for that particular loading.

4.9.1 PVC lined tube

The failure envelopes and theoretical loading paths for a PVC lined tube are shown in Figure 4-10. The predictions of the order of ply failure shown in the stress space graphs for a PVC lined tube are repeated in this graph.

4.9.2 Veil lined tube

Figure 4-11 shows the failure envelopes and theoretical loading paths in strain space for a veil lined tube. This figure also matches the order of ply failure predicted in the stress space graph for a veil lined tube.

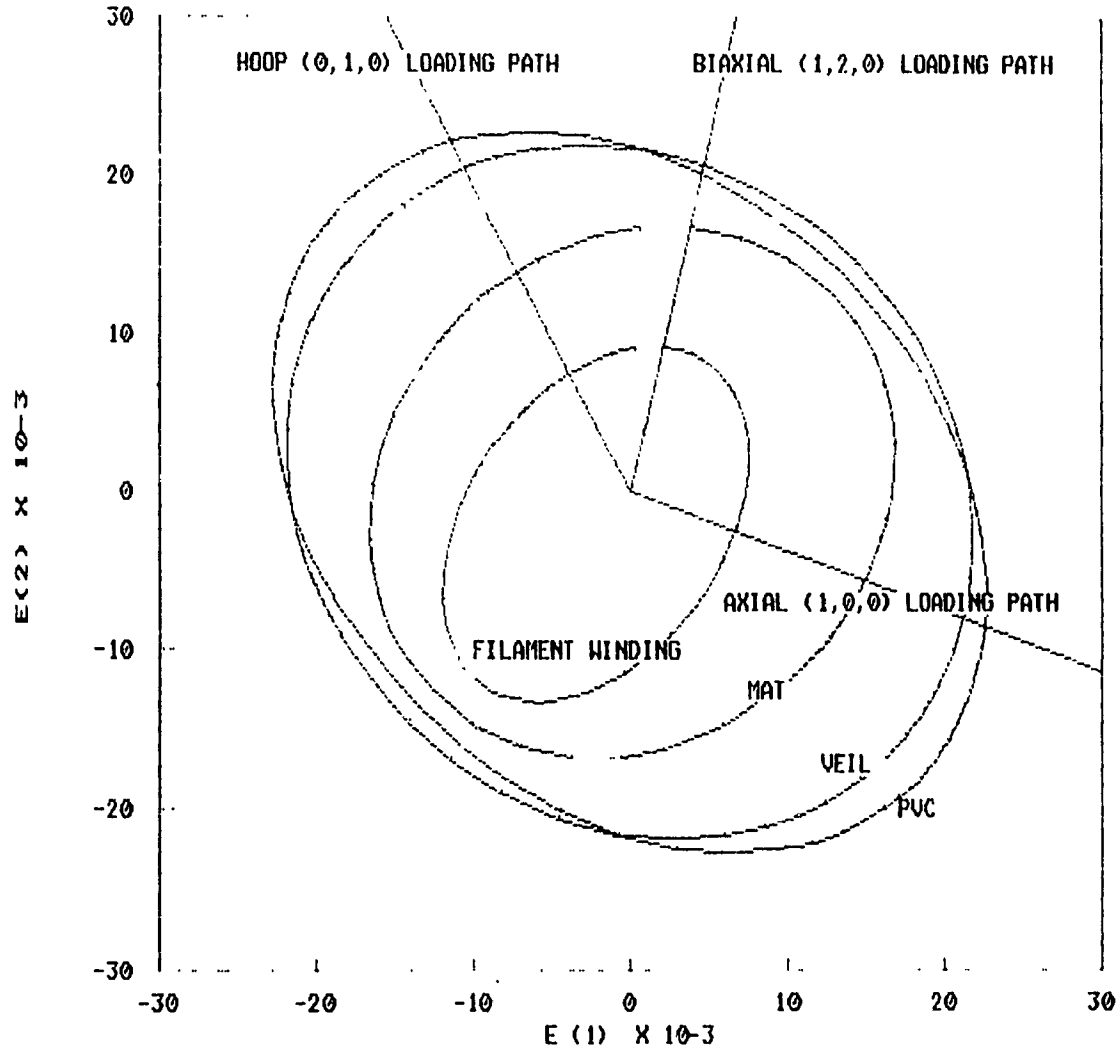

Fig. 4-10: Failure envelopes and loading paths in strain space. PVC lined tube.

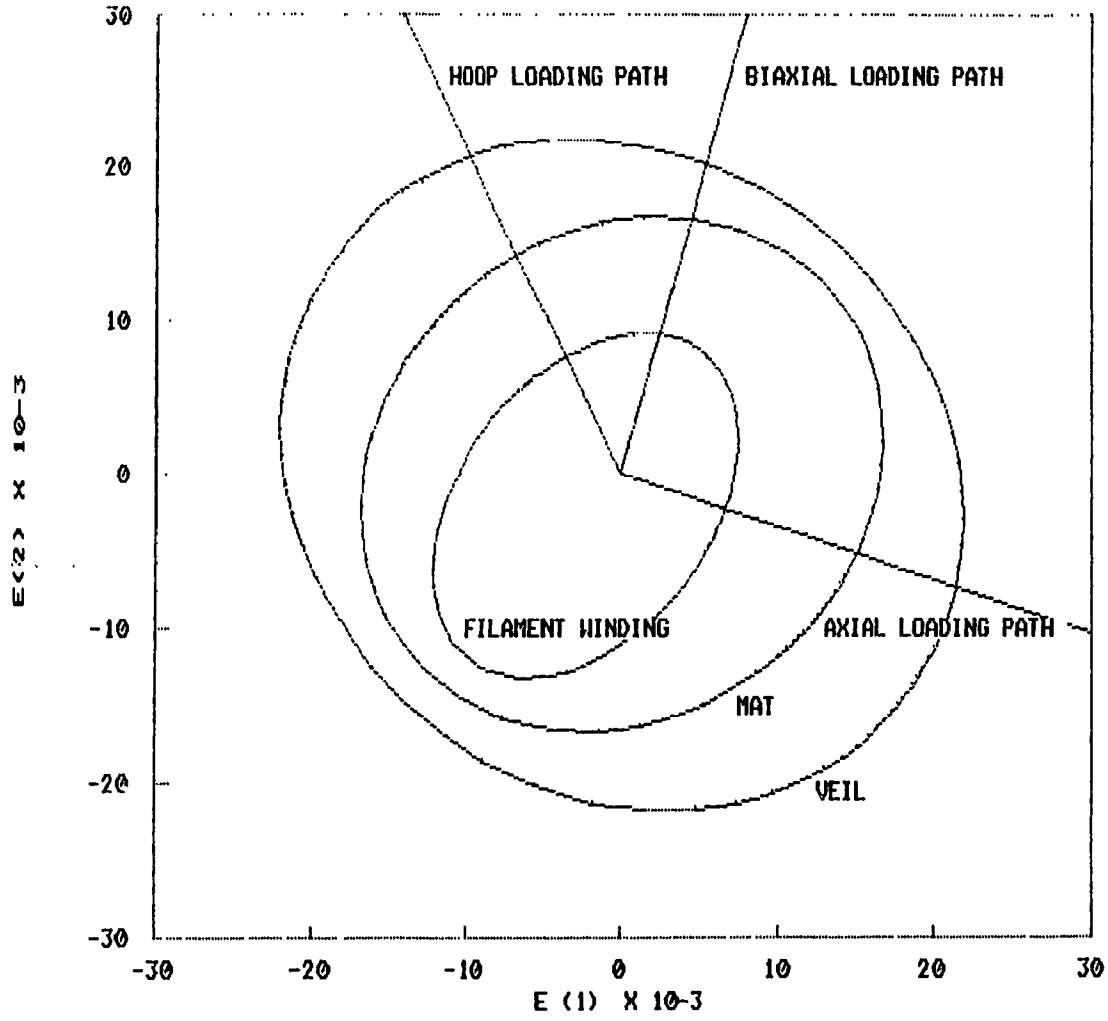

Fig. 4-11: Failure envelopes and loading paths in strain space. Veil lined tube.

4.10 Limitations of Laminate Analysis

While the quadratic interaction criterion is simple and quick to use, it does have some serious drawbacks. One drawback is that it does not explain the way the lay-up fails. Laminate theory, which uses the strength of a unidirectional fiber reinforced lamina as the criteria for failure, may predict a failure load that greatly underestimates the final rupture strength of a filament wound tube. For a $\pm 55^{\circ}$ filament wound tube under biaxial loading this underestimation may be as great as a factor of 10 [28].

CHAPTER 5. Experimental Exposure Results: Appearance Changes

As mentioned before, a given class of chemical solution can produce a characteristic appearance change in a laminate. This chapter presents the changes seen in the tubes' appearance after exposure to the project's environments.

5.1. Initial Colour and Appearance

After construction and preparation for aging, all the tubes of each liner group had the same general appearance.

Fig. 5-1 shows the initial appearance of a veil lined tube. Externally, the veil lined tubes were beige with the filament winding pattern clearly visible, due in part to incomplete wetting of the fibers (jackstrawing). These tubes were translucent, and when viewed from the interior outward the only discernible feature was numerous, tiny air bubbles trapped in the matrix. The inner surface varied from a smooth, circular, uniform layer of resin to a rough, non circular surface with areas of exposed, though wetted, veil.

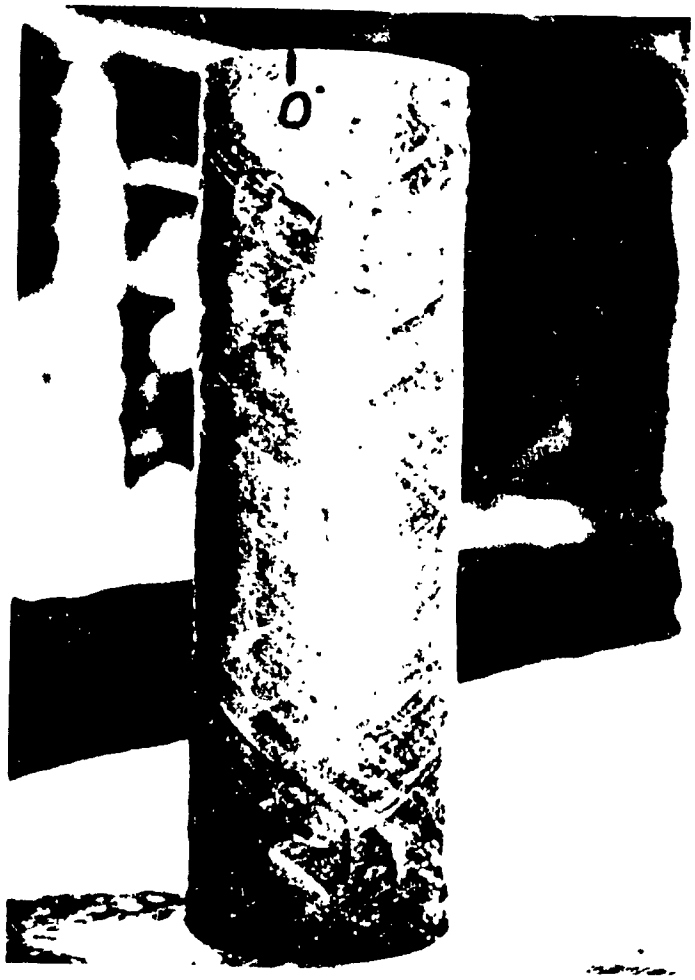

Fig. 5-1: The initial appearance of a veil lined tube.

When viewed across the wall thickness there are two concentric colour zones. The darker, inner one is the veil and chopped strand mat layers. The lighter, outer zone is the filament winding layer and individual layers of the filament winding are discernible to the naked eye. The thickness of these layers varied slightly. A cross section view of tube 4C-1A, shown in Fig. 5-1, is shown in Fig. 5-2.

Fig. 5-2: Photomicrograph: a cross section view of the wall of tube 4C-1A, shown in Fig. 5-1.

The initial appearance of the PVC lined tubes was similar to that of the veil lined tubes. Fig. 5-3 shows tube 30D-1B, a PVC lined tube that was sacrificed to help develop the hoop test.

Due to incomplete wetting of the fibers, the filament winding pattern is clearly visible. The colour is a slightly darker beige than the veil lined tubes. The tube is opaque and the inside of tube was a smooth, uniform grey surface with a constant diameter.

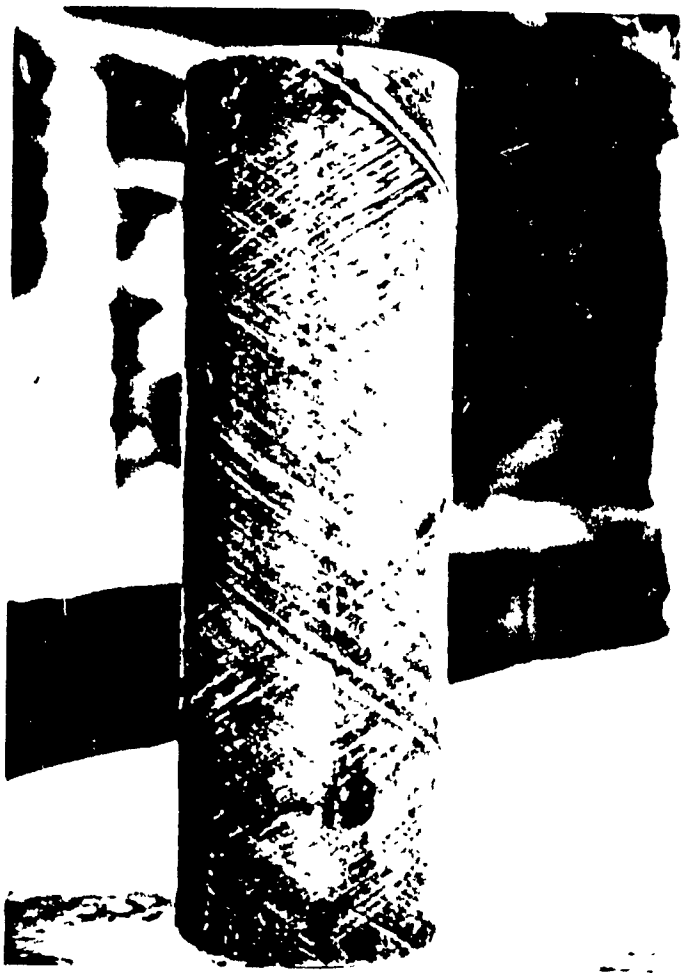

Fig. 5-3: The initial appearance of a PVC lined tube.

A cross sectional view of tube 30D-1A is shown in Fig. 5-4. Three distinct layers can be seen. The PVC liner is the uniform grey band. Above it is the veil and mat layer. This figure also demonstrates the unevenness of these layers. The thickness of the veil and mat layers

varied from roughly 0.25 mm to over 1.0 mm. The outer zone, lighter in tone from the intermediate zone, is the filament winding layer where the individual filament layers are visible. Also apparent is the variation in the thickness of the filament winding layer

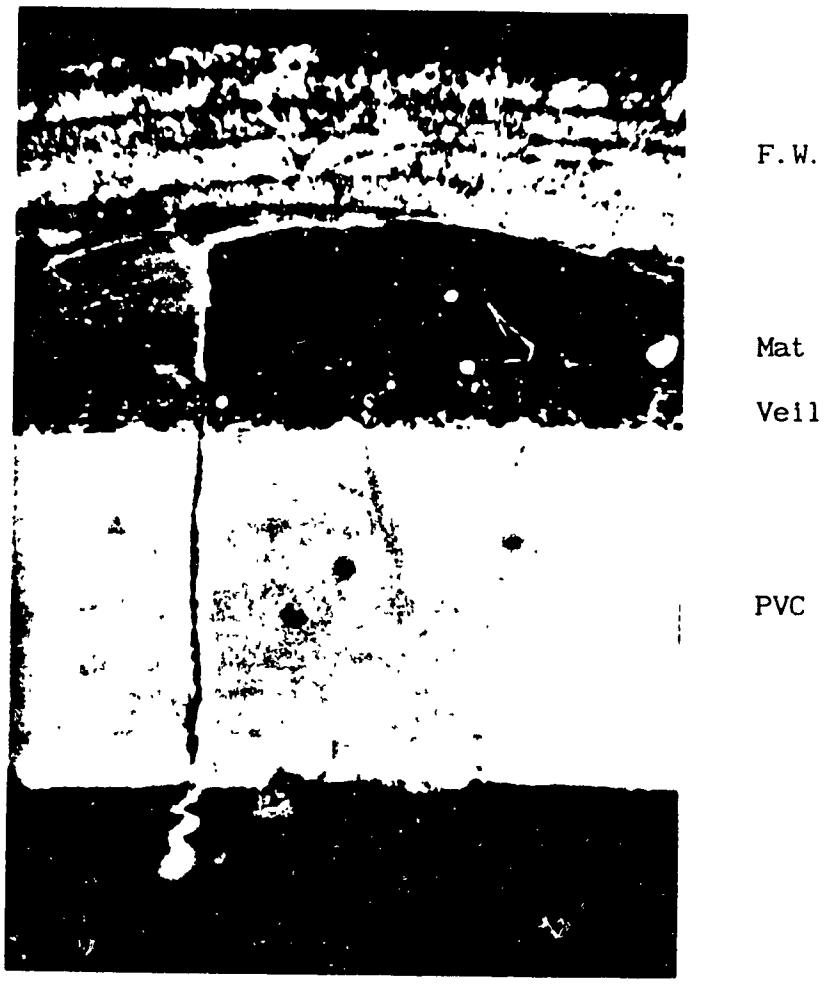

Fig. 5-4: Photomicrograph: a cross section view of the wall of tube 30D-1A, a PVC lined tube.

5.2 Changes in Appearance

5.2.1 Exposure to Room Temperature Air

There was no visible change in appearance with tubes exposed to room temperature air.

5.2.2 Exposure to Room Temperature Water

There was no visible change in appearance with tubes exposed to room temperature water.

5.2.3 Exposure to 80°C Water

When specimens were being pulled after six months of exposure for the first test point, there were obvious changes in both the veil lined and PVC lined tubes' appearance.

Fig. 5-5 shows the appearance of a veil lined tube after 7 months of exposure to 80°C water. The resin colour of the veil lined tubes changed to a reddish-yellow. This colour change was uniform along the length of the tube. The tube became less translucent and when looking at the inner surface, the randomly oriented glass fibers of the mat layer were discernible. The colour change of the resin was uniform across the wall thickness.

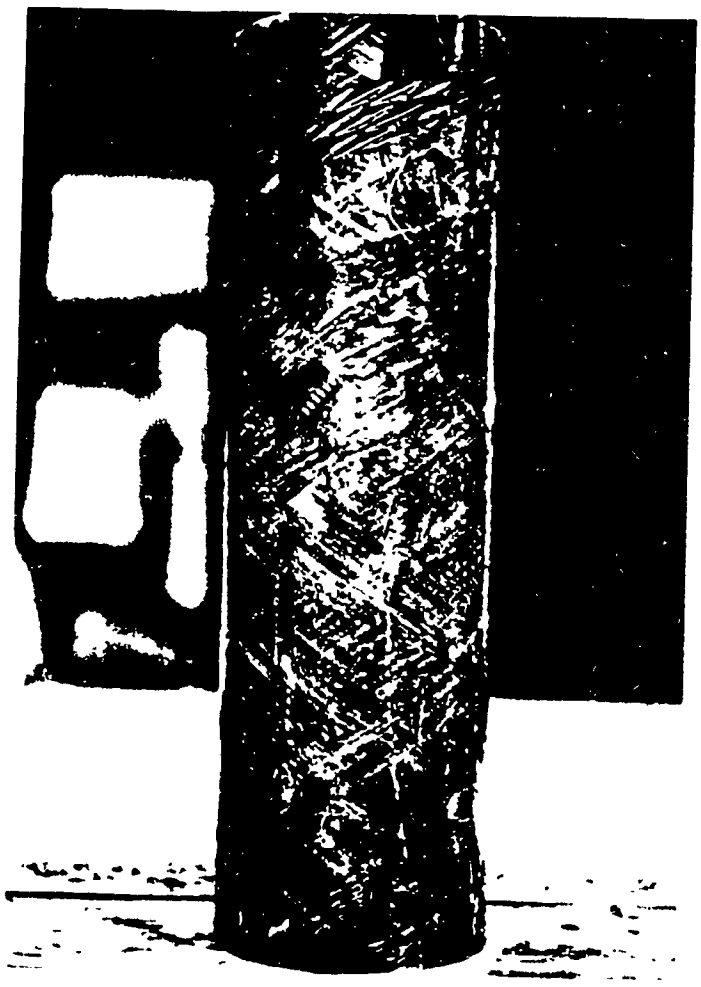

Fig. 5-5: The appearance of a veil lined tube after 7 months exposure to hot water.

The PVC lined tubes were similarly affected. After 7 months of exposure to hot water, the resin changed colour to a brownish yellow as shown in Fig. 5-6. The exposed surface of the PVC changed from uniform grey to a uniform light beige and the remaining thickness of PVC changed to purple. Looking across the thickness from the exposed inner wall surface and looking radially outwards, the colour change is seen as a gradual change from off-white to purple. There is no

distinct boundary between the colours as shown in Figure 5-7, a cross section of tube 22D-1A.

Fig. 5-6: The appearance of a PVC lined tube after 7 months exposure to hot water.

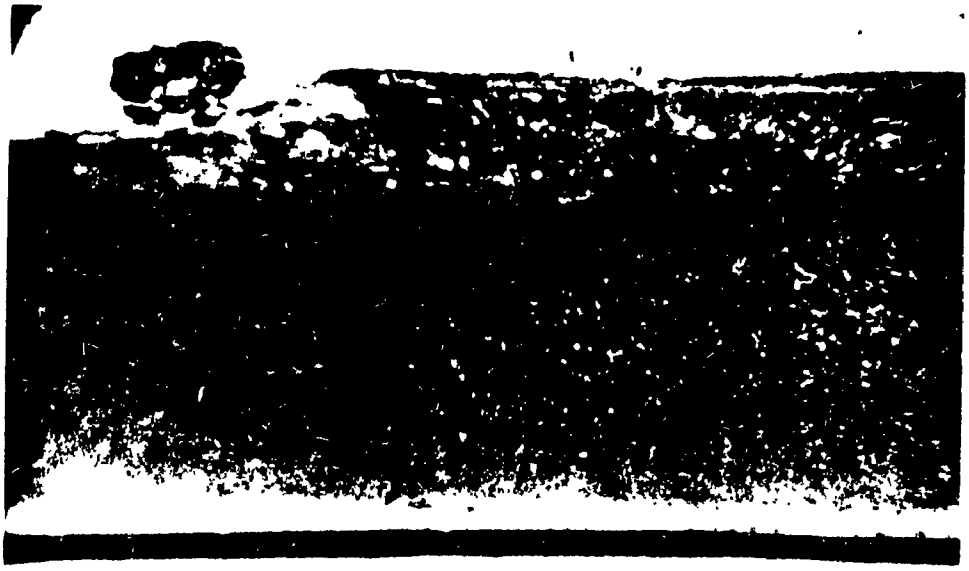

Fig. 5-7: Photomicrograph: The colour change across the thickness of a PVC liner after exposure to 80°C water for 7 months.

Swelling of the PVC was indicated by a slight decrease of the inner diameter. The area of PVC liner covered by the PVC end cap showed neither the color change nor swelling. However, the surface of the cap exposed to the hot water showed the same colour change characteristics. This indicated that this effect was due to the presence of water at elevated temperatures.

The colour changes due to exposure to hot water occurred with an exposure of less the 6 months and once they occurred they were stable after removal from the environment.

5.2.4 Exposure to Room Temperature Sulfuric Acid (98%)

Sulfuric acid was found to aggressively attack the resin. Veil lined tubes filled with sulfuric acid had their inner wall eaten away, exposing the veil and mat layers. Due to the severity of the damage this environment/liner combination was deleted from the remainder of the project.

The PVC lined tubes showed no effects from exposure to sulfuric acid as long as the acid did not come in contact with the resin. When sulfuric acid came in contact with a resin surface, the resin would change colour to an orange-red in a matter of hours. The PVC liner retained its original appearance throughout the exposure period.

5.2.5 Exposure to Room Temperature Hydrochloric Acid (35%)

Exposure to room temperature HCl on the veil lined tubes caused the resin to acquire a green colour. An example of this is shown in Fig. 5-8. This colour change was uniform along the length of the tube, and was apparent when the first tubes were pulled after six months of exposure. The inner wall of the tube also took on a purple tint that grew in intensity as the exposure time was increased, being almost non-existent at six months to obvious at three years of exposure. When examined across the wall thickness, the purple tint extended slightly into the corrosion liner forming a thin band. The tube appeared almost opaque and the glass fibers of the mat layer became easily visible.

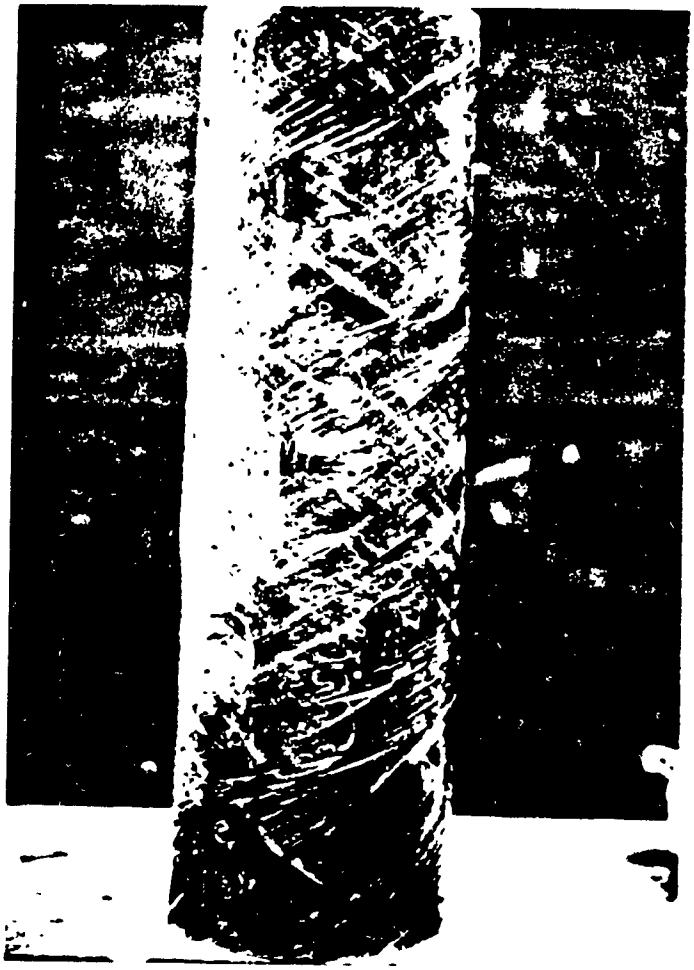

Fig. 5-8 : The appearance of a veil lined tube exposed to room temperature HCl.

The effect of exposure to room temperature HCl on the external appearance of the PVC lined specimens was negligible. The colour of the resin darkened slightly, as shown in Fig. 5-9, after 32 months of exposure. At first the PVC layer seemed unaffected, but as exposure time was increased the exposed surface of the PVC took on a purple tint.

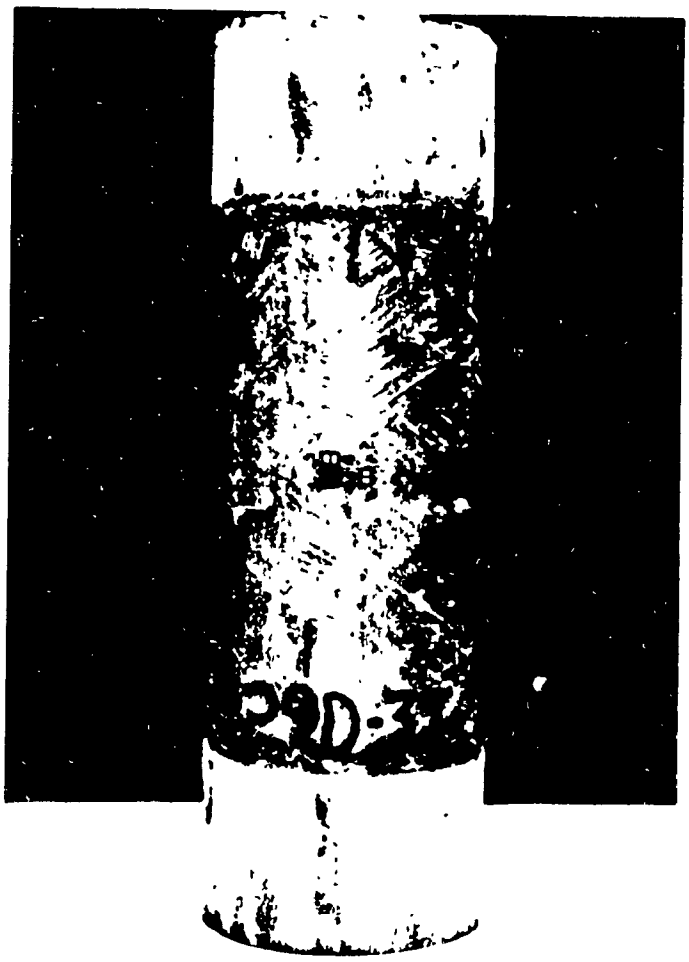

Fig. 5-9: External appearance of a PVC lined tube after 32 months exposure to room temperature HCl.

5.2.6 Exposure to 50°C (122°F) Hydrochloric Acid (35%)

The most dramatic and varied changes in the tubes were observed with those specimens exposed to Hydrochloric acid at 50°C. The first effects were seen when specimens were being pulled for test point one.

The resin color of the veil lined tubes changed to a uniform olive-green, as shown in Fig. 5-10. The veil lined tubes became more

Fig. 5-10: The change in colour to olive-green of a veil lined tube exposed for 6 Months to hot HCl.

opaque and the glass strands of the mat layer became visible. They appeared as randomly oriented silver lines. The inner wall became a translucent brown as shown in Fig. 5-11.

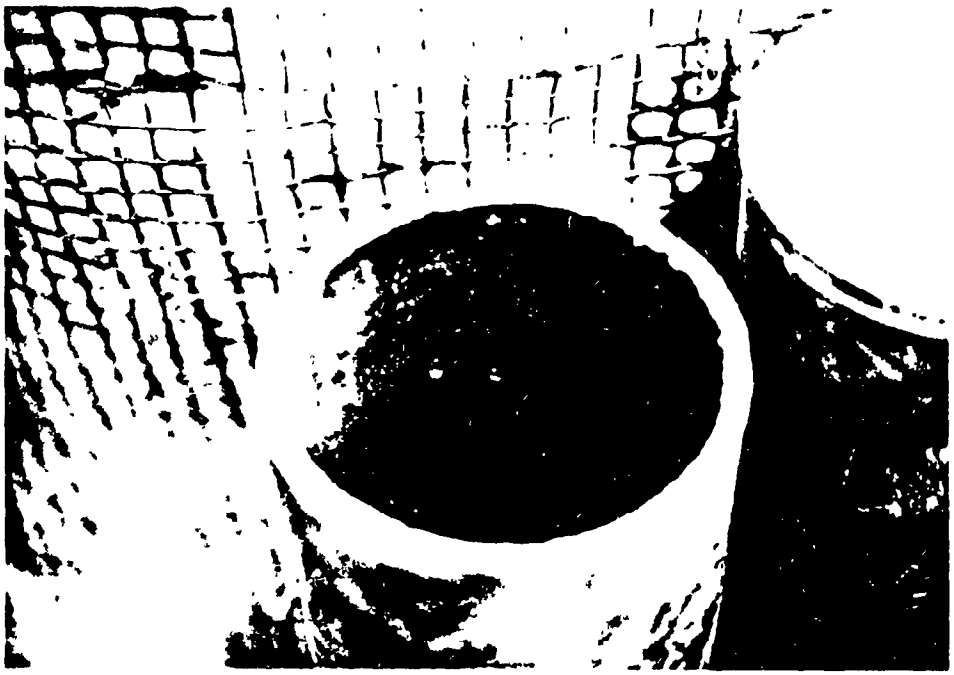

Fig. 5-11: Change in inner wall colour of a veil lined tube to a translucent brown.

When viewed across the wall thickness, the zone of filament winding appeared to be a green band, while the zone of the veil and mat layers were brown. There also appeared to be an area between the two zones where the colour changed gradually from one to another.

The PVC lined tubes showed several effects after exposure to hot HCl. After 6 months of exposure, the exposed surface of the PVC changed colour from grey to purple. When viewed across the wall thickness, it appeared that the PVC layer was composed of two different materials. Even when viewed under a microscope, the boundary between the two colours was quite distinct. Fig. 5-12 shows a cross section of tube 23C-1A which clearly shows this effect. Externally, the appearance of the tube had not change at this time.

Fig. 5-12: Photomicrograph: A cross section view of the PVC liner of tube 23C-1A showing change of PVC's colour from grey to purple and the sharp boundary between the two.

As exposure time to hot HCl increased, more of the PVC changed colour to purple in a fairly smooth radial pattern. By test point three, the colour of the resin of the tubes had started to change to green. When tubes 23E and 24A were pulled for testing after 17 months of aging, there were dark patterns along the length of the tubes that repeated at regular intervals. This mottle is shown in Fig. 5-13.

Fig. 5-13: Mottle found along the lengths of tubes 23E and 24B. 17 months exposure to hot HCl.

The cause of this mottling effect was the colour change of the PVC, from grey to purple, reaching the outer surface of the PVC tube. This is shown in Figs. 5-14 and 5-15. Light being reflected back through the resin was being reflected from two different coloured surfaces, a grey one and a purple one.

Fig. 5-14: Colour change of PVC liner, edge view. Tube 23E-1E.

Fig. 5-15: Colour change of PVC liner, exterior view. Tube 23E-1E.

5.3 Absorption of HCl at 50°C

Of all the environments used in this project, only those tubes subjected to hot HCl showed signs of having absorbed significant amounts of liquid.

At test point 1, it was observed that even after draining and flushing, both the PVC and veil lined tubes had a very strong odor of HCl. These fumes were strong enough to discolour photographs that some PVC lined tubes were left standing under.

At test point three, tube 10E (veil lined) was allowed to stand for several days after being drained and flushed, after which time yellowish-green beads were observed on the inner tube wall. Some of these beads can be seen in Fig. 5-11. Testing with Alkacid® test paper showed the drop to be have a very low pH, indicating a very strong acid. After several more hours a small puddle, estimated to be about 0.5 ml, was found under the tube. This droplet formation was observed with other similarly aged tubes and evidence of fuming was also observed.

After being cut to size for testing, Tube 23D developed several yellowish-green droplets on the cut edge. The smaller drops appeared to be forming over the veil/mat layer. The largest drop had an estimated volume of 1 to 2 ml and covered the thickness of the tube wall. This is shown in Fig. 5-16. Testing with alkacid test paper showed the liquid to have a very low pH.

Fig. 5-16: Beads of HCl on the cut edge of tube 23D-1C.

5.4 Blister Formation on Tubes Exposed to 50°C HCl

Another effect of the hot HCl environment upon both the veil lined and PVC lined tubes was the development of blisters on the inner wall.

Tube 9E-1C was found to have developed a blister about the size of a thumbnail in area and about 1 mm high. Exposure time was 13 months. This blister is seen at the 9 O'Clock position on the tube in Fig. 5-17.

Fig. 5-17: Blister that developed on inner wall of tube 9E-1C after exposure to hot HCl for 13 months.

Tube 23A-1C was found to have developed a large blister, shown in Figs. 5-18 and 5-19. The blister was oval shaped with its major length along the longitudinal axis of the tube. The blister measured 45 by 15 mm and was approximately 6 mm tall at its highest point. When opened the blister was dry, the cavity is shown in Fig. 5-20. The PVC had separated at about half its thickness and the thickness of the blister was uniform. Blisters were also observed on tube 24D.

Fig. 5-18: Blistering of PVC liner, tube 23A-1C.

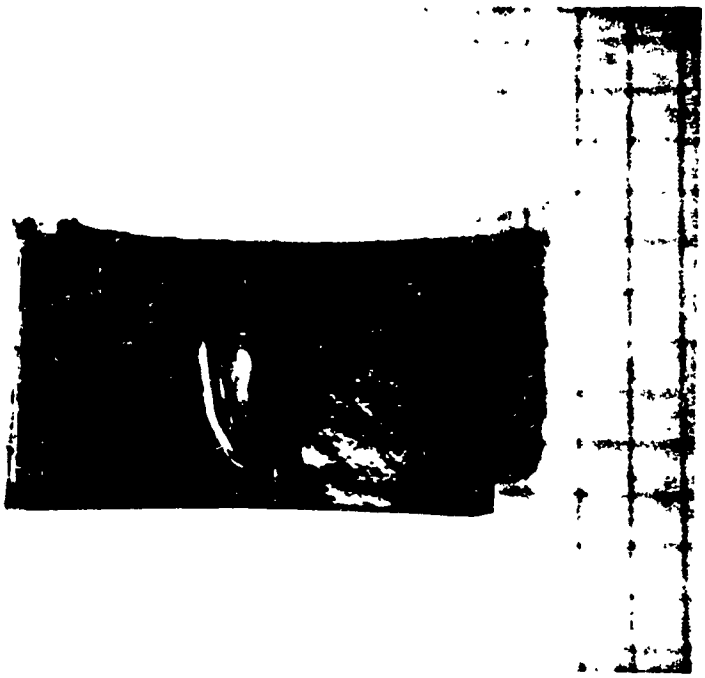

Figure 5-19: Top view of blister, tube 23A-1C.

Fig. 5-20: Dry cavity of blister, tube 23A-1C.

CHAPTER 6. Residual Strengths after Exposure to Environments

Along with the obvious physical changes, the performance of the tubes under stress can also be affected by exposure to the environments of this project. Indications include changes in stress-strain response, changes in failure pressure or load, and changes in failure pattern that can be associated with a given environmental exposure. This chapter presents the stress-strain response, the failure pressure or load, and the failure patterns observed.

6.1 Experimental Result Table Description

The Tables that present the experimental results for this project are composed of "cells". Each cell represents a particular liner/environment combination. When a test was scheduled but not carried out, the first line of the cell will be dashes and all other lines blank. A cell with a tube number on the first line and dashes on the second line represent tubes that were pulled and tested, but the test was deemed a failure.

A cell for a successful test has a tube number on the first line, and the exposure time in months on the second line. On the third line, the failure pressure, from the hoop and biaxial test, or the failure load, from the axial test, is presented. On the fourth line, in brackets, is the failure pressure in MPa or failure load in kN. When strain gages were used, the axial and hoop microstrain at failure is presented on

lines five and six respectively. The information that may be presented in a cell is summarized in Fig. 6-1.

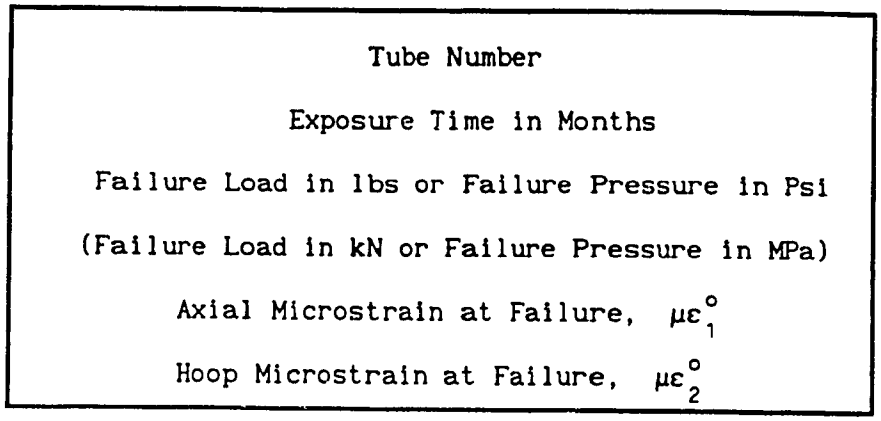

Fig. 6-1: The information that may be contained in a cell of the result Tables.

6.2 Hoop Test Results

6.2.1 Readings at Failure

Tables 6-1 to 6-6 show the readings recorded at failure for both the veil lined and PVC lined tubes under hoop stress for test points 1 to 6.

Due to the way data was collected in the early stages of the project, some of the strain values are linear extrapolations from the last two readings taken prior to failure. These are marked with an †. When tested under hoop stress, the veil lined tubes had two failure patterns and the PVC lined tubes had three failure patterns. These

will be discussed in section 6.2.2. For the veil lined tubes type I failure is indicated by the tube number alone on line one of the cell, a * after the tube number indicates type II failure. For the PVC lined tubes a "crack and spray" failure is indicated by the tube number standing alone on line one of the cell, a ‡ after the tube number indicates an explosive failure. A * after a PVC lined tube's number also indicates a type II failure.

Table 6-1: Hoop test readings at failure, test point 1

		WATER		HCl (35%)		H_2SO_4
	AIR	20°C	80°C	20°C	50°C	(98%)
VEIL	4C-1A 9 2100 (14.48)	2B-1A 11 1600 (11.03)	5C-1A 7 920 (6.34)	6B-1A 12 1450 (9.99)	10A-1A• 6 1000 (6.90)	
	4C-1B 9 2000 (13.79)	2B-1B 12 1620 (11.17) -6050 10270	5E-1B• 8 820 (5.65) -2350 5595†	6B-1B 12 1460 (10.07)	10B-1B• 6 1200 (8.27) -2950 5225	
PVC	30D-1A 10 1680 (11.58)	32D-1A 10 2000 (13.79)	22D-1A 7 1980 (13.65)	27E-1A 12 1850 (12.76)	23C-1A 6 1500 (10.34)	25C-1A 12 2800 (19.30) -9320† 20396†
	30E-1B 14 1750 (12.07) --- 13222	32D-1B 10 1920 (13.23) -6710† 13190	22D-1B 7 1790 (12.34) -7917† 13073†	27E-1B 12 2190 (15.10)	23B-1B 6 1980 (13.65) -8860† 16981†	25C-1B 12 2540 (17.51) -11858† 18547†

Refer to Fig. 6-1 for a description of cell information.
† extrapolated
• type II failure

Table 6-2: Hoop test readings at failure, test point 2.

		WATER		HCl (35%)		H_2SO_4
	AIR	20°C	80°C	20°C	50°C	(98%)
VEIL	11E-1C 17 1800 (12.41) -7088 11341	1A-1C 17 1830 (12.62) -6094 7930	5D-1C* 13 830 (5.72) -2205 4862	6C-1C ---	9E-1C* 13 680 (4.69) -1934 3121	
	14C-1D 17 1820 (12.55)	1A-1D 17 1670 (11.51)	5D-1D* 13 750 (5.17)	6C-1D ---	9D-1D* 13 660 (4.55)	
PVC		31B-1C 17 2070 (14.27) -10611 16183	21D-1C 13 1380 (9.52) -5283 11407	28B-1C 18 2000 (13.79) -9900 17891	23A-1C ---	26A-1C 15 2520 (17.38) -12021 16541†
		31B-1D 17 1910 (13.17)	21D-1D 13 1300 (8.96)	28B-1D 18 1590 (10.96)	23A-1D‡ 13 2960 (20.41)	26A-1D 15 2510 (17.31)

Refer to Fig. 6-1 for a description of cell information.
‡ explosive failure
* type II failure

Table 6-3: Hoop test readings at failure, test point 3.

		WATER		HCl (35%)		H_2SO_4
	AIR	20°C	80°C	20°C	50°C	(98%)
VEIL	14D-1E 23 2010 (13.86) -6799 12236	1C-1E* 21 1530 (10.55) -5294 8083	5D-1E* 17 610 (4.21) -1681 3968	8A-1E 19 2190 (15.10) -9555 13679	10D-1E* 17 1000 (6.90) -3367 6020	
	14D-1F 23 1860 (12.82)	1C-1F 21 1700 (11.72)	16B-1F ---	6E-1F 19 2010 (13.86)	10D-1F* 17 1000 (6.90)	
PVC		31B-1E 21 1840 (12.69) -10154 14829	21A-1E 17 1370 (9.45) -5367 9156	28D-1E‡ 19 2280 (15.72) -11187 13433	23E-1E‡ 17 2160 (14.89) -11439 15546	26C-1E‡ 19 3410 (23.51) -15187 ---
		31D-1F 21 1930 (13.31)	20C-1F* 17 1210 (8.34)	28D-1F‡ 19 1910 (13.17)	23E-1F 17 1550 (10.69)	26C-1F 19 2300 (15.86)

Refer to Fig. 6-1 for a description of cell information.
* type II failure
‡ explosive failure

Table 6-4: Hoop test readings at failure, test point 4.

		WATER		HCl (35%)		H_2SO_4
	AIR	20°C	80°C	20°C	50°C	(98%)
VEIL	15A-1G 27 1790 (12.34) -6931 10807	1E-1G 26 1930 (13.31) -5743 8347	5A-1G* 23 830 (5.72) -2121 4524	8B-1G 25 1690 (11.65) -7534 13182	11A-1G* 23 750 (5.17)	
	15A-1H 27 1760 (12.13)	1E-1H 26 1380 (9.52)	16E-1H 17 980 (13.65)	8B-1H 25 1710 (11.79)	11A-1H* 23 680 (4.69)	
PVC		32B-1G‡ 26 2030 (14.00) -10205 17549	21E-1G 17 1020 (7.03) -2797 6051	29A-1G 25 2520 (17.37) -11434 19686	24B-1G 23 1570 (10.83) -5165 10156	26E-1G 25 2110 (14.55) -7558 14307
		32B-1H 26 1730 (11.93)	21B-1H 21 1320 (9.10)	29A-1H 25 2560 (17.65)	24B-1H 23 1490 (10.27)	26E-1H 25 2180 (15.03)

Refer to Fig. 6-1 for a description of cell information.
* type II failure
‡ explosive failure

Table 6-5: Hoop test readings at failure, test point 5.

		WATER		HCl (35%)		H_2SO_4
	AIR	20°C	80°C	20°C	50°C	(98%)
VEIL	15D-1I 34 1780 (12.27) -6447 11449	2D-1I 33 1600 (11.03) -6443 8866	7A-1I 29 840 (5.79) -2194 4369	8D-1I 32 1710 (11.79) -11837 13869	11D-1I 30 880 (6.07) -3770 9017	
	15D-1J 34 1660 (11.44)	2E-1J 33 1600 (11.03)	7A-1J 29 930 (6.41)	8E-1J 32 1680 (11.58)	11D-1J ---	
PVC		33C-1I* 33 1810 (12.48) -7483 10447	22B-1I 29 1790 (12.34) -7462 13101	29C-1I 32 2130 (14.68) -8625 14609	24D-1I* 30 640 (4.41) -1559 3042	27B-1I 32 1760 (12.14) -6068 8808
		33C-1J 33 1640 (11.31)	22B-1J 29 1790 (12.34)	29C-1J 32 1360 (9.38)	24D-1J ---	27B-1J‡ 32 2460 (16.96)

Refer to Fig. 6-1 for a description of cell information.
* type II failure
‡ explosive failure

Table 6-6: Hoop test readings at failure, test point 6.

		WATER		HCl (35%)		H_2SO_4
	AIR	20°C	80°C	20°C	50°C	(98%)
VEIL	15E-1K 41 1700 (11.72) -6829 11790	3A-1K* 38 1650 (11.38) -5232 8271	16D-1K 34 1090 (7.52) -2950 4923	9B-1K 38 1440 (9.93) -4463 7903	10C-1K* 36 650 (4.48) -1897 4247	
	15E-1L 41 1610 (11.10)	3A-1L 38 1440 (9.93)	16D-1L 34 1180 (8.14)	9A-1L 38 1510 (10.41)	10C-1L ---	
PVC		34C-1K 38 1800 (12.41) -7578 11975	20E-1K 34 1590 (10.96) -5803 9560	29E-1K 38 2280 (15.72) -10938 19372	25A-1K‡ 36 3160 (21.79) -16728 ---	27D-1K 38 1980 (13.65) -5566 ---
		34C-1L 38 1970 (13.58)	20E-1L 34 1370 (9.45)	29E-1L‡ 38 3050 (21.03)	25A-1L‡ 36 3150 (21.72)	27D-1L 38 1770 (12.20)

Refer to Fig. 6-1 for a description of cell information.
* type II failure
‡ explosive failure

6.2.2 Hoop Test Failure Patterns

Reviewing the video of the tubes' tests revealed that the veil lined tubes had two failure patterns, and the PVC lined tubes had three failure patterns.

In the case of the veil lined tubes, the first visible sign of distress in all the tests was the development of a small, thin line oriented along the the length of the tube that would grow into an axially elongated patch of whitening. The length and position of this patch in the test section, the length of tube between the O-rings of the test fixture, would vary from tube to tube.

When the development of this patch was instantaneous, a tick sound might be heard. Generally, its length would be half the tube's length or longer. Those that appeared gradually had no detectable noise associated with them. Some would seem to start at a point and grow up and down along the tube's length, others would fade in. As the pressure continued to increase the patch would continue to grow along the axial direction and other axial patches would appear around the tube. The area of whitening around the older patches would spread outwards (in the hoop direction).

There were two distinct patterns by which fluid would escape from the tube.

Type I failure was failure by weepage, and occurred when pressure was lost due to the test fluid leaking through the tube's wall and escaping as a spray.

With type I failure, a zone of delamination could be seen to develop in the filament winding layer over a section of the axial whitening patch as the applied pressure was increased. This delamination zone would spread silently and unevenly, becoming lighter in colour as it approached the tube's exterior. The delamination would stay centered over the axial patch and spread no more than a few centimeters either side. Weepage was in the form of a fan of spray along the filament winding direction from the edge of the whitest area of delamination. Figures. 6-2 to 6-4 show the appearance of various tubes after failure by weepage.

Visual inspection of the inside of the tube revealed that there was an axial crack in the veil layer, above which there was an irregular whitening in which the strands of the chopped strand mat were visible. The axial crack was clean, and longer than the area of whitening. Inspection of the exterior seemed to show that delamination of the plies of the filament winding layer had taken place.

To further investigate the damage to a veil lined tube after failure by weepage, a section of tube 4C-1A was cut out. Figures 6-5 and 6-6 show the same crack in the liner at the two edges of the cut out section at a magnification of 99.225 X

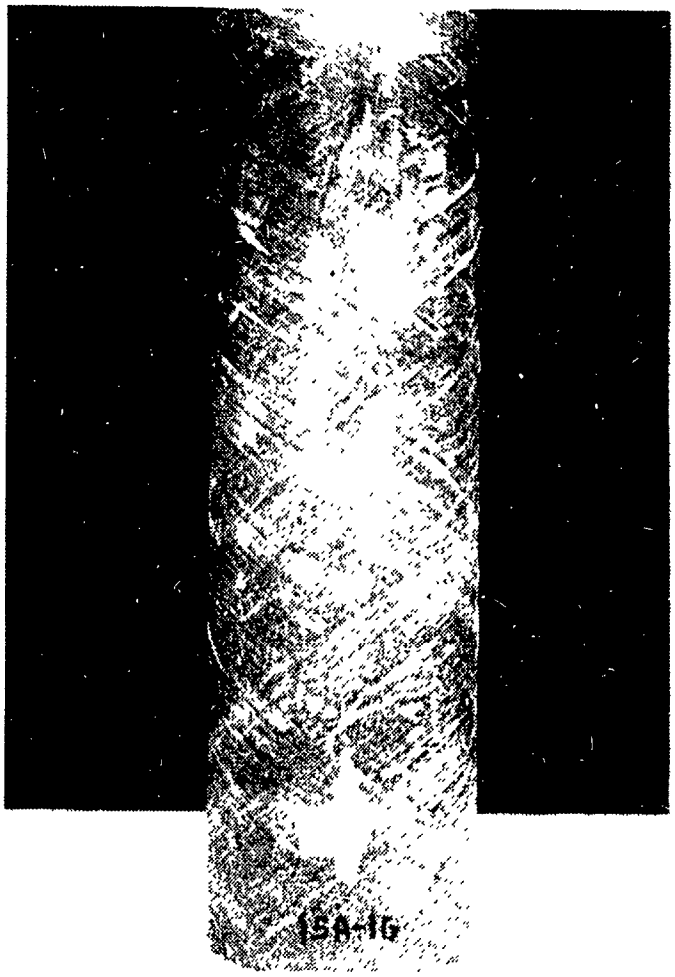

Fig. 6-2: Appearance of veil lined tube 15A-1G (air, test point 5) after failure by weepage.

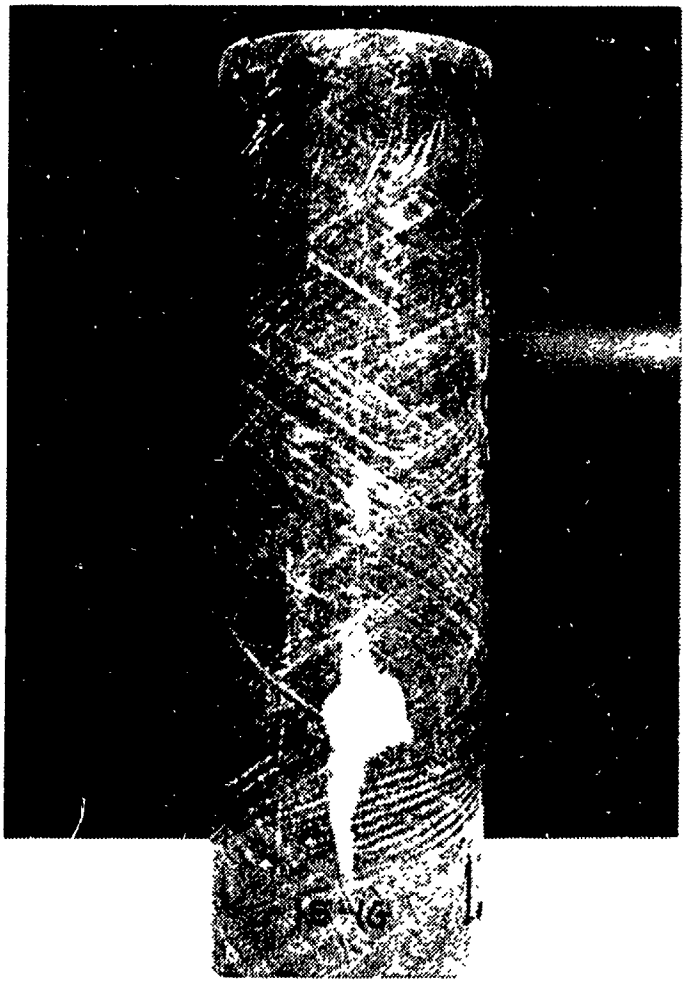

Fig. 6-3: Appearance of veil lined tube 1E-1G (water, test point 5) after failure by weepage.

Fig. 6-4: Appearance of veil lined tube 6E-1B (HCl, test point 1) after failure by weepage.

Backlighted, cracks appear as dark lines. In both Figs. 6-5 and 6-6 there is a clean crack in the veil layer that is perpendicular to the inner wall. In Fig. 6-5 this crack meanders slightly as it passes through the mat layer. At the filament winding layer, the direction of the crack changes to follow the filament winding layers around the tube. This change in direction marks the point that the crack becomes an interlaminar crack.

In Fig. 6-6, after passing through the veil layer the crack branches out into the mat layer where it stops. Above this, there are two interlaminar cracks, separated by a layer of filament winding, that are joined by a transverse crack. Together, Figures 6-5 and 6-6 demonstrate the way different cracks can combine to form a path for the fluid to take through the tube wall.

Type II failure, indicated by a * after the tube number, occurred when pressure was lost due to a crack in the veil layer allowing fluid past the O-ring. Type II failure was associated with half of the hot water and two-thirds of the hot HCl exposed tubes. Examples of the tube's appearance after failure are shown in Figs. 6-7 and 6-8. The arrows on the tube in Fig. 6-7 point to the lines of whitening. While it is obvious that type II failure can be considered as a failed test since weepage through the tube wall did not occur, it still represents a change in tube behavior that can be associated with a particular environment.

Fig. 6-5: Photomicrograph: View across the wall thickness of tube 4C-1A at the failure site. Side A.

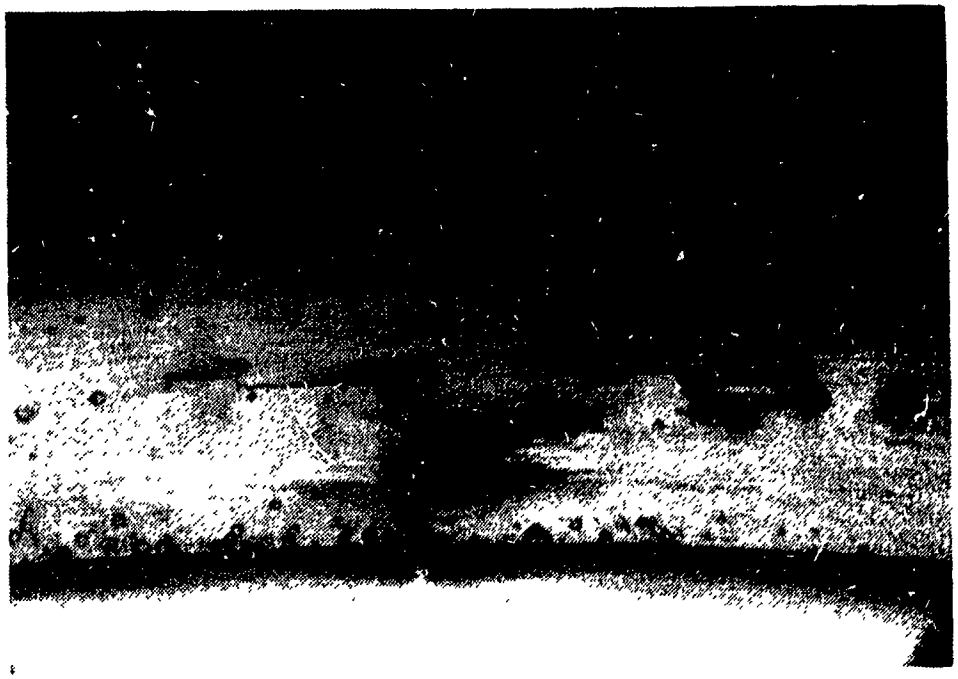

Fig. 6-6 Photomicrograph: View across the wall thickness of tube 4C-1A at the failure site. Side B.

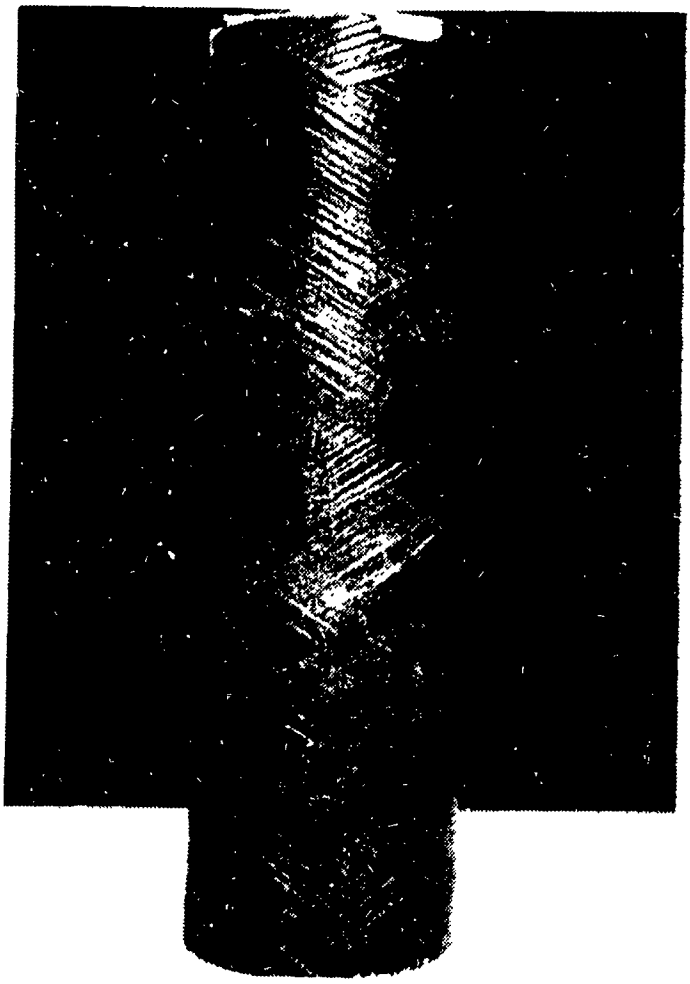

Fig. 6-7: Appearance of a tube exposed to hot HCl that failed due to fluid leaking past O-ring. Arrows point to lines of whitening.

Fig. 6-8: Appearance of a tube exposed to hot water that failed due to fluid leaking past O-ring.

Under hoop stress the PVC lined tubes failed in one of three ways: "crack and spray", explosive or type II failure.

The most common type of failure, crack and spray, was so named as it described the failure. Aside from the occasional tick from the tube during testing, there was no indication of impending failure. When failure occurred, a quick, sharp "crack" would be heard followed immediately by a spray of fluid.

Internally, the visible damage to the tube consisted of a single axial crack in the PVC liner that would always run the length of the test section. Externally, centered over the liner crack, would be a wide zone of delamination that was usually the length of the test section. This delamination damage would taper off at the ends of the tube. When the test fluid reached the surface of the tube it would form multiple spray fans, the base of which would follow the direction of the filament winding layer.

The external appearance of several PVC lined tubes after this type of failure is shown in Figs. 6-9 to 6-13.

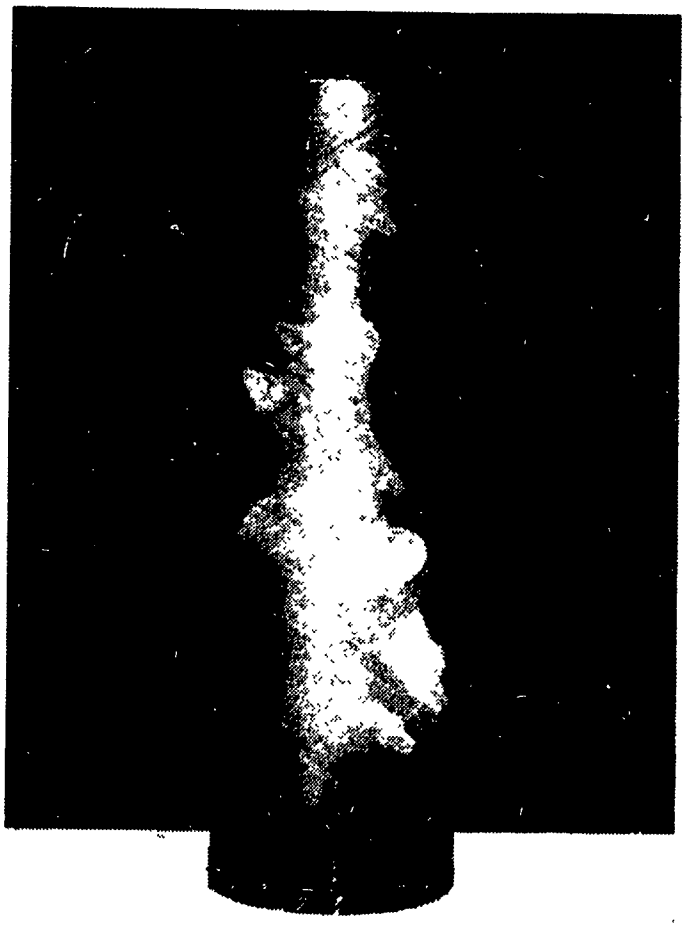

Fig. 6-9: External appearance of PVC lined tube 34C-1L (cold water) after failure. Hoop test, test point 6.

Fig. 6-10: External appearance of PVC lined tube 22D-1A (hot water) after failure. Hoop test, test point 1.

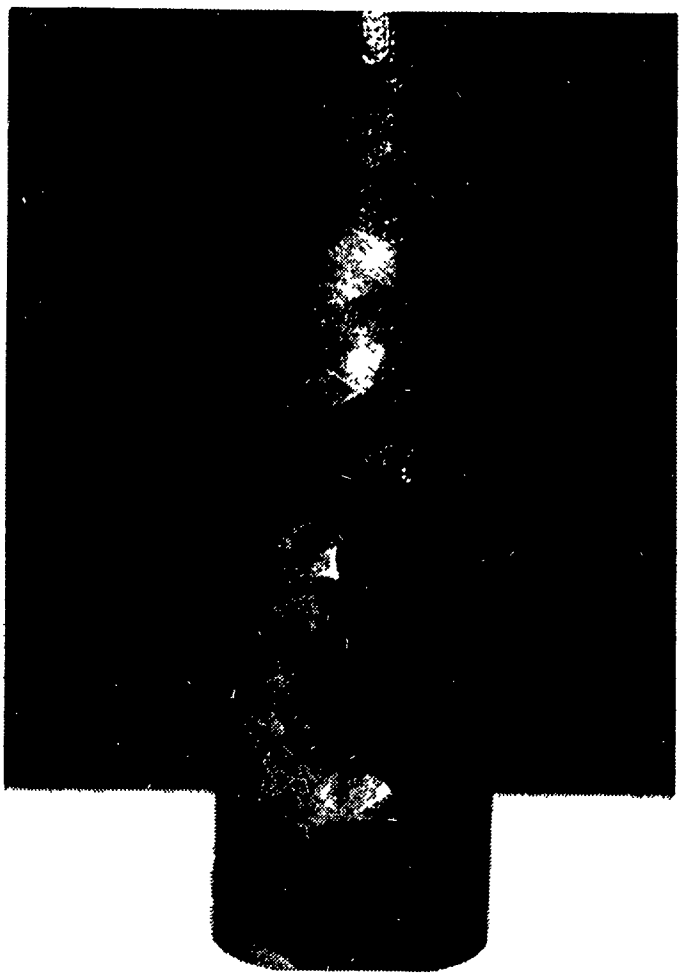

Fig. 6-11: External appearance of PVC lined tube 29C-1I (cold HCl) after failure. Hoop test, test point 5.

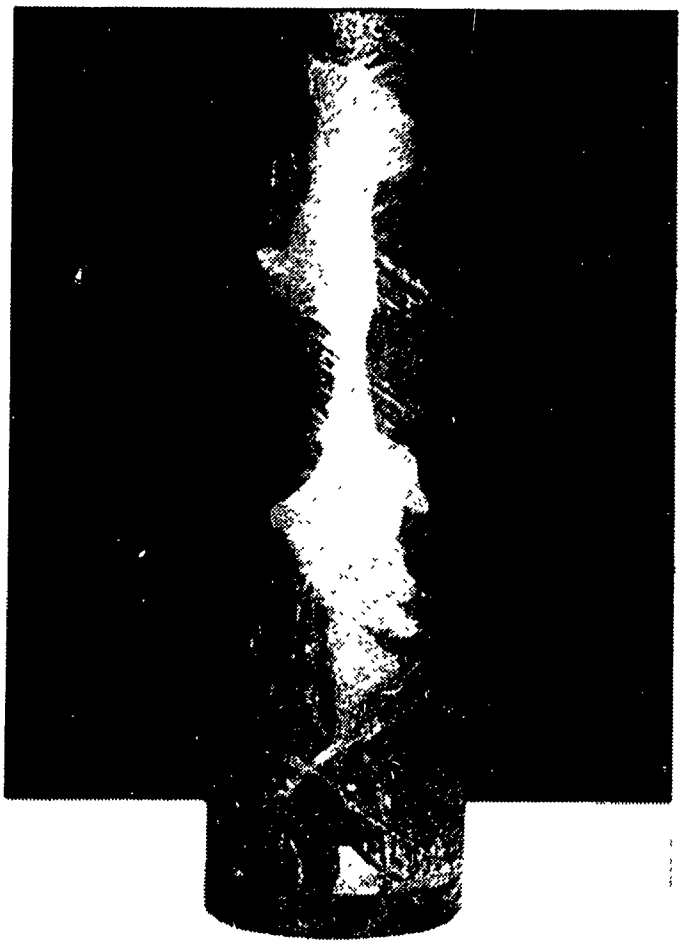

Fig. 6-12: External appearance of PVC lined tube 24B-1H (hot HCl) after failure. Hoop test, test point 5.

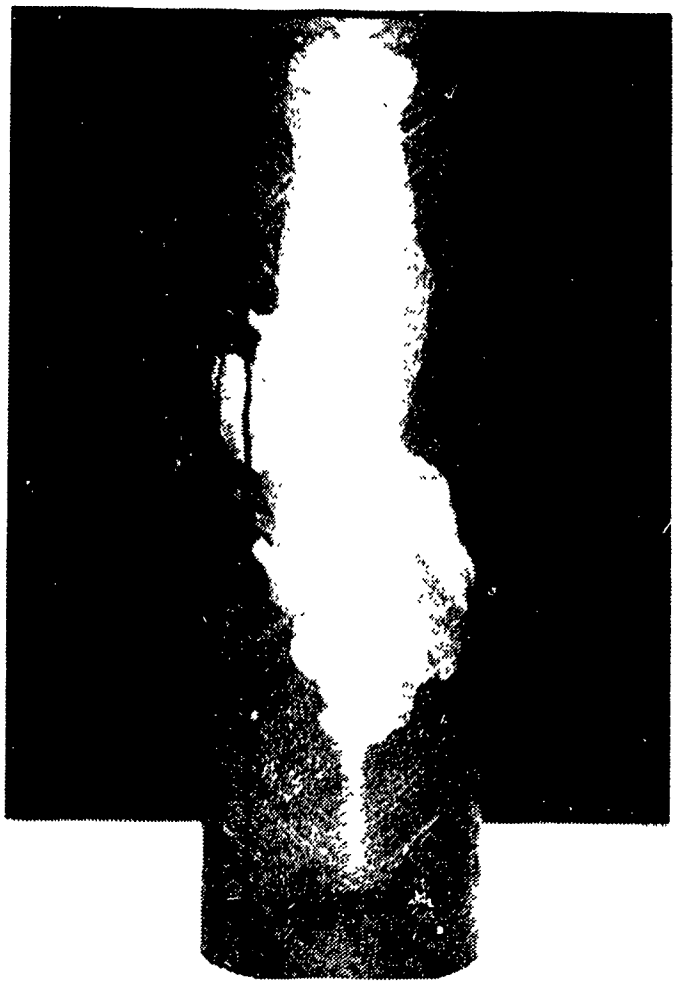

Fig. 6-13: External appearance of PVC lined tube 26E-1G (sulfuric acid) after failure. Hoop test, test point 5.

A section of tube 30D-1A was cut out, polished and the crack in the PVC liner was examined under a microscope at 99.225 X. Fig. 6-14 shows the view.

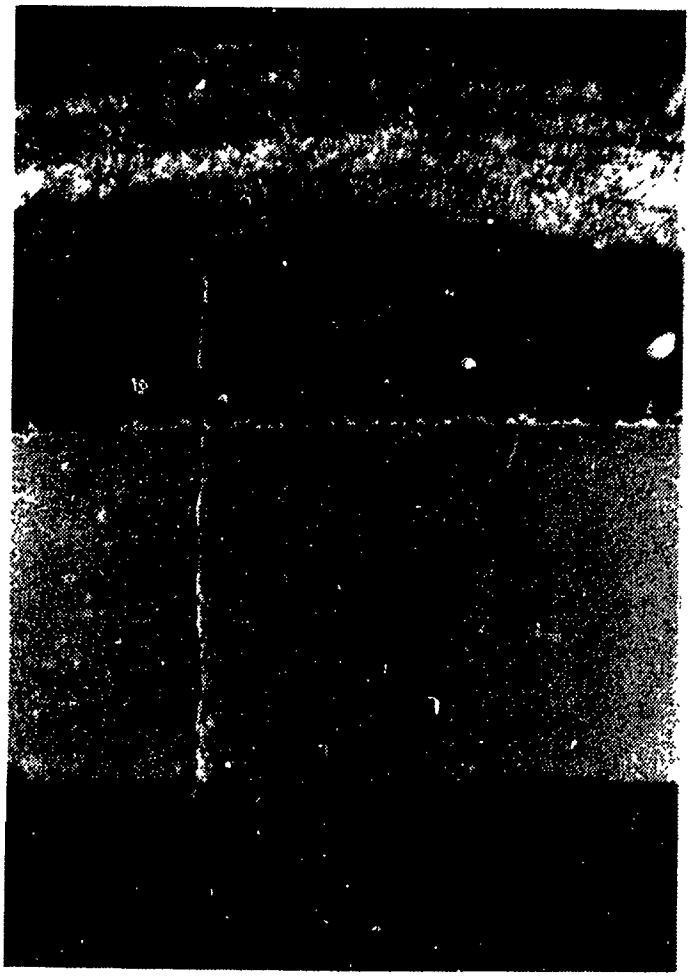

Fig. 6-14: Photomicrograph: View across the wall thickness of tube 30D-1A at the failure site.

The path of the crack is similar to that observed with the veil lined tubes. The crack passes straight through the PVC, veil and mat layers, travelling perpendicular to the inner wall surface. At the interface between the veil and filament winding layers, the crack changes direction 90° and proceeds to work its way through the filament winding layers until a branch reaches the surface.

A variation of this type of failure is where there would be the "crack" and the PVC would split but there would be no penetration of the test fluid through the filament winding layer. Pressure would be lost by the test fluid leaking past the seals at the ends of the test fixture (type II failure). This occurred with tubes 20C-1F, 24D-1I and 33C-1I. The external appearance of tube 33C-1I is shown in Fig. 6-15.

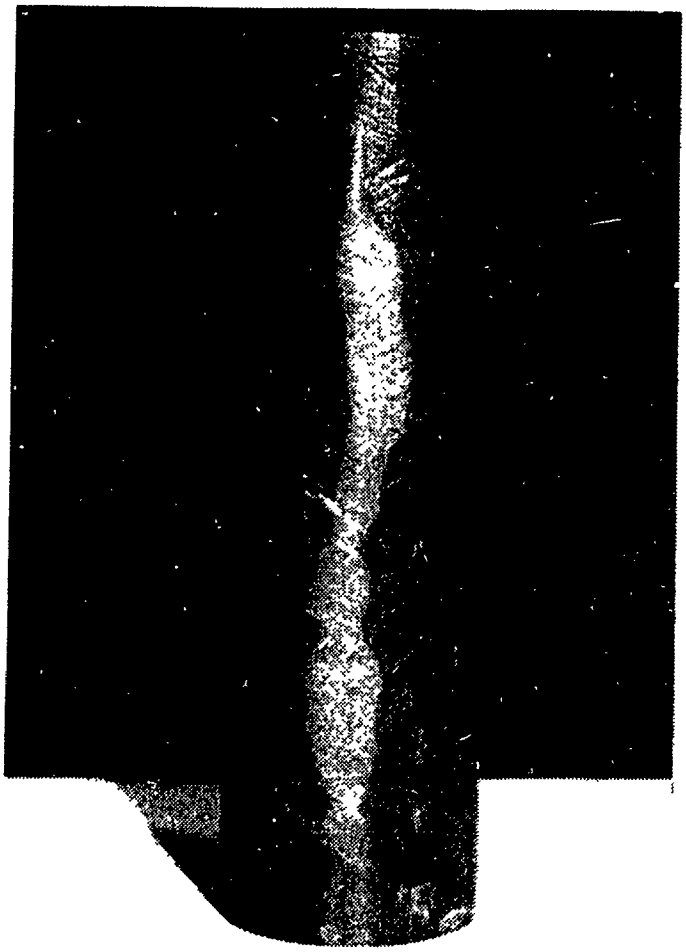

Fig. 6-15: External appearance of PVC lined tube 33C-1I (cold water) after failure. Hoop test, test point 5.

Explosive failure occurred in ten of the sixty tubes tested and these are listed in Table 6-7.

Table 6-7: List of tubes that failed explosively.

Tube	Test Point	Environment
23A-1D	2	HCl 50°C
23E-1E	3	HCl 50°C
26C-1E	3	H_2SO_4
28D-1E	3	HCl 20°C
28D-1F	3	HCl 20°C
32B-1G	4	WATER 20°C
27B-1J	5	H_2SO_4
25A-1K	6	HCl 50°C
25A-1L	6	HCl 50°C
29E-1L	6	HCl 20°C

Unlike the two previous PVC lined tube failure patterns there were clear indications of impending failure. Figure 6-16 shows the first visual indication of impending explosive failure, the silent appearance of a small spot of whitening. As the pressure was increased further, this whitening would slowly grow in diameter as shown in Fig. 6-17.

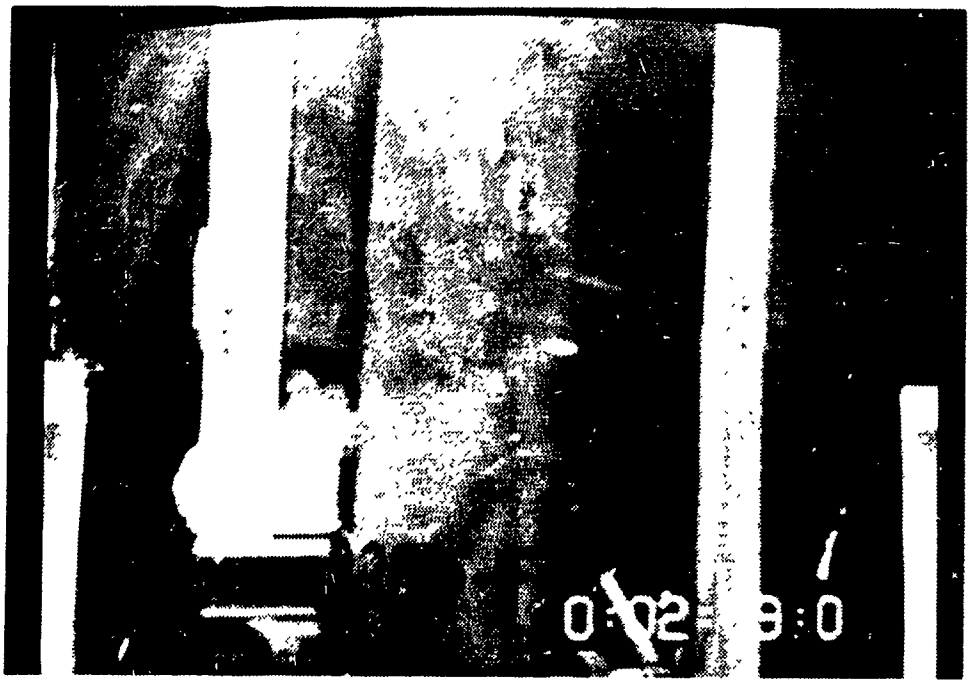

Fig. 6-16: The first indication of impending failure, the silent appearance of a small spot of whitening.

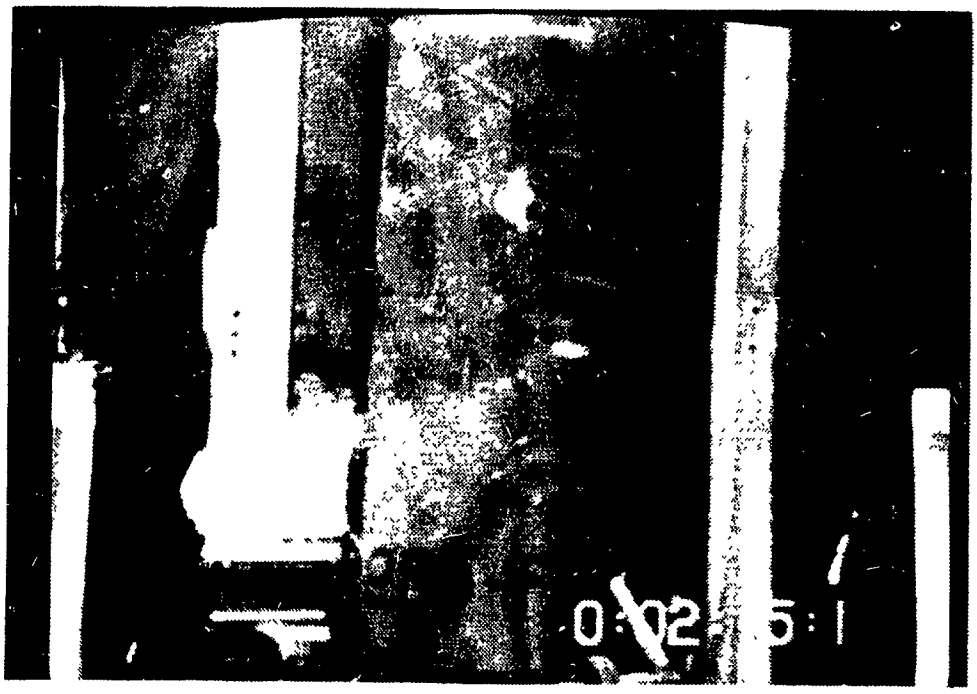

Fig. 6-17: As the pressure was increased this whitening would slowly grow in diameter.

Then suddenly, the rate of growth of the patch would increase and the explosive failure would occur as shown in Figs. 6-18 to 6-20. The explosive failure was characterized by the tearing of the filament winding layer and the violent ejection of liner material.

Fig. 6-18: Start of explosion.

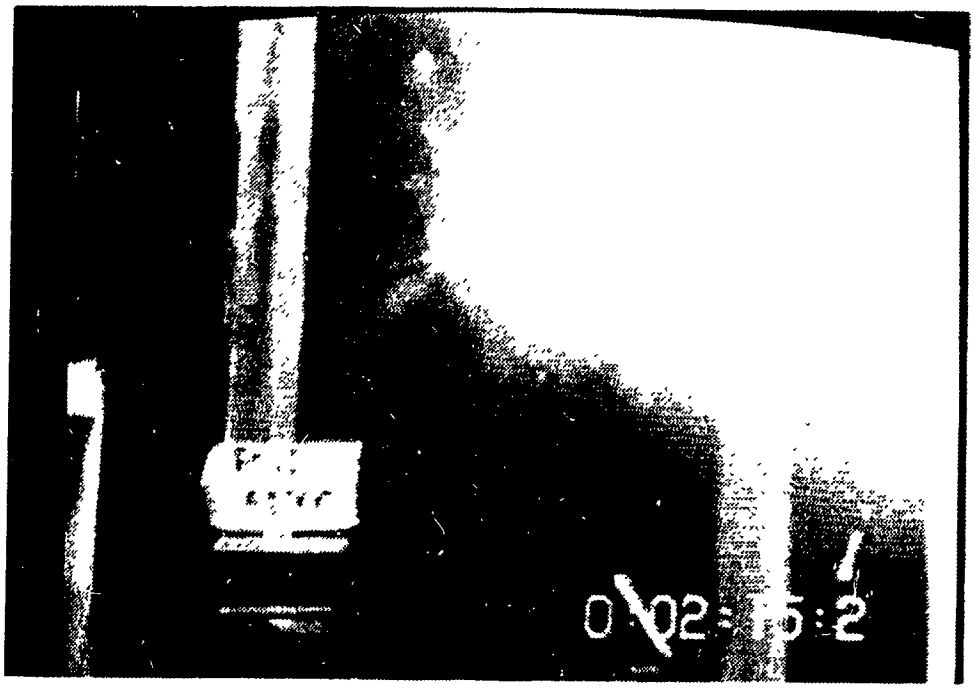

Fig. 6-19: Mid-explosion.

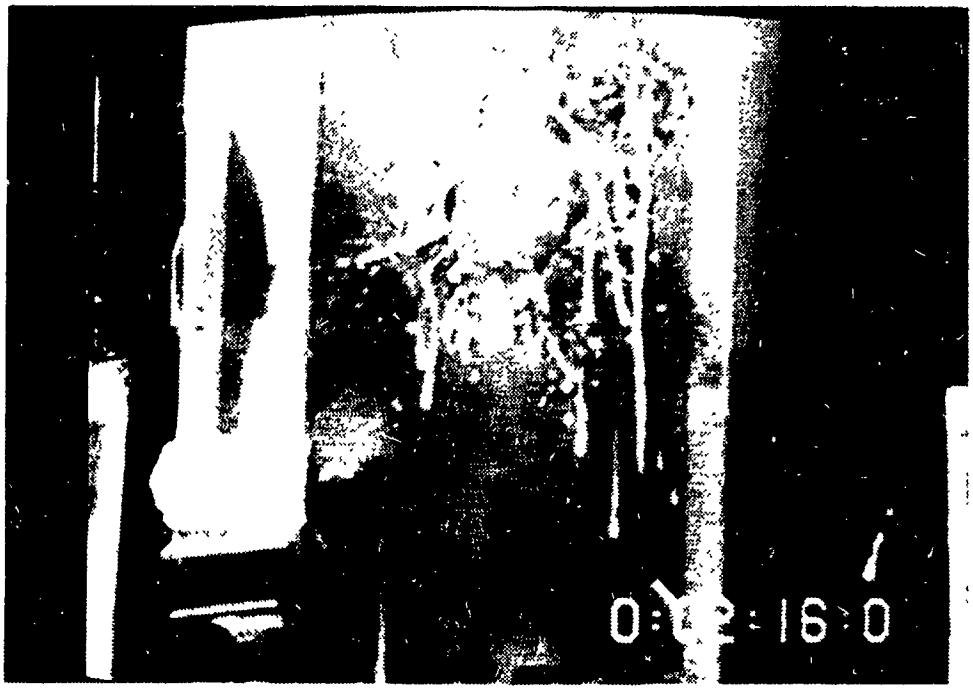

Fig. 6-20: End of explosion. Note hole blown in plexiglass shield.

With the exception of one cold water and one sulfuric acid exposed tube, all the explosive failures were observed with tubes exposed to cold or hot HCl. Figure 6-21 shows the typical external appearance of a PVC lined tube after explosive failure. Figure 6-22 shows the damage to the PVC liner of the tube in Fig. 6-21.

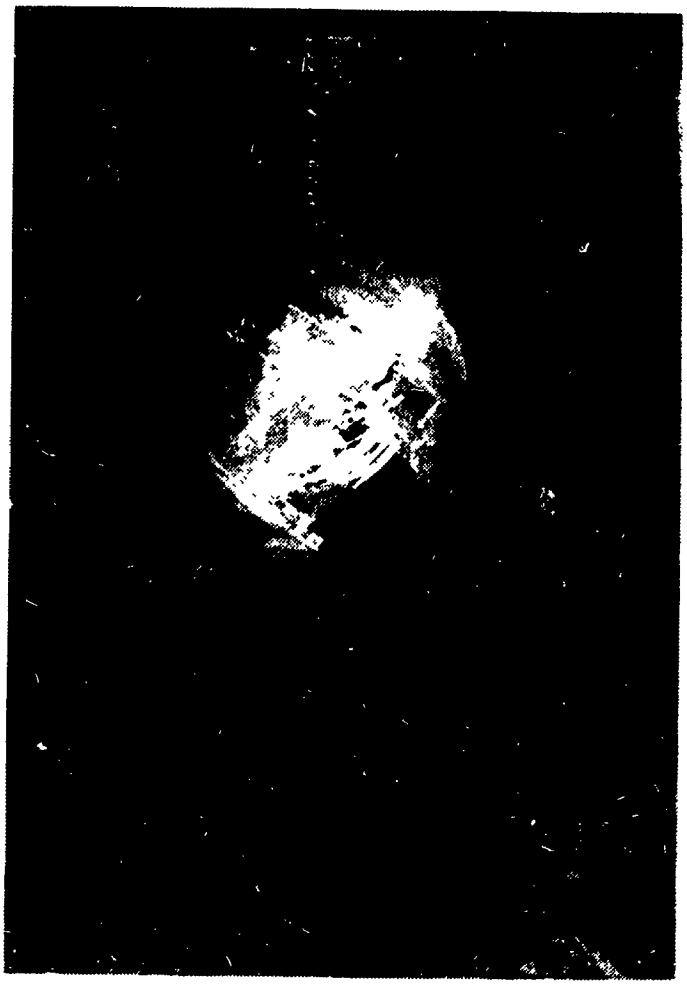

Fig 6-21 Typical external appearance of a PVC tube after explosive failure.

Fig 6-22: The damage to the PVC liner of the tube in Fig 6-21.

6.2.3 Strain Versus Pressure

Figure 6-23 shows surface stains ε_1, ε_2 and the Poisson's ratio υ_{21} versus pressure for tube 29A-1G. This graph shows the typical pattern observed in all the other strain versus stress graphs for hoop loading of PVC lined tubes.

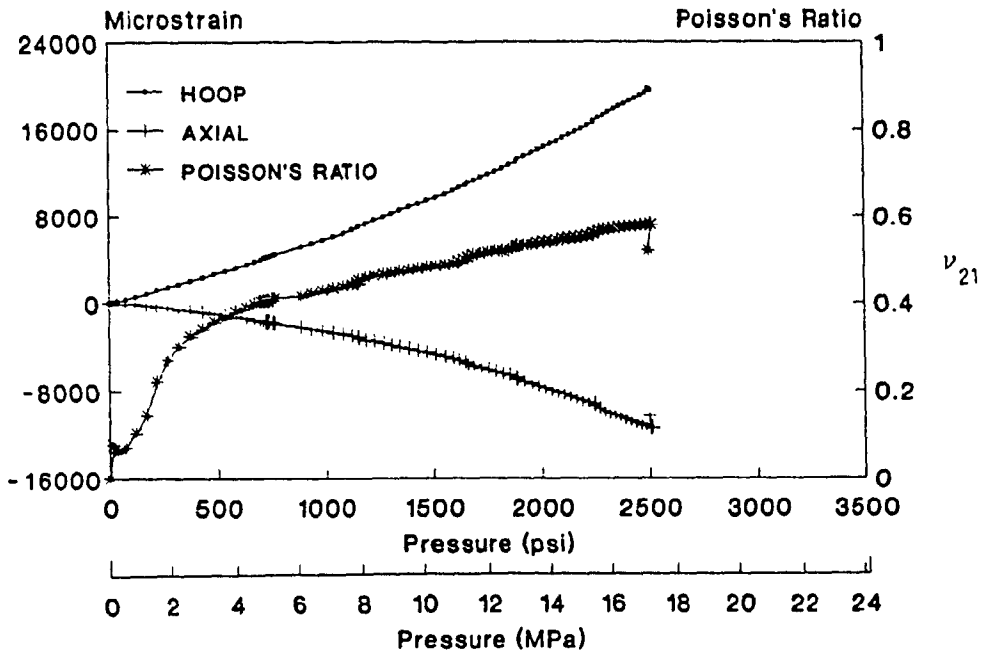

Fig. 6-23: Strain and Poisson's ratio versus pressure graph for PVC lined tube 29A-1G.

The hoop strain is positive and non-linear. As the load increases so does the slope of the hoop strain line. The axial strain is negative and non-linear. Again, as the load is increased the slope of the axial strain line increases.

From 0 psi the Poisson's ratio increases rapidly and by 500 psi the Poisson's ratio starts to flatten out, usually maintaining an even slope until failure.

Figure 6-24 shows ε_1, ε_2 and υ_{21} versus pressure for the veil lined tube 11E-1C. It has the same characteristics as for the PVC lined tube under hoop loading. This was also the typical pattern for the veil lined tubes under hoop loading.

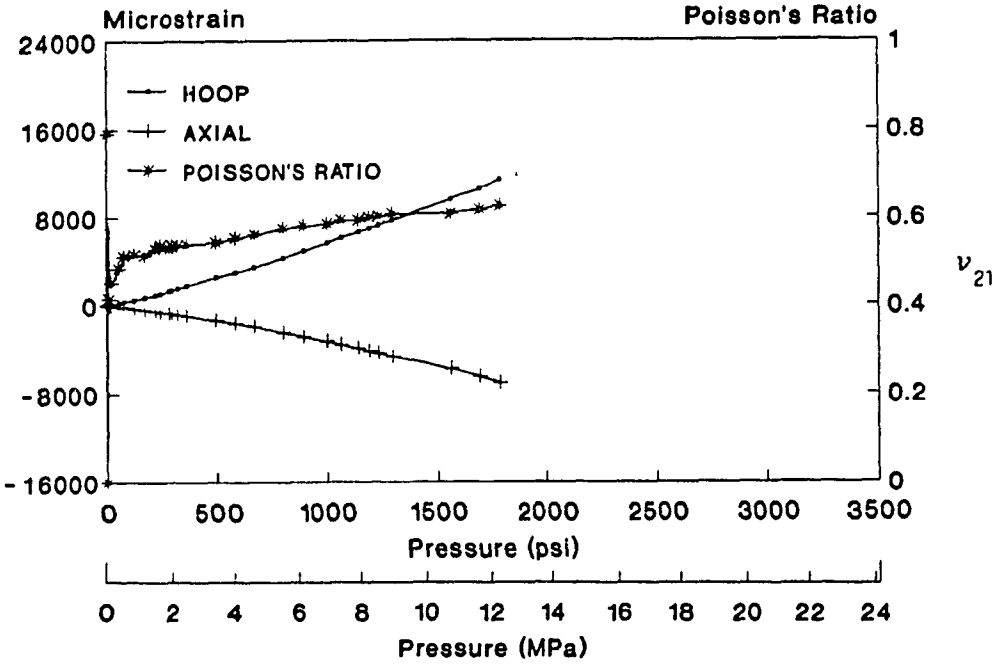

Fig. 6-24: Strain and Poisson's ratio versus pressure graph for veil lined tube 11E-1C.

Comparing Figures 6-23 and 6-24 with Fig. 2-3 it is apparent that the response of vinyl ester tubes is similar to that observed with E-glass/epoxy tubes under hoop stress.

6.3 Biaxial Test Results

6.3.1 Readings at Failure

Tables 6-8 to 6-13 show the readings recorded at failure for both the veil lined and PVC lined tubes under biaxial stress for test points 1 to 6.

Table 6-8: Biaxial test readings at failure, test point 1.

		WATER		HCl (35%)		H_2SO_4 (98%)
	AIR	20°C	80°C	20°C	50°C	
VEIL	4C-2A ---	1B-2A ---	---	6A-2A 12 1430 (9.86) 1189 5413	10A-2A 6 1500 (10.34)	
VEIL	4E-2B 13 2170 (14.96)	2A-2B 24 1540 (10.61)	---	6B-2B 12 1560 (10.76) 1125 4688	10B-2B 6 1460 (10.07) 1297† 5510†	
PVC	30D-2A ---	31C-2A 24 1570 (10.83) 1793 8640	---	27E-2A 12 1730 (11.93) --- 2688	23B-2A ---	25D-2A 12 2880 (19.86) --- 5532
PVC	---	32C-2B 24 1820 (12.55)	---	28A-2B 12 1730 (11.93) 1181 6678	23C-2B 6 1100 (7.58)	25C-2A 12 2450 (16.89) 3352 ---

Refer to Fig. 6-1 for a description of cell information.

Table 6-9: Biaxial test readings at failure, test point 2.

		WATER		HCl (35%)		H_2SO_4
	AIR	20°C	80°C	20°C	50°C	(98%)
VEIL	14C-2C 17 1900 (13.10) 1655 7964	---	---	6D-2C 15 1280 (8.83) 861 3416	9E-2C 13 1420 (9.79) 1038 7923	
	11E-2C ---	---	---	6D-2D 15 1630 (11.24)	9E-2D 13 840 (5.79)	
PVC		---	---	28C-2C 18 1720 (11.86) 4665 12676	23D-2C 13 900 (6.21) 1358 4293	26B-2C 15 2470 (17.03) 5234 10828
		---	---	28C-2D 18 1790 (12.34)	23D-2D 13 960 (6.62)	26B-2D 15 2180 (15.03)

Refer to Fig. 6-1 for a description of cell information.

Table. 6-10: Biaxial test readings at failure, test point 3.

		WATER		HCl (35%)		H_2SO_4
	AIR	20°C	80°C	20°C	50°C	(98%)
VEIL	---	---	16A-2E ---	8A-2E 19 1870 (12.89) 1790 8666	10E-2E 17 1510 (10.41) 2592 8190	
	---	---	16B-2F ---	8A-2F 19 1890 (13.03)	10E-2F 17 1550 (10.69)	
PVC		---	20C-2E ---	28E-2E‡ 19 1770 (12.20) 1241 6717	24A-2E 17 1110 (7.65) 888 4123	26D-2E 19 2030 (14.00) 3012 10786
		---	21C-2F ---	28E-2F‡ 19 1630 (11.24)	24A-2F 17 1210 (8.34)	26D-2F 19 2430 (16.75)

Refer to Fig. 6-1 for a description of cell information.
‡ explosive failure

Table 6-11: Biaxial test readings at failure, test point 4.

		WATER		HCl (35%)		H_2SO_4
	AIR	20°C	80°C	20°C	50°C	(98%)
VEIL	15A-2G ---	1E-2G 26 1830 (12.62) 2420 7462	5A-2G 23 1020 (7.03) 1672 4377	8C-2G 25 1920 (13.24) 1870 7634	11A-2G 23 1330 (9.17) 4684 8173	
	15B-2H 27 1880 (12.96)	2C-2H 26 1650 (11.38)	16E-2H ---	8B-2H 25 1810 (12.47)	11B-2H 23 950 (6.55)	
PVC		32B-2G 26 1930 (13.30) 5350 10440	21B-2G ---	29A-2G 25 2150 (14.82) 4684 8721	24B-2G ---	26E-2G 25 2060 (14.20) 1961 8501
		33B-2H 26 2280 (15.72)	21E-2H ---	29B-2H 25 2180 (15.03)	24C-2H 23 890 (6.14)	27A-2H 25 1610 (11.10)

Refer to Fig. 6-1 for a description of cell information.

Table 6-12: Biaxial test readings at failure, test point 5.

		WATER		HCl (35%)		H_2SO_4
	AIR	20°C	80°C	20°C	50°C	(98%)
VEIL	15C-2I 34 1780 (12.27) 487 6639	2D-2I 33 1500 (10.34) 1950 5854	7C-2I 29 1040 (7.17) 1118 4719	8D-2I ---	11C-2I 30 1000 (6.90) 2068 6285	
	15C-2J 34 1910 (13.17)	2D-2J 33 1780 (12.27)	7A-2J 29 770 (5.31)	8D-2J 32 1390 (9.58)	11D-2J ---	
PVC		34B-2I 33 2460 (16.96) 3222 8918	22B-2I 29 1660 (11.45) 2250 7913	29C-2I 32 2230 (15.38) 3558 ---	24D-2I ---	27C-2I 32 2210 (15.24) --- ---
		33C-2J 33 1760 (12.13)	22C-2J 29 1490 (10.27)	29D-2J 32 2480 (17.10)	24E-2J ---	27C-2J 32 1710 (11.79)

Refer to Fig. 6-1 for a description of cell information.

Table 6-13: Biaxial test readings at failure, test point 6.

		WATER		HCl (35%)		H_2SO_4
	AIR	20°C	80°C	20°C	50°C	(98%)
VEIL	15E-2K 41 1900 (13.10) 3328 9018	3A-2K ---	7D-2K 34 930 (6.41) 602 1562	9A-2K 38 1800 (12.41) 326 6997	9C-2K 36 1350 (9.31) 1648 3541	
	4A-2L 41 1960 (13.51)	3B-2L ---	16D-2L 34 1150 (7.93)	9A-2L 38 1170 (8.07)	9C-2L 36 1500 (10.34)	
PVC		34C-2K 38 2280 (15.72) 3876 11514	20F-2K 34 1640 (11.31) 2848 7662	29E-2K ---	25A-2K ---	27D-2K ---
		34D-2L ---	22E-2L ---	30A-2L ---	25B-2L ---	25E-2L ---

Refer to Fig. 6-1 for a description of cell information.

6.3.2 Biaxial Test Failure Patterns

For the veil lined tubes under biaxial stress a single failure mode, similar to the type I failure seen under hoop stress, was observed.

The first indication of distress shown by most of the tubes was named "pump and tick". After each incremental increase in pressure the tube would tick. The frequency of this ticking would be high immediately after a rise in pressure and would gradually decrease in frequency during the time between pressure increases.

The next indication of distress was the same as that observed during the hoop test, the appearance of lines that grew into axially elongated patches of whitening. The development of these areas varied from developing quickly with a "crack" and growing in steps with increasing pressure and more noise, to silently appearing and growing gradually outwards. These areas had varying lengths and were spaced randomly around the tube.

Next, areas of delamination would start over some of the patches. The delamination was generally limited to the area above and 3 cm (1.25 in.) or less either side of the axial patch and varied in intensity.

The rate of failure varied from tube to tube. Some tubes would fail quickly, others would slowly go through the stages and it was possible to watch the development of the axial patches and delamination.

Final failure of the tube is characterized by the presence of one to several axial patches above which would be areas of varying degrees of delamination. At failure, fluid would spray from the edges of the delamination. This is shown in Fig. 6-25.

Fig. 6-25: Spray from the edges of the delamination area.
Veil lined tube, biaxial test.

The external appearance of the veil lined tubes after failure was similar to that observed during the hoop test, an example is shown in Fig. 6-26.

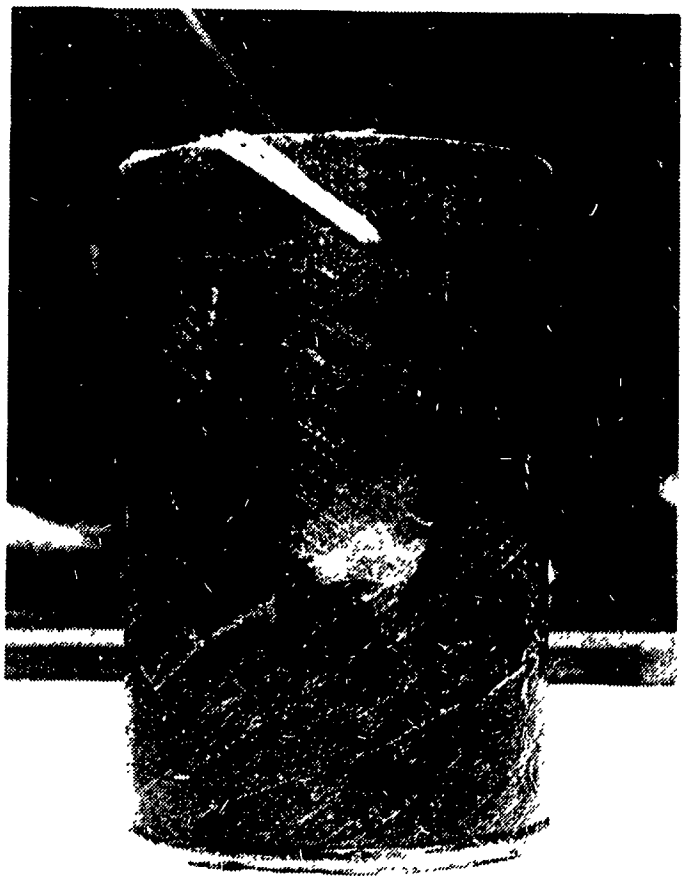

Fig. 6-26: The external appearance of a veil lined tube after failure by weepage. Biaxial test.

The "pump and tick" phenomena was also present when the PVC lined tubes were tested under biaxial loading. In some tests the ticks were associated with the appearance of thin whitening bands along the filament winding direction (transverse cracks). The next stage in failure was a sudden "crack" and then the test fluid spraying from the tube at multiple locations (crack and spray).

Examination of the tubes after testing revealed damage that was similar to that seen in the hoop test. Instead of just one crack there were multiple axial cracks in the PVC around the tube. The cracks meandered along the axial direction of the tube except at the ends just below the edge of the end cap. Here, the axial crack would branch off and encircle the tube until another crack was met. The damage above these cracks was the same sort of delamination as was seen with the hoop test. Sprays of test fluid generally appeared at several locations, however some tubes had only a single spray. The external appearance of tube 26D-2F taken at 0°, 120° and 270° around the tube are shown in Figures 6-27, 6-28 and 6-29 respectively.

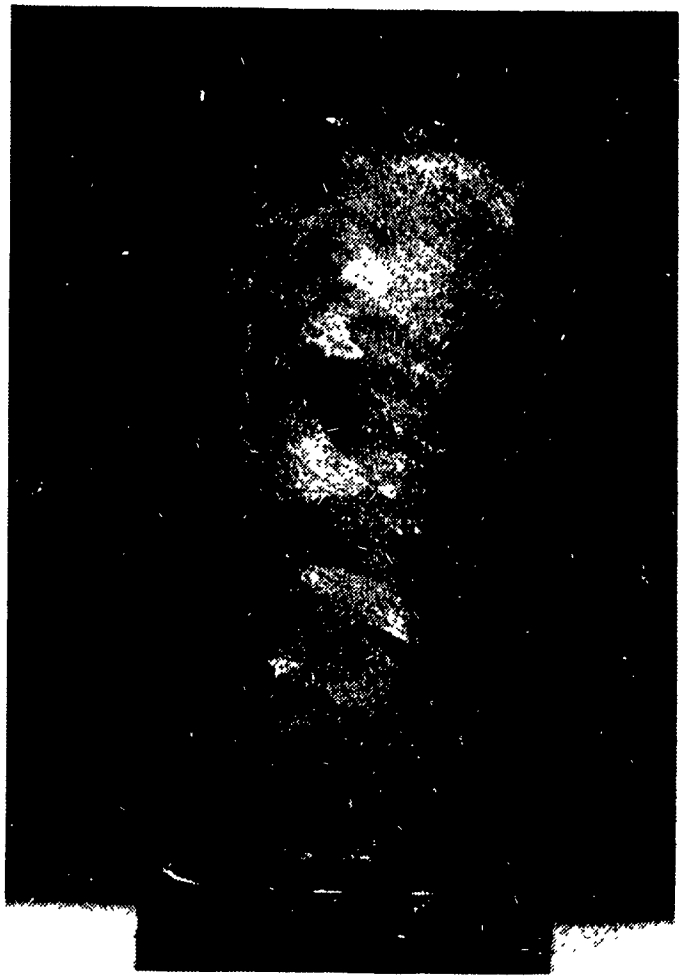

Fig. 6-27: The external appearance of tube 26D-2F at 0°.

Fig. 6-28: The external appearance of tube 26D-2F at 120°.

Fig. 6-29: The external appearance of tube 26D-2F at 270°.

Two PVC lined tubes, 28E-2E and 28E-2F, had explosive failures. The appearance of 28E-2F after failure is shown in Figure 6-30.

Figure 6-30: Appearance of tube 28E-2F after an explosive failure.

6.3.3 Strain Versus Pressure

Fig. 6-31 shows ε_1, ε_2 and υ_{21} versus pressure for PVC lined tube 31C-2A under biaxial loading. It shows that hoop and axial strain are both positive, and the Poisson's ratio is negative. Both the hoop and axial strain are non linear. The hoop strain is always greater than the axial strain. The Poisson's ratio is fairly consistent throughout the test.

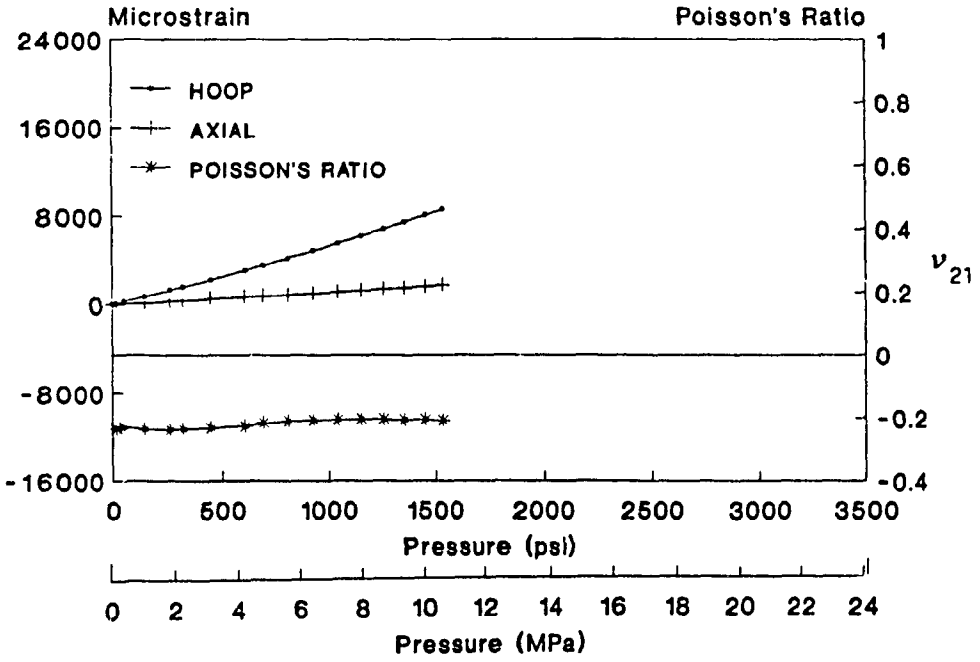

Fig. 6-31: Strain and Poisson's ratio versus pressure graph for PVC lined tube 31C-2A.

Figure 6-32 show the graph for tube 1E-2G, a veil lined tube under biaxial load. It shows the same characteristics as the PVC lined tubes under biaxial loading. Both graphs show the typical pattern for the results from the biaxial test.

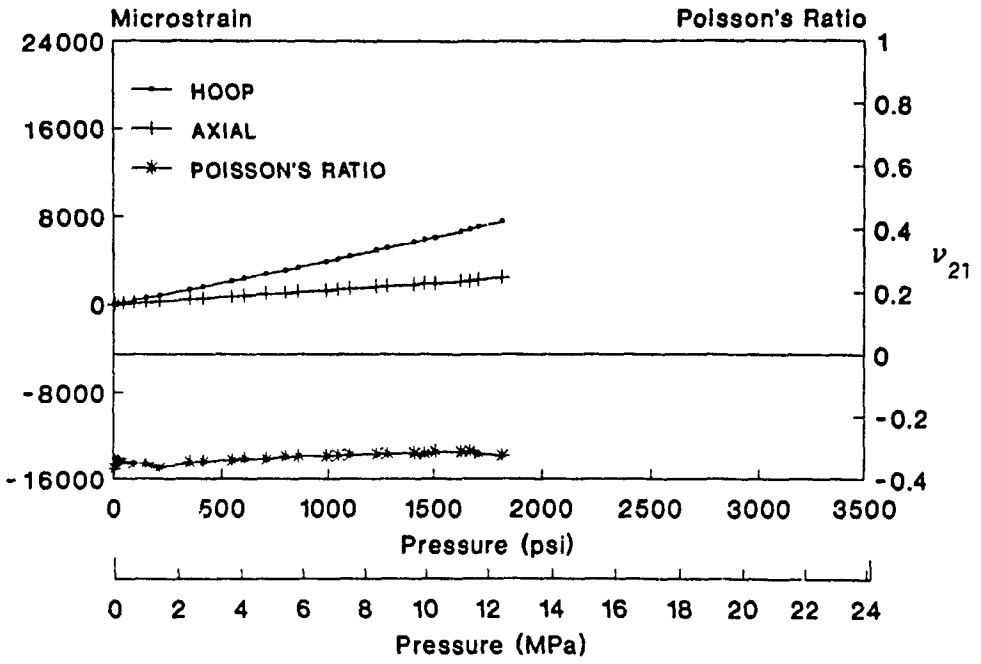

Fig. 6-32: Strain and Poisson's ratio versus pressure graph for veil lined tube 1E-2G.

At first, a comparison of the stress strain behavior shown in Figs. 6-31 and 6-32 with that shown in Fig. 2-2 would seem to show that vinyl ester tubes behave differently compared to epoxy tubes. However, since we are dealing with failure due to weepage only the portion of Fig. 2-2 below 100 MN/m^2 should be considered. In this case the hoop strain of both tube types appears to be linear while the vinyl ester tube's axial strain is linear and the epoxy tube's axial strain is non-linear.

6.4. Axial Test Results:

6.4.1. Readings at Failure

The results in the following tables are the readings at the point of initial failure.

Table 6-14: Axial test readings at failure, test point 1.

		WATER		HCl (35%)		H_2SO_4
	AIR	20°C	80°C	20°C	50°C	(98%)
VEIL	4E-3A 12 21000 (93.41)	2A-3A 13 24875 (110.5)	5C-3A 7 16375 (59.49)	6A-3A 12 24450 (108.8) 7639 ---	10A-3A 6 21875 (97.30)	
	4E-3B 14 20050 (89.18) 13044 -3667	2A-3B 13 24760 (110.1)	5C-3B 7 16000 (71.17)	6A-3B 12 24500 (108.9)	10B-3B 6 19000 (84.51) 4958 ---	
PVC	30E-3A 12 22875 (101.7) 12286 ---	31C-3A 14 20275 (90.18) 9675 ---	22D-3A 7 19000 (84.51) 8099 ---	28A-3A 12 16450 (73.17) 5415 ---	23C-3A 6 18150 (80.73) 6635 ---	25D-3A 12 21000 (93.41) 8741 ---
	30E-3B 14 20000 (88.96) 10374 -3988	31C-3B 14 16800 (74.73)	21D-3B 9 21500 (95.63)	28A-3B 12 18000 (80.06)	23B-3B 6 19000 (84.51)	25D-3B 12 22500 (100.1)

Refer to Fig. 6-1 for a description of cell information.

Table 6-15: Axial test readings at failure, test point 2.

		WATER		HCl (35%)		H_2SO_4
	AIR	20°C	80°C	20°C	50°C	(98%)
VEIL	11E-3C 17 21500 (95.63) 6973 -2838	1B-3C 17 20750 (92.30) 5090 -1821	5E-3C 13 14325 (63.72) 3029 -1541	6C-3C 15 24600 (109.4) 7196 -3178	9D-3C 13 17750 (78.95) 5231 -1951	
	14C-3D 17 26750 (119.0)	1B-3D 17 17500 (77.84)	5E-3D 13 15500 (68.94)	6D-3D 15 24450 (108.8)	9D-3D 13 18250 (81.17)	
PVC		32C-3C 17 22025 (97.97) 7396 -3578	21A-3C 13 21500 (95.63) 8691 -3463	28B-3C 18 17000 (75.62) 4287 -1684	23A-3C 13 20750 (92.29) 9323 -2608	26A-3C 15 17775 (79.06) 5719 -1895
		32C-3D 17 20725 (92.18)	21A-3D 13 22500 (100.1)	28C-3D 18 17050 (75.84)	23D-3D 13 20500 (91.18)	26B-3D 15 20500 (91.18)

Refer to Fig. 6-1 for a description of cell information.

Table. 6-16: Axial test readings at failure, test point 3.

		WATER		HCl (35%)		H_2SO_4
	AIR	20°C	80°C	20°C	50°C	(98%)
VEIL	14E-3E 22 25150 (111.9) 11555 -3535	1C-3E 21 21975 (97.74) 10301 -3469	16A-3E 17 18400 (81.84) 6594 -2047	6E-3E 14 25350 (112.8) 11202 -3607	10D-3E 17 19000 (84.51) 10849 -2929	
	14D-3F 22 24500 (109.0)	1A-3F 21 21500 (95.63)	16A-3F 17 17900 (79.62)	6E-3F 19 18500 (82.28)	10E-3F 17 17300 (76.95)	
PVC		31D-3E 21 17950 (79.84) 8026 -3263	21C-3E 17 20300 (90.29) 5476 -1896	28D-3E 19 17150 (76.28) 6758 -2723	23E-3E 17 18575 (82.62) 7507 -1977	26C-3E 19 22975 (102.2) 9195 -3413
		31D-3F 21 18500 (82.29)	21C-3F 17 17300 (76.95)	28E-3F 19 14790 (65.79)	24A-3F 17 17800 (79.17)	26D-3F 19 22550 (100.3)

Refer to Fig. 6-1 for a description of cell information.

Table. 6-17: Axial test readings at failure, test point 4.

		WATER		HCl (35%)		H_2SO_4
	AIR	20°C	80°C	20°C	50°C	(98%)
VEIL	15B-3G 27 21000 (93.41) 6580 -3451	2C-3G 26 22050 (98.08) 7375 -2340	5A-3G 23 14375 (63.94) 3601 -752	8C-3G 25 18375 (81.73) 7942 -2469	11B-3G 23 12375 (55.04) 5390 -1595	
	15B-3H 27 20500 (91.18)	2C-3H 26 22650 (100.7)	16E-3H 17 17400 (77.39)	8C-3H 25 18050 (80.29)	11B-3H 23 12750 (56.49)	
PVC		33B-3G 26 18750 (83.40) 5367 -1702	21B-3G 21 21300 (94.74) 7896 -2643	29B-3G 25 20700 (92.07) 9107 -2883	24C-3G 23 15600 (69.39) 4313 -2072	27A-3G 25 17625 (78.40) 5376 -2402
		33B-3H 26 19175 (85.29)	21E-3H 17 16600 (73.84)	29B-3H 25 22300 (99.19)	24C-3H 23 14500 (64.50)	27A-3H 25 15650 (69.61)

Refer to Fig. 6-1 for a description of cell information.

Table 6-18: Axial test readings at failure, test point 5.

		WATER		HCl (35%)		H_2SO_4
	AIR	20°C	80°C	20°C	50°C	(98%)
VEIL	15C-3I 34 21550 (95.63) 9522 -4139	2E-3I 33 19800 (88.07) 6044 -635	7C-3I 29 18750 (83.40) 4484 -1697	8E-3I 32 15125 (67.27) 7697 -2855	11D-3I 30 14400 (64.05) 4851 -2393	
	15D-3J 34 21075 (93.74)	2E-3J 33 22600 (100.5)	7C-3J 29 18125 (80.62)	8E-3J 32 19000 (84.51)	11C-3J 30 13950 (62.05)	
PVC		34B-3I 33 20575 (91.52) 7691 -3479	22C-3I 29 15550 (69.17) 4892 -1550	29D-3I 32 17750 (78.95) 7031 -1978	24D-3I 30 12275 (54.60) 2774 -1199	27B-3I 32 14600 (64.94) 3782 -1294
		34B-3J 33 19500 (86.73)	22C-3J 29 17750 (78.95)	29D-3J 32 16750 (74.50)	24E-3J 30 14000 (62.27)	27C-3J 32 16625 (73.94)

Refer to Fig. 6-1 for a description of cell information.

Table. 6-19: Axial test readings at failure, test point 6.

		WATER		HCl (35%)		H_2SO_4
	AIR	20°C	80°C	20°C	50°C	(98%)
VEIL	4A-3K 41 24850 (110.5) 10859 -3748	3B-3K 38 21750 (96.74) 6231 -2454	7D-3K 34 16875 (75.06) 4691 -1054	9B-3K 38 25000 (111.2) 8964 -4616	9C-3K 36 16850 (74.95) 13946 -3854	
	4A-3L 41 25075 (111.5)	3B-3L 38 19325 (85.96)	7D-3L 34 18175 (80.84)	9B-3L 38 23100 (102.7)	10C-3L 36 14000 (62.27)	
PVC		34D-3K 38 21250 (94.52) 8032 -2804	22E-3K 34 12000 (53.37) 4390 -1073	30A-3K 38 20100 (89.40) 9499 -3975	25B-3K 36 17225 (76.62) 5387 -2651	25E-3K 38 21725 (96.63) 7679 -3203
		34D-3L 38 19625 (87.29)	22E-3L 34 18375 (81.73)	30A-3L 38 21000 (93.41)	25B-3L 36 15250 (67.83)	25E-3L 38 19000 (84.51)

Refer to Fig. 6-1 for a description of cell information.

6.4.2 Axial Test Failure Patterns

Under axial loading the failure of the veil lined tubes was slow and progressive. Failure of these tubes can be considered to have occurred in two stages.

In the first stage of failure, the first indication of distress would be that the tube would start to tick. The first sign of failure would be the appearance of a small patch of whitening along the hoop direction. The tube would then bend slightly and the patch would spread around the tube. Damage to the tube was a crack in the corrosion liner, and above this area failure of the resin of the filament winding layer. This was considered the failure point of the tube and the event resulted in a drop in applied load. Further increase in load would cause the resin of the filament winding layer to break up further, causing the whitening band to grow axially. The filament winding layer would rotate slightly, and some slight necking could be seen.

After the initial failure, some tubes would enter the final stage of failure. The final stage of failure was the result of the glass filaments breaking. This would often start as a small, localized failure followed by a wave of breaking filaments moving around the tube. The appearance of a tube that failed in this single band of failure manner is shown in Fig. 6-33.

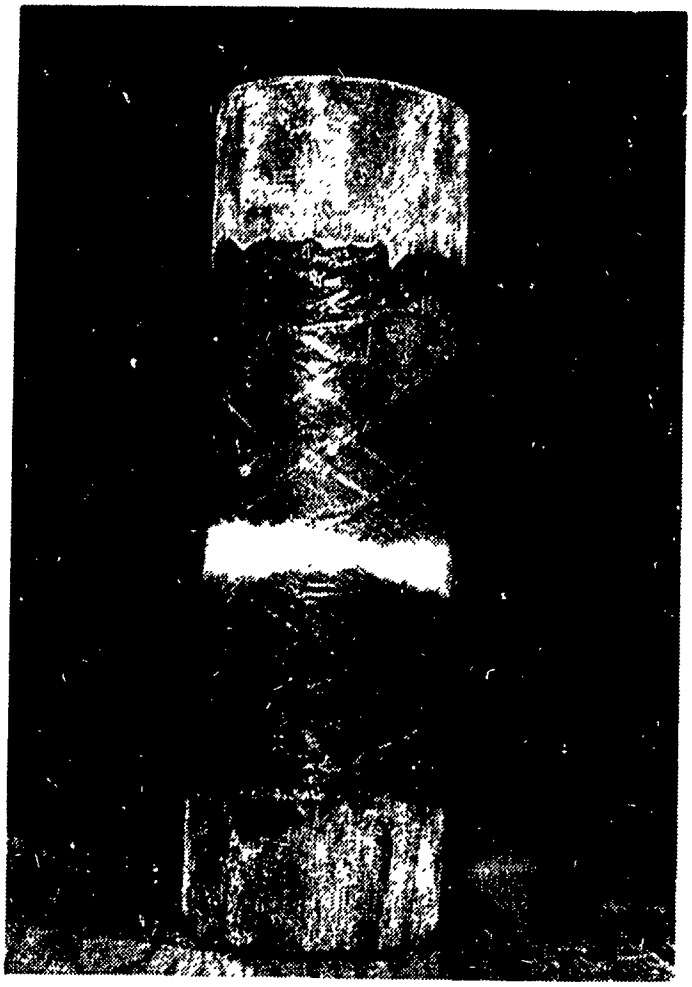

Fig. 6-33: Single band type of failure, veil lined tube.

Other tubes would repeat the first failure stage, and these bands would grow and merge axially until a third of the tube length was involved and necking was observed. The failure load of a subsequent failure would generally be higher than the failure load preceding it. Eventually, the tube would move into the final stage of failure. Fig. 6-34 shows the appearance of a tube that failed in this manner.

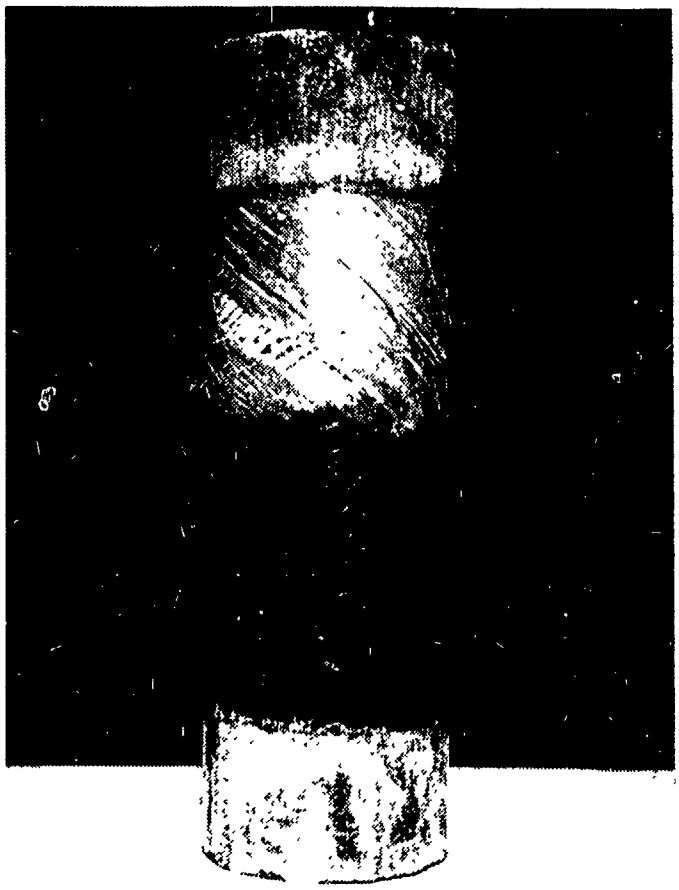

Fig. 6-34: Multiple bands of failure that have merged, veil lined tube.

The appearance of the tube in Fig. 6-34 is similar to the typical appearance of a E-glass/epoxy after final failure shown in Fig. 2-4.

With some tubes, the initial whitening patch would give rise to a band of delamination that spread along the filament winding direction, resulting in a spiral delamination. This was the result of one angle of the filament winding breaking while the other separated due to transverse cracks in the matrix. Fig. 6-35 shows a tube that failed in this manner.

Fig. 6-35: Spiral type failure, veil lined tube.

Failure of the PVC lined tubes under axial loading was sharp and quick.

Like the veil lined tubes, the PVC lined tubes would first indicate distress during loading by starting to "tick". However, unlike the veil lined tubes, no small, localized cracks or areas of whitening were observed to develop.

The first visible sign of damage was the sudden appearance of a band of whitening that would encircle the tube and be about 7 mm in width axially. A sharp "crack" and an abrupt drop in load marked the moment of development. As the applied load was brought back up, the area of whitening grew axially.

Before final failure, several failures in the same manner of the first could occur as loading continued. The load of these subsequent failures varied, being slightly higher or lower than the previous failure load, but rarely above the initial failure load. Where the bands are spaced close enough together, the whitening zones could merge and then the tube would neck and the filament winding layer would rotate towards the axial direction. The necking became noticeable when roughly a quarter of the tube was covered with the whitening band.

Final failure, as with the veil lined tubes, was when the glass filaments broke. Breakage started at a small area and spread around the tube, the speed of which varied from tube to tube. Examples of the appearance of PVC lined tubes after testing are shown in Figs. 6-36, 6-37 and 6-38. An example of a tube necking during testing is shown in Fig. 6-39.

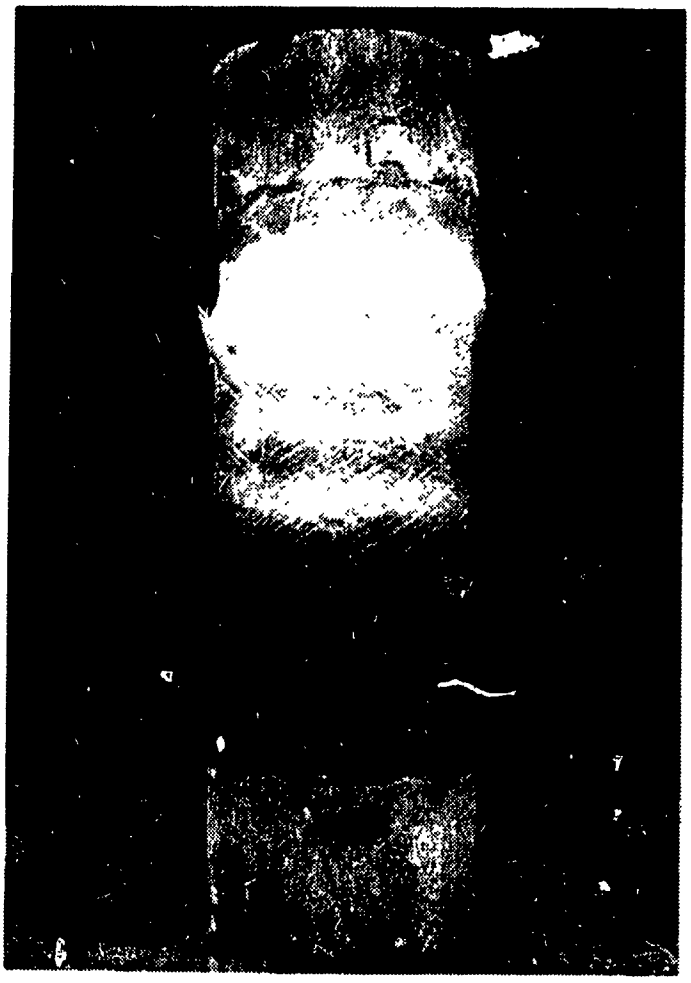

Fig. 6-36: Appearance after testing, tube 31D-3F.

Fig. 6-37: Appearance after testing, tube 33B-3G.

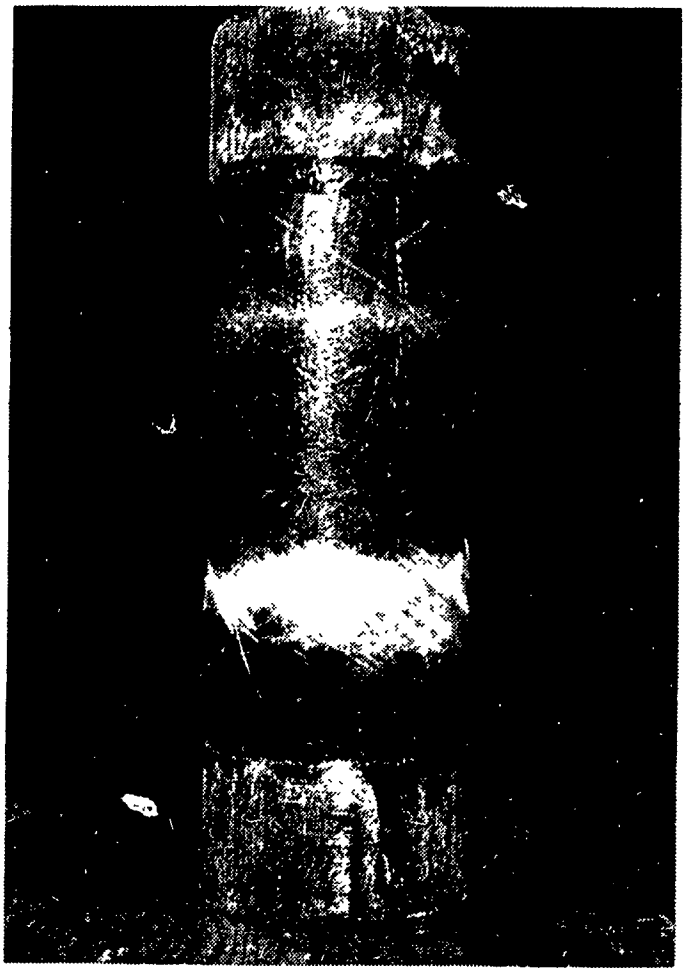

Fig. 6-38: Appearance after testing, tube 28E-3F.

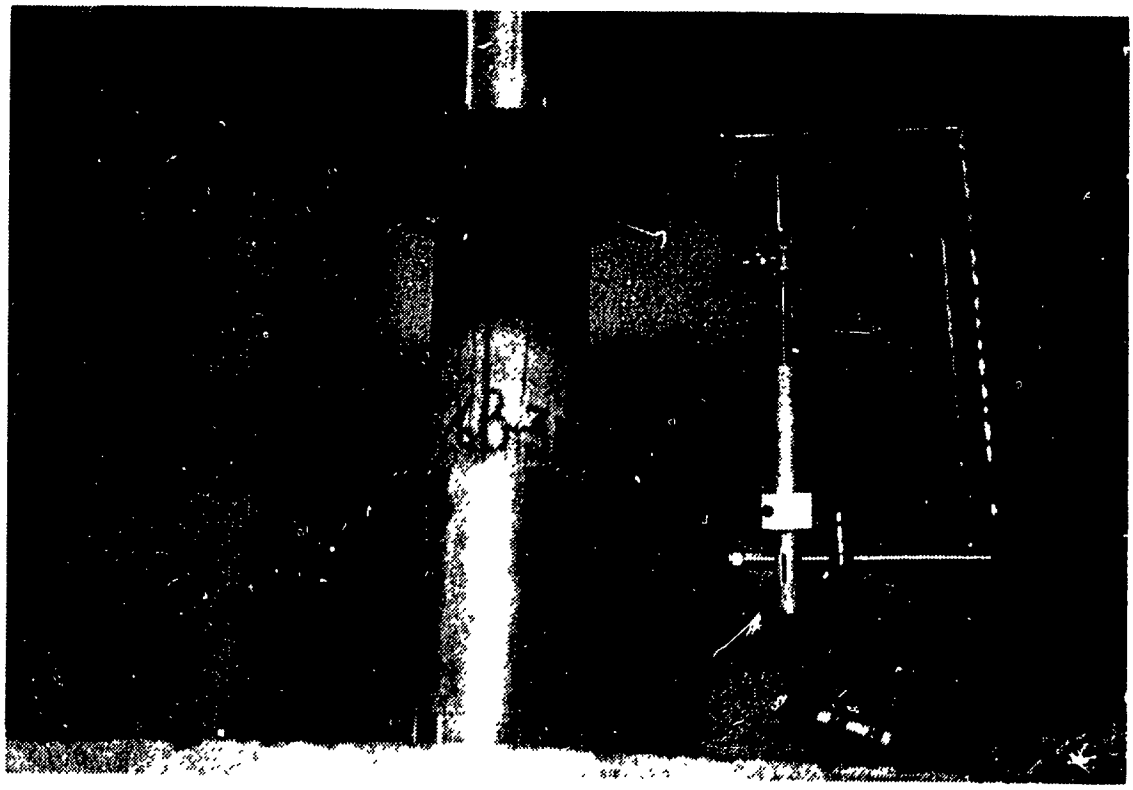

Fig. 6-39: Necking of tube during testing.

6.4.3 Strain versus Load

Figure 6-40 shows ε_1, ε_2, and the Poisson's ratio υ_{12} versus applied load for PVC lined tube 21A-3C under axial loading. The results show that the axial strain is positive and the hoop strain is negative. Both strains are non linear. The slope of the strain lines increases as load increases. The Poisson's ratio keeps the same slope throughout the test.

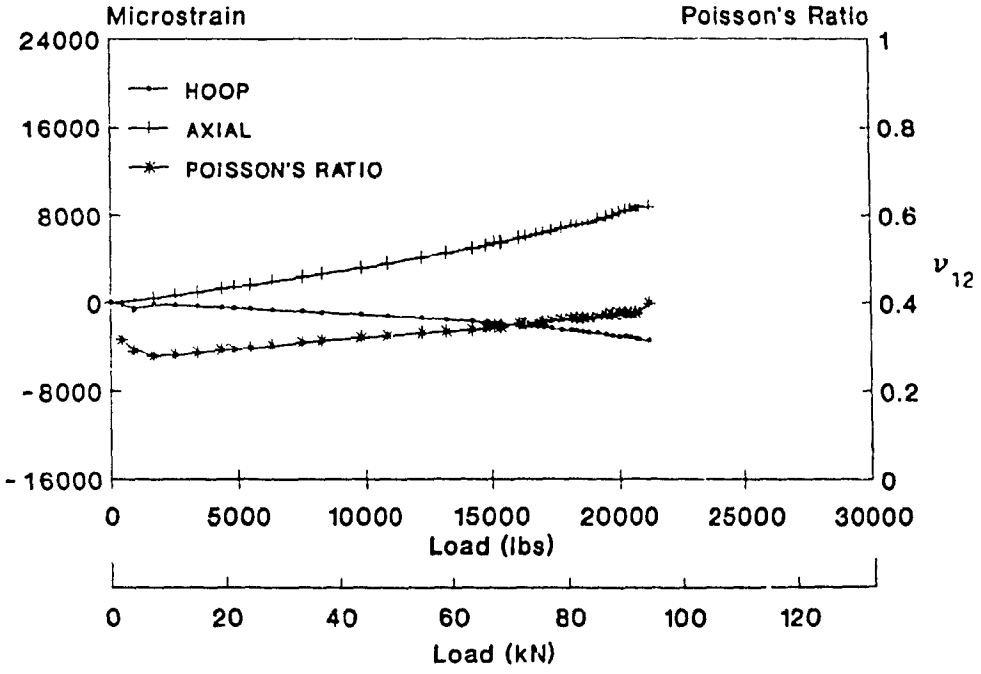

Fig 6-40: Strain and Poisson's ratio versus load graph for PVC lined tube 21A-3C

Figure 6-41 shows ε_1, ε_2 and the Poisson's ratio υ_{12} for a veil lined tube under axial loading. This graph shows the same trends as the PVC lined tubes under axial loading.

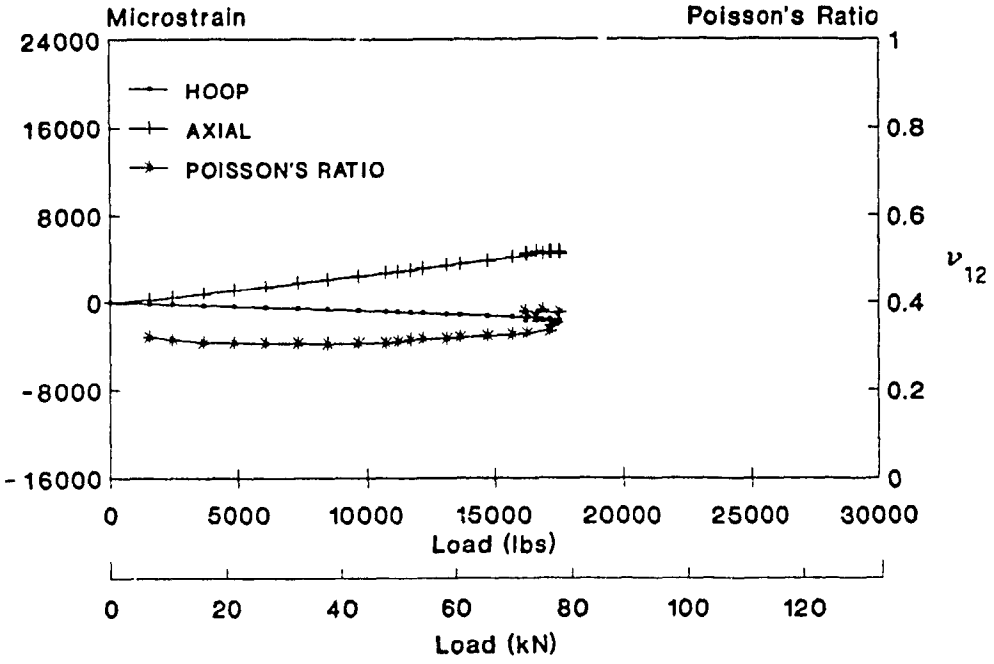

Fig. 6-41: Strain and Poisson's ratio versus load graph for veil lined tube 7C-3I.

CHAPTER 7. Analysis of Test Results

The purpose of this section is to analyze the test results for indications of how the tubes were affected by their environments.

7.1 Applied Stress at Failure Versus Exposure Time

Perhaps the most obvious analysis of the experimental results is the plotting of failure pressure or failure load versus exposure time.

7.1.1. Veil Lined Tubes

The results from the hoop, biaxial and axial tests for the air aged veil lined tubes are presented in Figures 7-1, 7-2, and 7-3 respectively. For the hoop and biaxial tests, Figures 7-1 and 7-2 show that the failure pressure remained fairly constant over time with a minimum of scatter. The axial test results show a much higher degree of scatter than the hoop and biaxial test, but in general the failure load remained fairly constant.

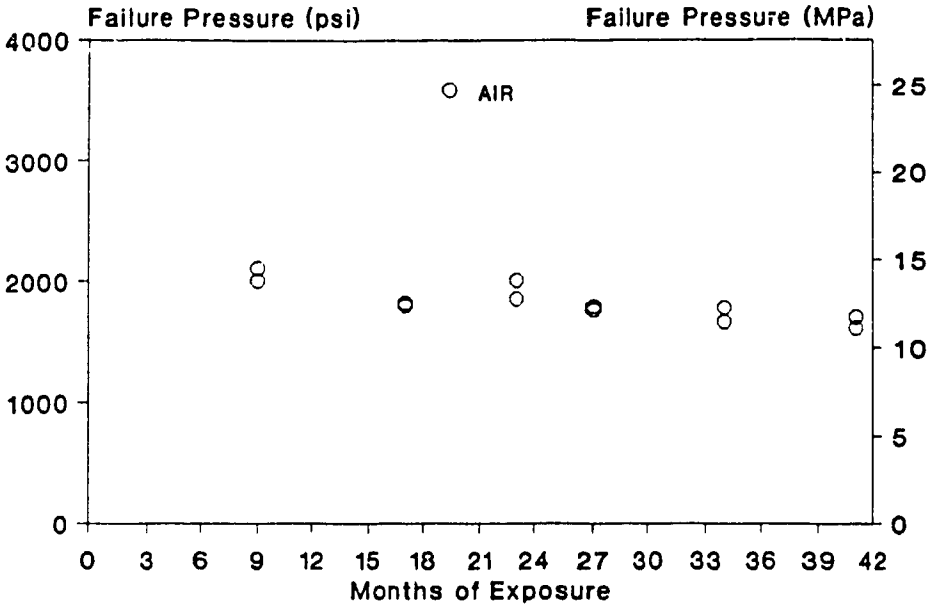

Fig. 7-1: Hoop test failure pressure versus exposure time, veil lined tubes exposed to air.

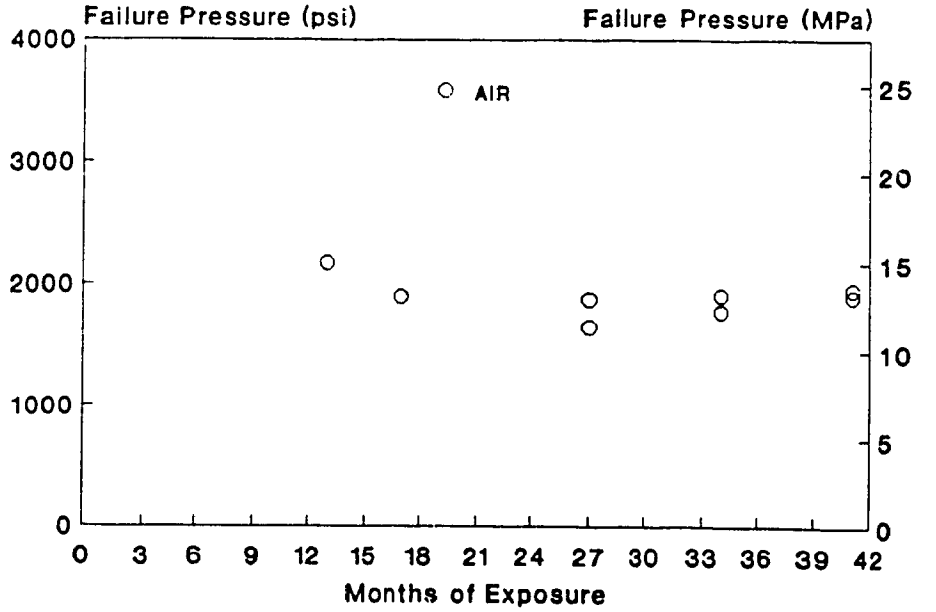

Fig. 7-2: Biaxial test failure pressure versus exposure time, veil lined tubes exposed to air.

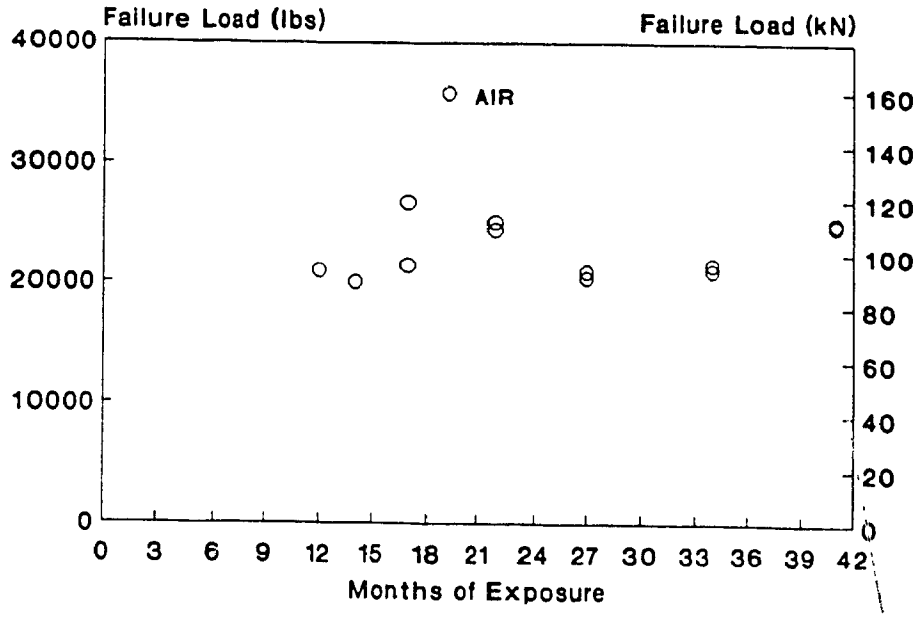

Fig. 7-3: Axial test failure load versus exposure time, veil lined tubes exposed to air.

Figure 7-4 shows the results from the hoop test for hot and cold water aged tubes. This graph has two interesting features. First it shows that despite different failure modes, there is little difference between type I and type II failure pressure for a given environment. Secondly, it shows that the hot water exposed tubes failed at lower pressure than the tubes exposed to room temperature water.

Figures 7-5 and 7-6 show the results from the biaxial and axial tests respectively for the hot and cold water aged veil lined tubes. Again, they show the failure pressure or load of the hot water aged tubes is less than that of the cold water aged tubes. The reduction in

performance of the hot water aged tubes is apparent after 6 months exposure and changed little with continued exposure. Again, the scatter with the axial test results is much greater than with the hoop and biaxial test results.

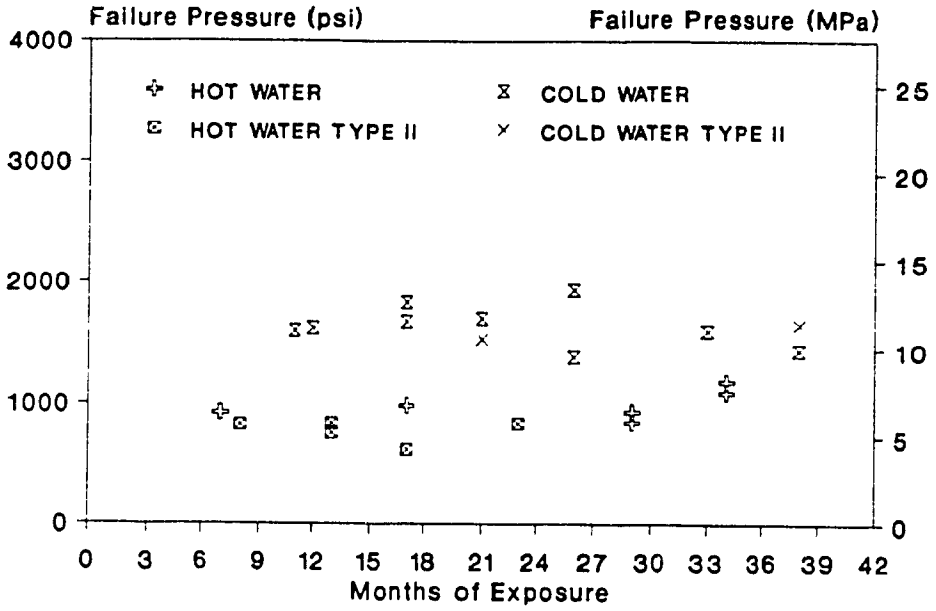

Fig. 7-4: Hoop test failure pressure versus exposure time, veil lined tubes exposed to hot and cold water.

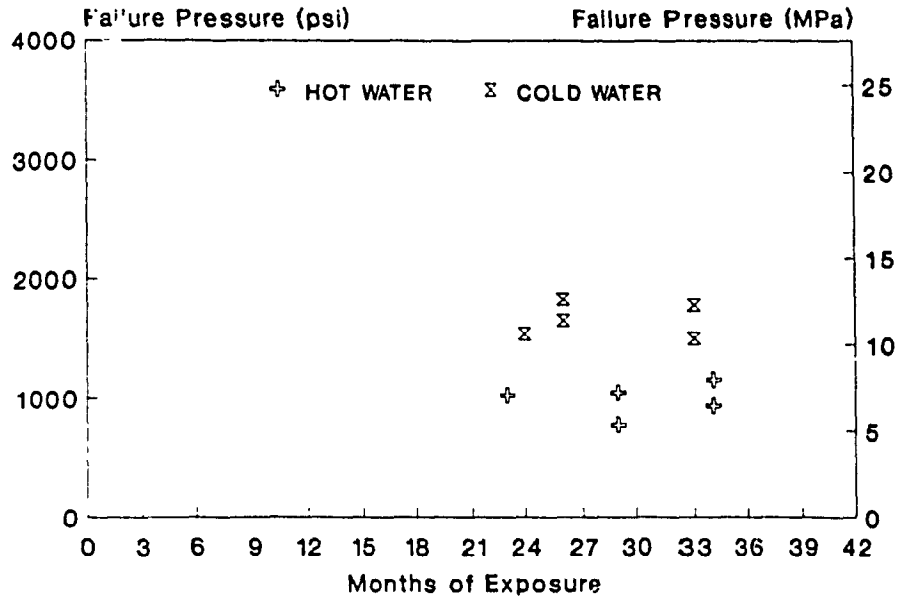

Fig. 7-5: Biaxial test failure pressure versus exposure time, veil lined tubes exposed to hot and cold water.

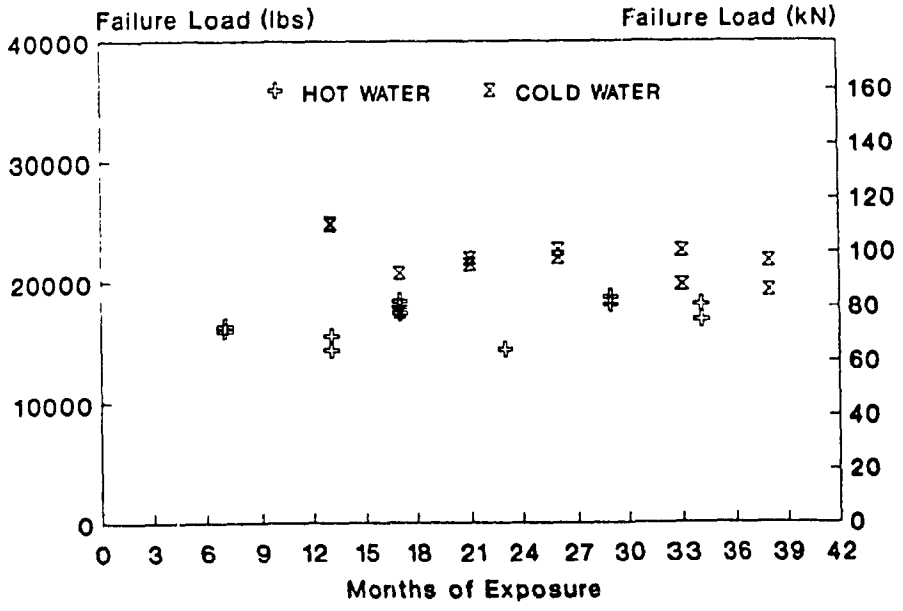

Fig. 7-6: Axial test failure load versus exposure time, veil lined tubes exposed to hot and cold water.

The next comparison for the veil lined tubes is for the results from the cold and hot HCl aged tubes. Figures 7-7, 7-8, and 7-9 show the results for the hoop, biaxial and axial test respectively. The first obvious feature of this group is the level of scatter. It is much greater than the preceding six Figures. In general, the hot HCl exposed tubes failed at a lower pressure or load than the cold HCl exposed tubes. Again, the drop in performance occurred during the first six months of exposure and then leveled off. Despite the difference in failure modes seen in the hot HCl exposed tubes during the hoop test, the failure pressure of the two modes was roughly the same.

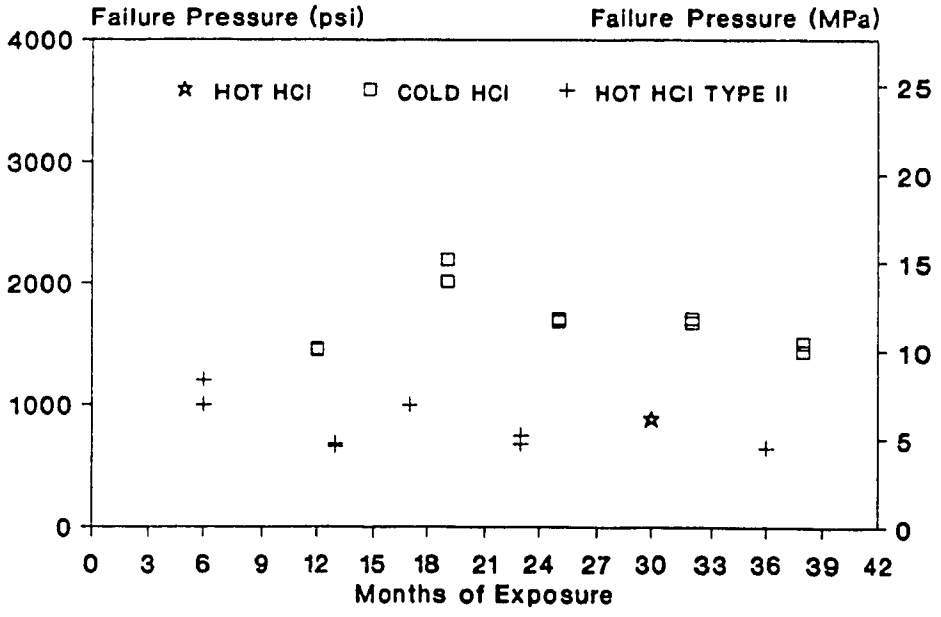

Fig. 7-7: Hoop test failure pressure versus exposure time, veil lined tubes exposed to hot and cold HCl.

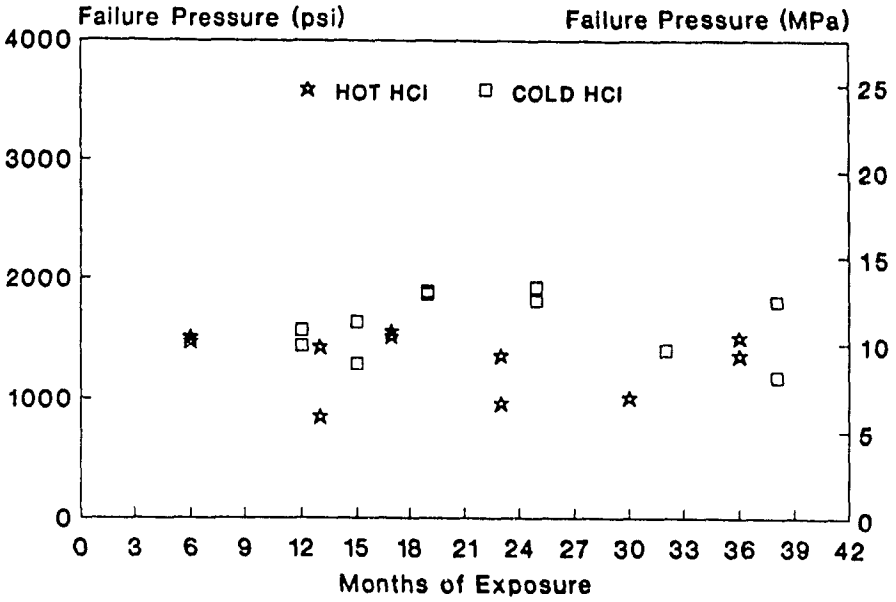

Fig. 7-8: Biaxial test failure pressure versus exposure time, veil lined tubes exposed to hot and cold HCl.

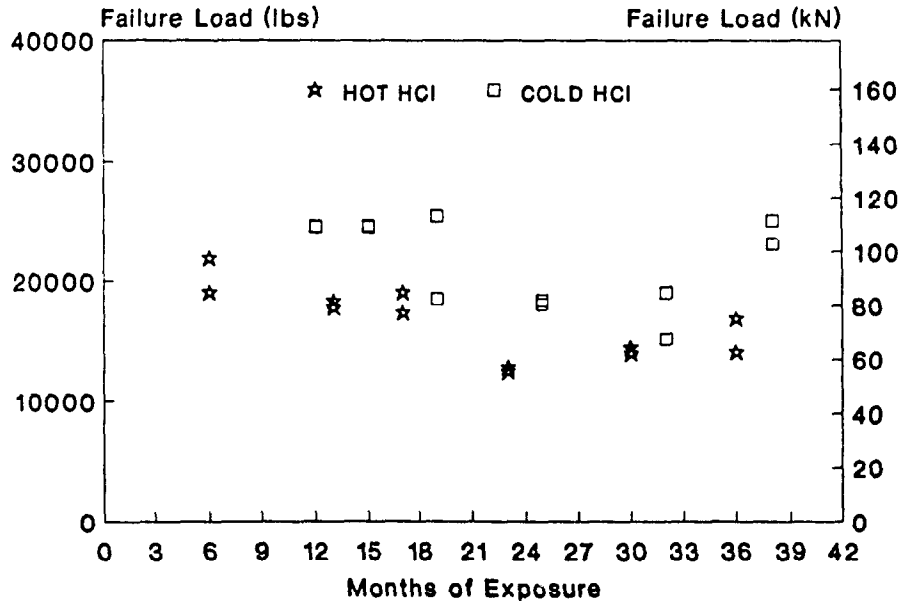

Fig. 7-9: Axial test failure load versus exposure time, veil lined tubes exposed to hot and cold HCl.

The final comparison for the veil lined tubes is to plot all the results for a given test on the same graph to compare the different environments. Figures 7-10 and 7-11 show the results of plotting failure pressure versus exposure time for the hoop test and biaxial test respectively. Figure 7-12 plots failure load versus exposure time for the axial test.

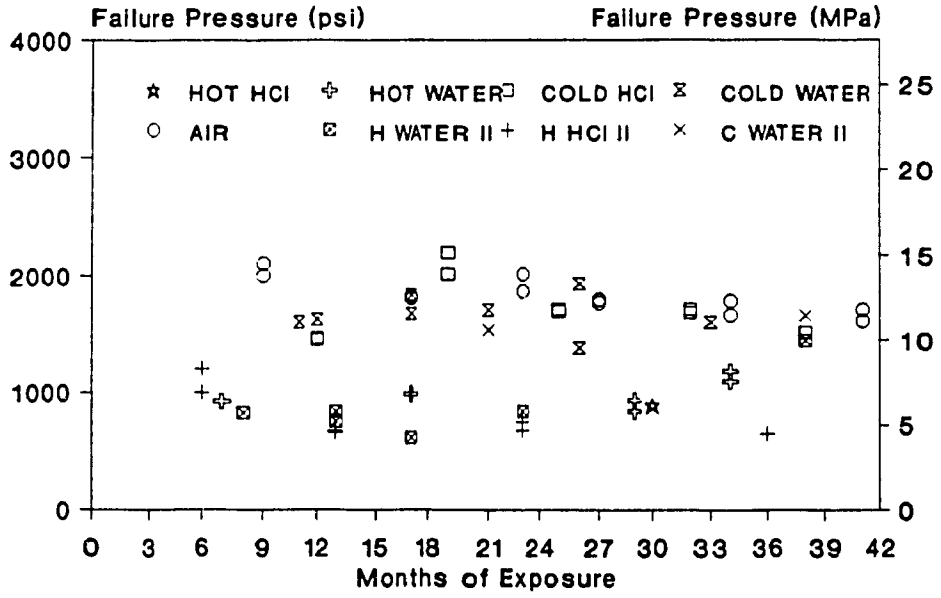

Fig. 7-10: Hoop test failure pressure versus exposure time, veil lined tubes, all environments.

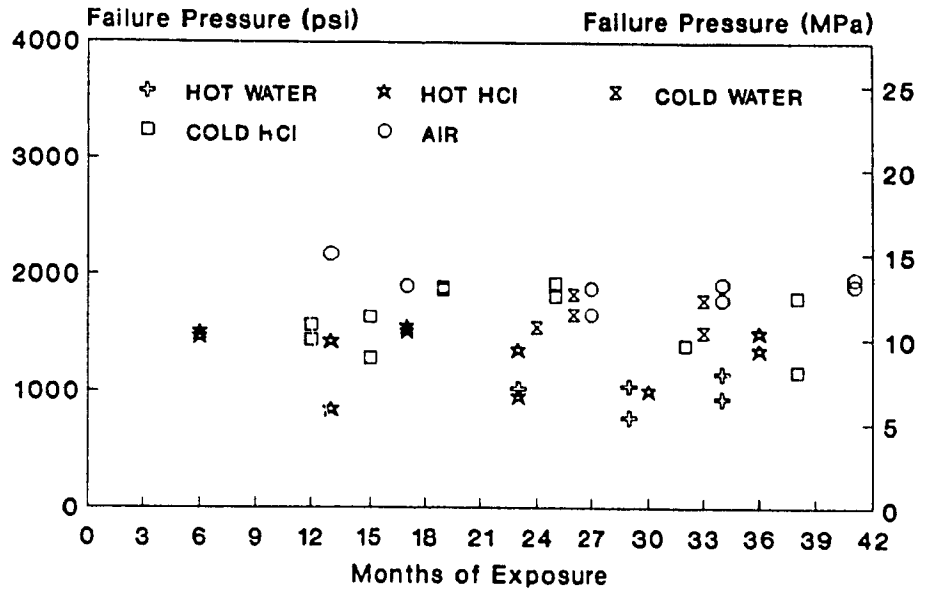

Fig. 7-11: Biaxial test failure pressure versus exposure time, veil lined tubes, all environments.

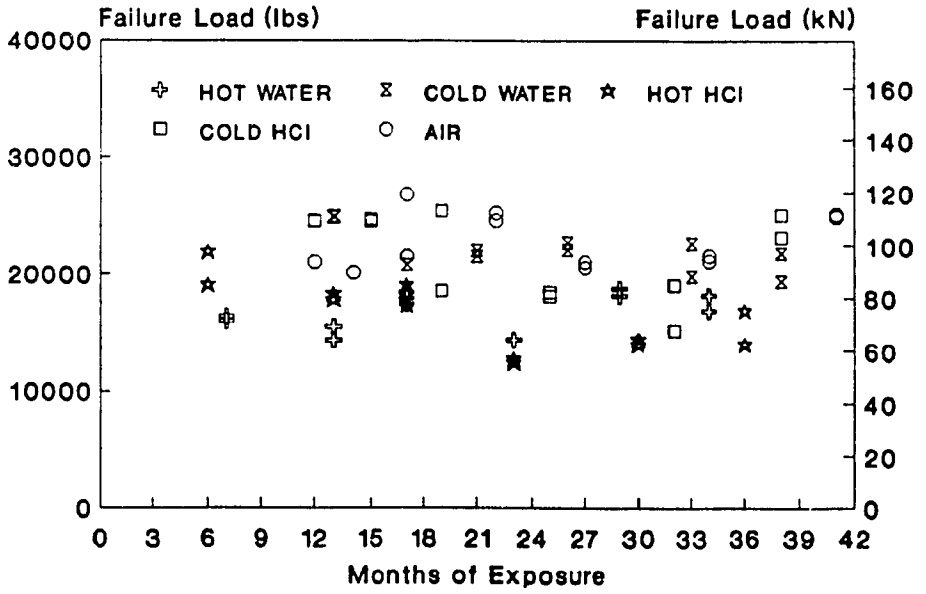

Fig. 7-12: Axial test failure load versus exposure time, veil lined tubes, all environments.

Despite a fair amount of scatter and differences in failure modes there is a common pattern in these three graphs. With reference to the air aged samples, those tubes exposed to the room temperature environments had roughly the same failure pressure or load as the air aged tubes. Tubes exposed to hot water or hot HCl had a significantly lower failure pressure or load than the air aged samples.

7.1.2 PVC Lined Tubes

Starting with the results from those tubes exposed to hot and cold water, Figure 7-13 shows hoop test failure pressure versus exposure time. There are several interesting features. First, for the cold water exposed tubes there is little difference in failure pressure between the explosive and crack and spray failures. Second, there is a fair amount of scatter in the hot water exposed tubes' results and third, the difference between the failure pressure of the hot water exposed tubes and the cold water exposed tubes is not as obvious as that seen with the hot and cold water aged veil lined tubes.

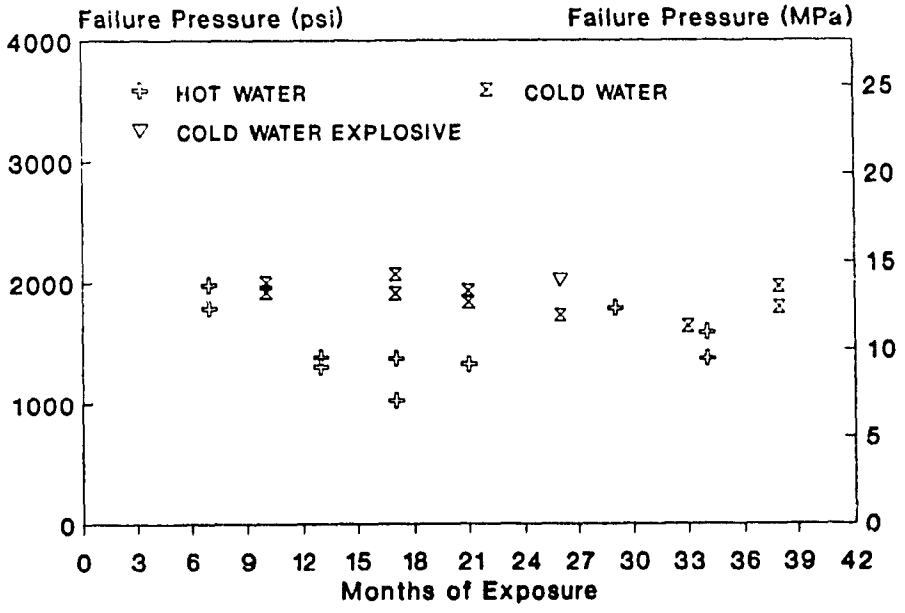

Fig. 7-13: Hoop test failure pressure versus exposure time, PVC lined tubes exposed to hot and cold water.

As a result, while it can be said that in general hot water exposed tubes fail at a lower pressure than those exposed to room temperature water, the highest failure pressure of the hot water tubes matches or slightly exceeds the room temperature exposed tubes lower failure pressures.

Failure pressure versus exposure time for the biaxial test results is shown in Fig. 7-14. This Figure appears to show that the hot water exposed tubes failed at pressures roughly equal to the room temperature aged tube's lowest failure pressure.

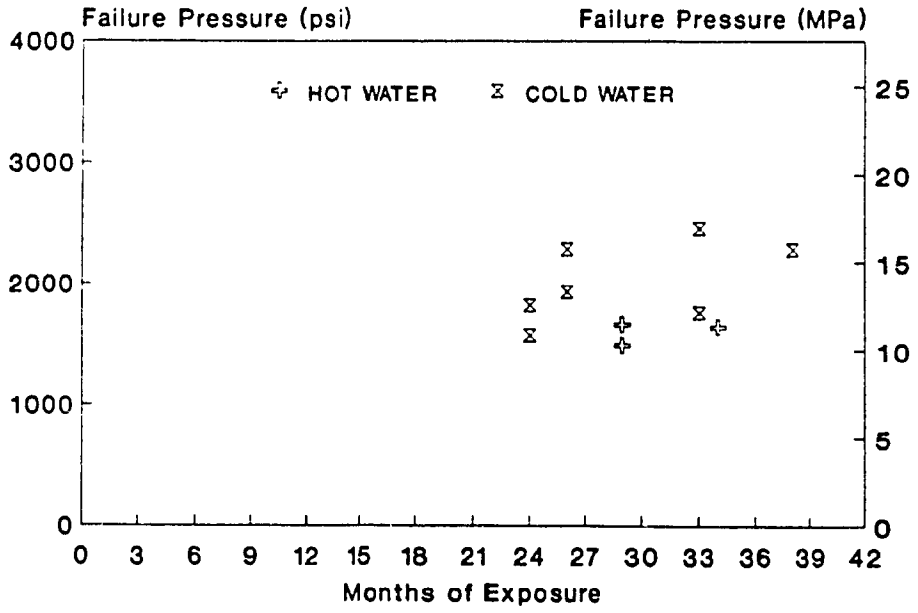

Fig. 7-14: Biaxial test failure pressure versus exposure time, PVC lined tubes exposed to hot and cold water.

The axial test results, shown in Fig. 7-15, are so close that in this case the two groups of tubes appear to be about equal in terms of performance.

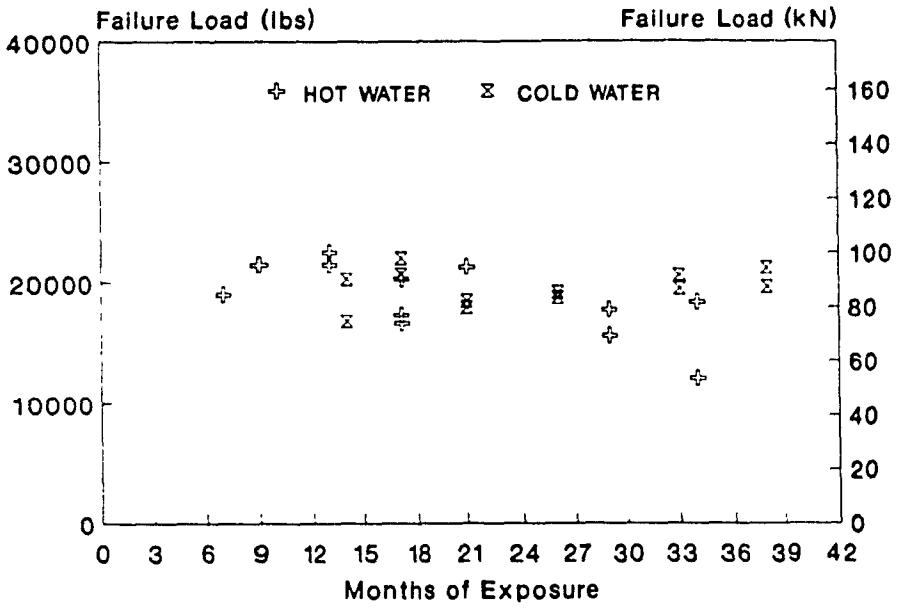

Fig. 7-15: Axial test failure load versus exposure time, PVC lined tubes exposed to hot and cold water.

Plotting failure pressure versus exposure time for the hoop and biaxial test results of the PVC lined tubes exposed to hot and room temperature HCl are shown in Figures 7-16, and 7-17.

Even when the different failure modes are accounted for, Figure 7-16 shows a very high degree of scatter in the results. Comparing the crack and spray type failure results (non-explosive) it appears that the cold HCl exposed tubes fail at a higher pressure than the hot HCl exposed tubes. The hot HCl explosive failures where also higher than the hot HCl non-explosive failures. No clear conclusion can be reached with the cold HCl explosive failures.

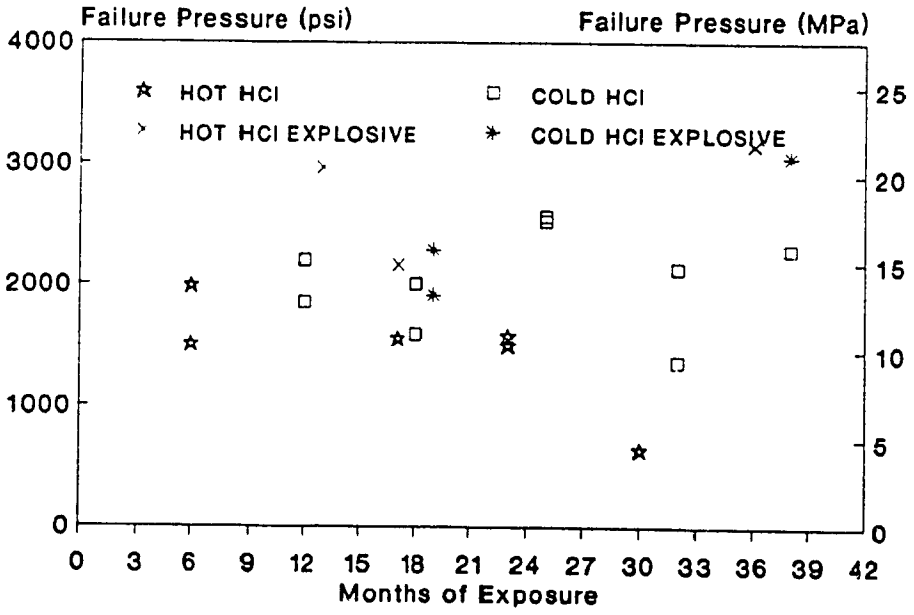

Fig. 7-16: Hoop test failure pressure versus exposure time, PVC lined tubes exposed to hot and cold HCl.

The results for the biaxial test, shown in Figure 7-17, shows that the hot HCl exposed tubes failed at lower pressures than the cold HCl exposed tubes.

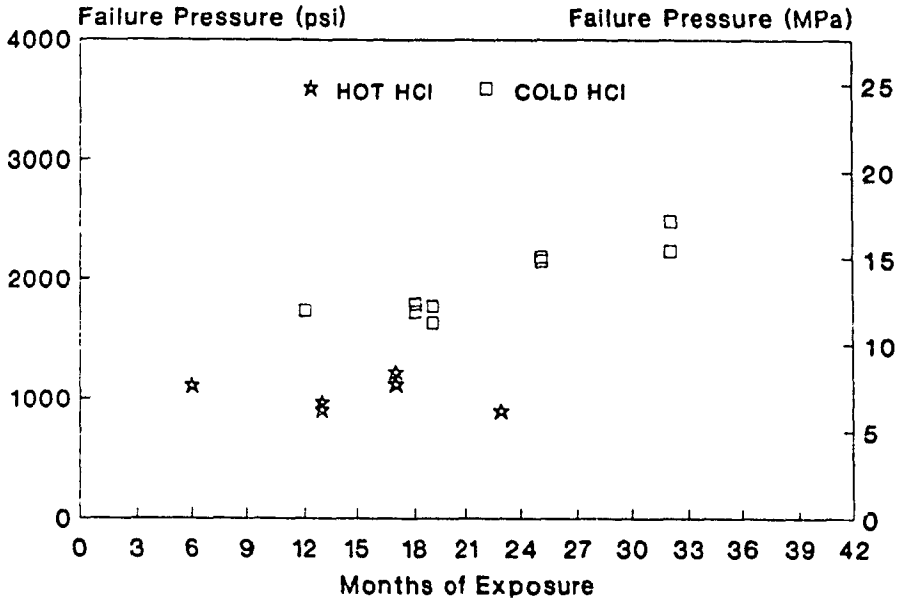

Fig. 7-17: Biaxial test failure pressure versus exposure time, PVC lined tubes exposed to hot and cold HCl.

Plotting failure load versus time for the PVC lined tubes exposed to hot and cold HCl, Figure 7-18, shows that there was little difference in the failure load of the hot and cold HCl exposed tubes. The result is similar to that seen in Fig. 7-15.

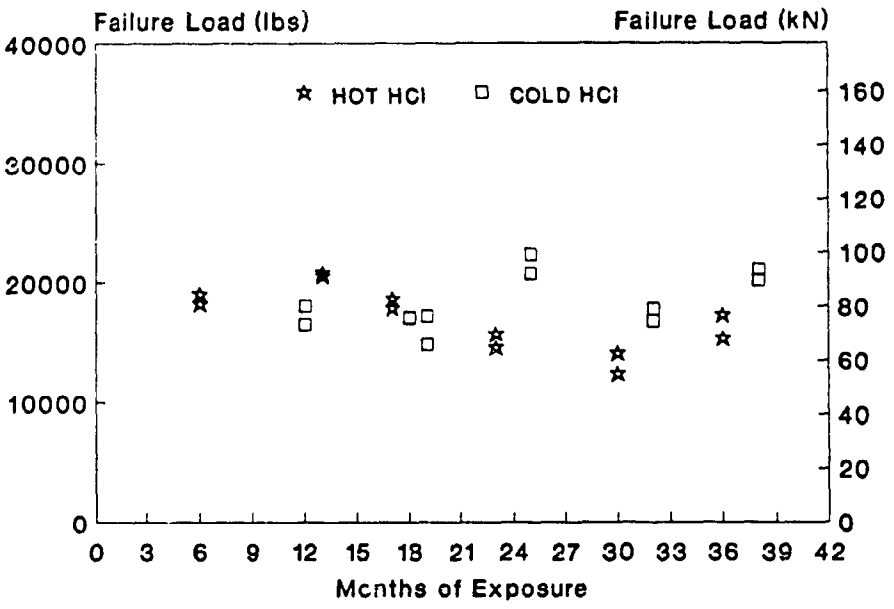

Fig. 7-18: Axial test failure load versus exposure time, PVC lined tubes exposed to hot and cold HCl.

The final two environments to be considered are air and sulfuric acid. From the hoop test results, Figure 7-19 shows that the non-explosive failure pressure of the sulfuric acid exposed tubes seems to decrease with increasing exposure time. The pressure of the first explosive failure was significantly higher than the highest non-explosive failure pressure. The pressure of the second explosive failure is slightly lower than the highest non-explosive failure pressure, but significantly higher than its test point companion. In both cases the tubes share a common mother tube, 26C for test point 3 (19 months) and 27B for test point 5 (32 months). The two results from air exposed tubes had failure pressures slightly below the lowest results for sulfuric acid exposure.

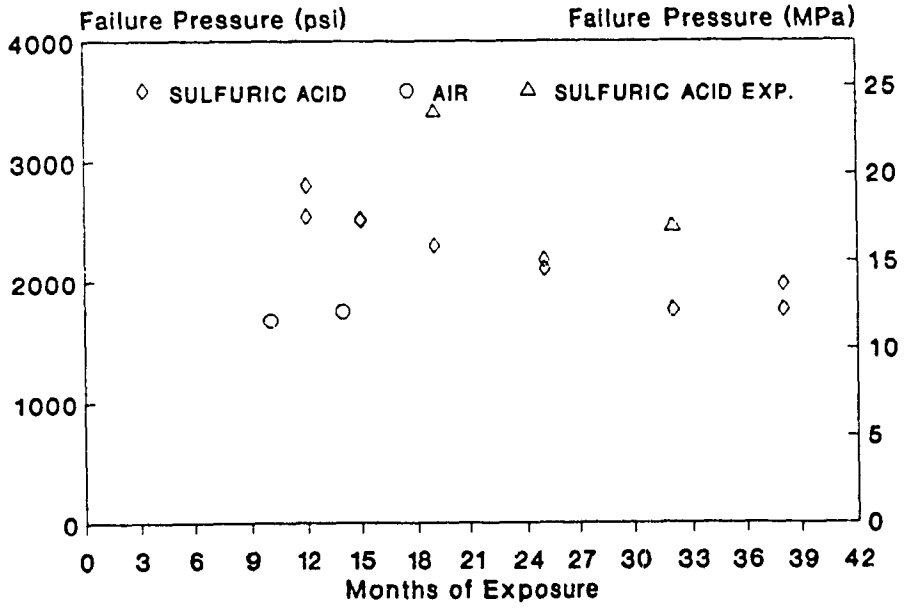

Fig. 7-19: Hoop test failure pressure versus exposure time, PVC lined tubes exposed to sulfuric acid and air.

From the biaxial test results, Fig. 7-20 also shows that the sulfuric acid aged tubes seemed to have a decreasing failure pressure with increasing exposure time.

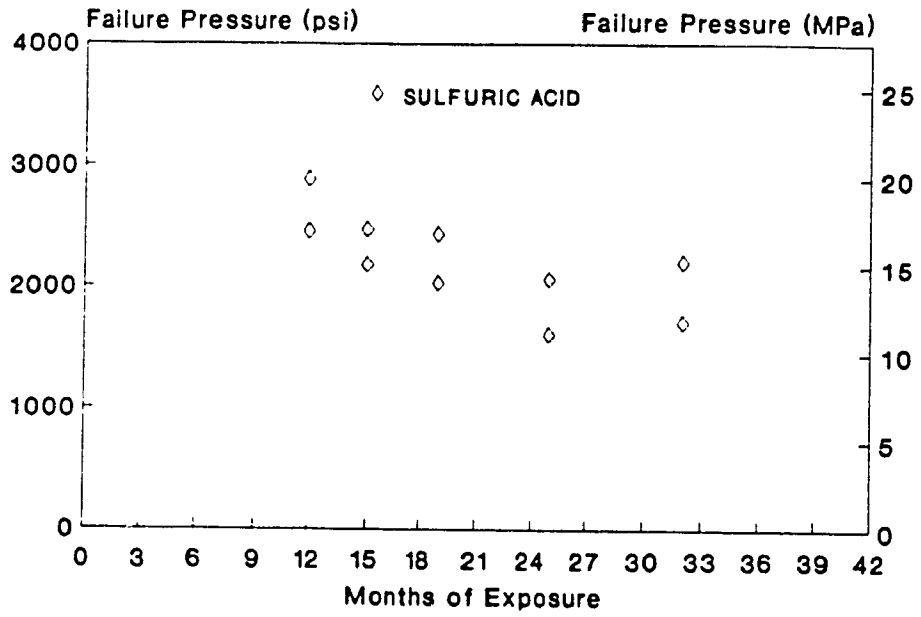

Fig. 7-20: Biaxial test failure pressure versus exposure time, PVC lined tubes exposed to sulfuric acid.

From the axial test results, the failure load of the sulfuric acid and air aged tubes versus exposure time is shown in Fig. 7-21. It shows that the air exposed tubes' failure load is comparable to that of the sulfuric acid aged tubes. For the sulfuric acid exposed tubes, the scatter in the results obscures any tends in the results.

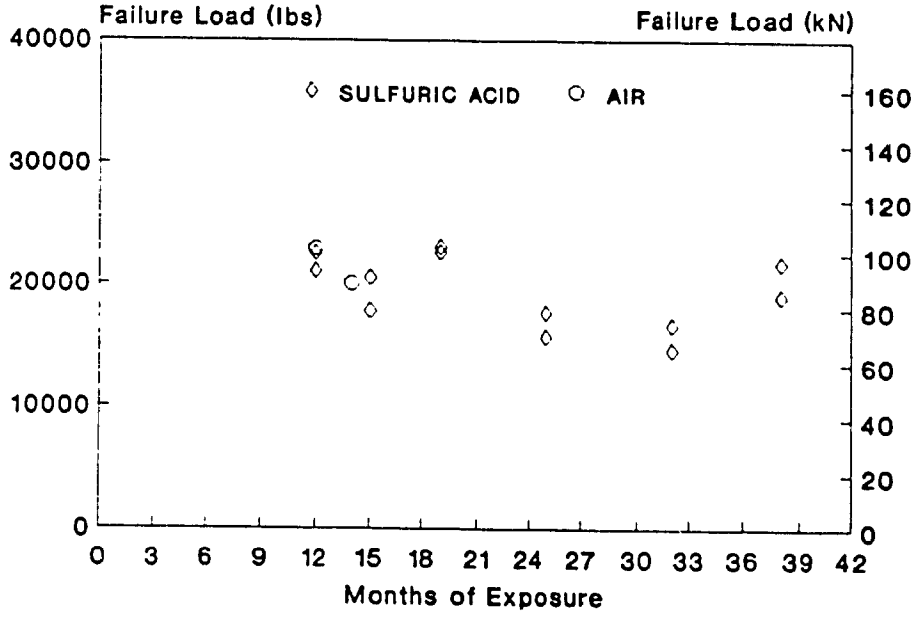

Fig. 7-21: Axial test failure load versus exposure time, PVC lined tubes exposed to sulfuric acid and air.

The final three graphs, Figures 7-22, 7-23, and 7-24, show the results for the PVC lined tubes from each test with all the environments graphed together.

From the hoop test results, Fig. 7-22, it appears that the lower failure pressures tended to be from hot water and hot HCl exposed tubes with non-explosive failure.

In Fig. 7-23, combining the biaxial test results showed that the hot HCl exposed and hot water exposed tubes had the lowest failure pressures.

In Fig. 7-24, combining the axial test results showed that all tubes had about the same performance.

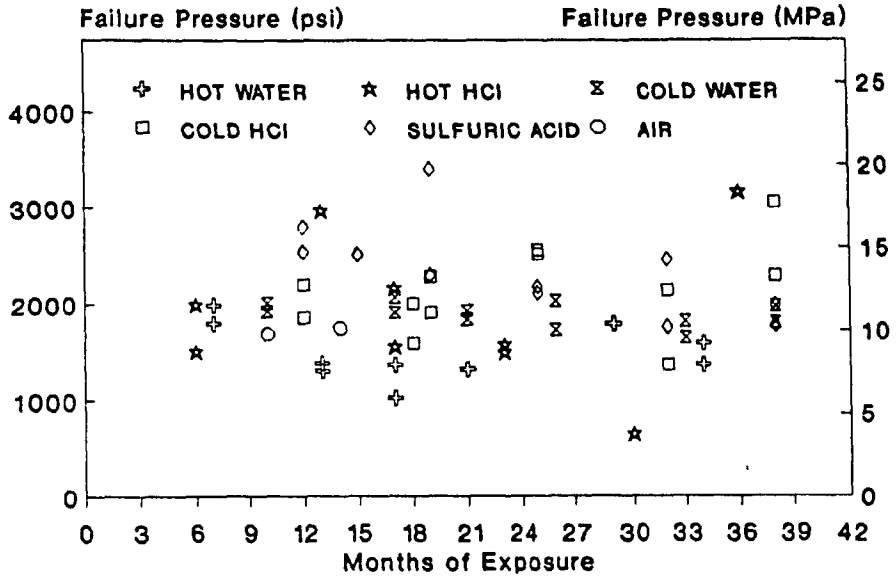

Fig. 7-22: Hoop test failure pressure versus exposure time, PVC lined tubes, all environments.

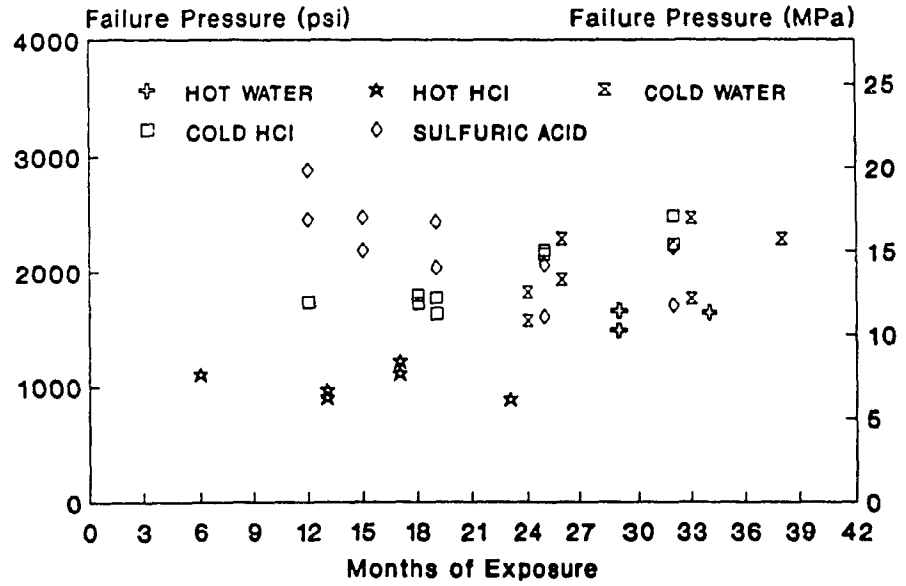

Fig. 7-23: Biaxial test failure pressure versus exposure time, PVC lined tubes, all environments.

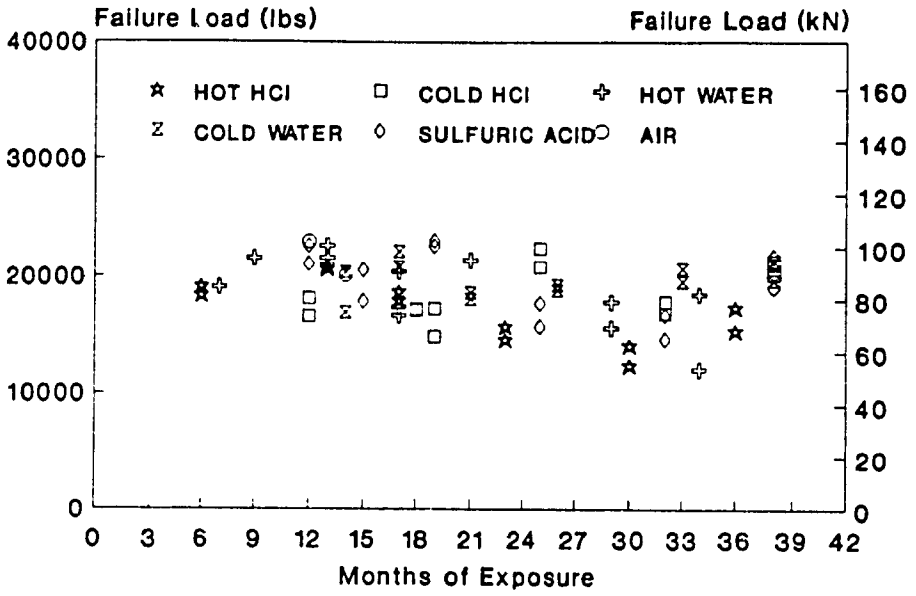

Fig. 7-24: Axial test failure load versus exposure time, PVC lined tubes, all environments.

7.2 $\bar{x}$, s and V of Failure Pressure or Load

The next obvious step is to calculate the mean ($\bar{x}$), standard deviation (s) and coefficient of variance (V) for the failure pressure and failure load results for each liner/environment combination.

For the hoop test results the mean, standard of deviation and coefficient of variance are given in Table 7-1. Note that the PVC lined tubes' results are only for the crack and spray failure results.

Table 7-1: Mean failure pressures, standard deviation, and coefficient of variance. Hoop test results.

		WATER		HCl (35%)		H_2SO_4
	AIR	20°C	80°C	20°C	50°C	(98%)
VEIL TYPE I	12.57 1.01 8.1%	11.29 1.12 9.4%	6.83 0.85 12.5%	11.62 1.72 14.8%	5.86 1.33 22.7%	
VEIL TYPE II	---	10.96 ---	5.28 0.65 12.2%	---	5.83 1.41 24.1%	
PVC	11.82 ---	12.97 0.89 6.9%	10.47 1.99 19.0%	14.16 2.76 19.6%	11.14 1.41 12.7%	15.49 2.41 15.5%

$\bar{x}$ and s are in MPa

For the veil lined tubes Table 7-1 shows that air has the highest mean failure pressure followed closely by cold water then cold HCl. There is then a significant drop to the mean failure pressure of hot water which is followed closely by hot HCl. The coefficient of variance varies

For the PVC lined tubes, Table 7-1 shows that the highest mean failure pressure was from tubes exposed to sulfuric acid. The next highest mean failure pressure was from tubes exposed to cold HCl, then cold water, air, hot HCl and the lowest was hot water.

Table 7-2 gives the mean, variance and coefficient of variance for the results from the biaxial test. For the veil lined tubes the highest mean failure pressure was from specimens exposed to air. The next highest was cold water followed closely by cold HCl. There is a significant drop to the mean failure pressure of the hot HCl tubes and another significant drop to the lowest mean failure pressure, that for hot water exposed tubes.

Table 7-2: Mean failure pressure, standard deviation, and coefficient of variance. Biaxial test results.

		WATER		HCl (35%)		H_2SO_4
	AIR	20°C	80°C	20°C	50°C	(98%)
VEIL	13.29 0.82 6.3%	11.45 0.99 8.6%	6.77 0.98 14.5%	11.12 1.83 16.4%	9.03 1.76 19.5%	
PVC		13.89 1.26 16.3%	11.00 0.63 5.8%	13.38 2.00 14.9%	7.09 0.90 12.7%	15.19 2.61 17.2%

$\bar{x}$ and s are in MPa

For the PVC lined tubes under biaxial stress, Table 7-2 shows the highest mean failure pressure is found with the sulfuric acid aged specimens followed by cold water, and cold HCl. The mean failure pressure of tubes exposed to hot water is some 2.3 MPa below cold HCl and tubes exposed to hot HCl have a mean failure pressure 6.54 MPa below cold HCl.

Table 7-3 shows the mean, standard deviation, coefficient of variance for the results from the axial test.

For the veil lined tubes the highest mean failure load is shown by air exposed specimens. The second highest failure load is shown by cold HCl followed closely by cold water. There is a significant drop in mean failure load for the hot HCl specimens which is followed closely by the hot water aged tubes which have the lowest mean failure load.

Table 7-3: Mean failure load, standard deviation, and coefficient of variance. Axial test results.

		WATER		HCl (35%)		H_2SO_4
	AIR	20°C	80°C	20°C	50°C	(98%)
VEIL	101.19 10.29 10.2%	96.20 9.39 9.8%	74.95 6.85 9.1%	96.56 16.02 16.6%	73.21 12.07 17.9%	
PVC	95.35 9.04 9.5%	87.16 6.56 7.5%	82.91 13.52 16.3%	81.19 9.98 12.3%	75.47 11.80 15.6%	86.19 12.88 14.9%

$\bar{x}$ and s are in kN

For the PVC lined tubes, Table 7-3 shows that the highest mean failure load is shown by the air aged tubes. In descending order, the mean failure load is as follows: cold water, sulfuric acid, hot water, cold HCl, and hot HCl.

In general, these results show that the highest failure loads/pressures are found with tubes that are aged in air or sulfuric acid. The next highest failure loads/pressures are found with the room temperature water and HCl. The lowest failure loads/pressures are found with the hot HCl and hot water exposed specimens. This trend was found with both the PVC lined and veil lined tubes.

7.3 Experimental Strain at Failure versus Theoretical

By plotting the experimental strain at failure onto the appropriate strain space failure envelope and loading path graph, it is possible to compare the experimental and theoretical results.

7.3.1 Veil Lined Tubes

The surface strain at failure from the hoop, biaxial and axial tests for the veil lined tubes are plotted onto the theoretical strain space failure envelope for the veil lined tubes in Fig. 7-25.

The results from the biaxial and axial tests form clusters along their respective theoretical loading paths while the hoop test results form a cluster just to the left of their theoretical loading path. The results for all test start well inside the failure envelope. The result from the hoop and axial tests extend to the mat layer failure envelope while the biaxial results extend to the edge of the filament winding layer failure envelope.

Figure 7-26 shows the hoop test results alone. The results from the hot water, water and air aged specimens form distinct clusters. The results from the hot HCl exposed tubes are spread out slightly along the hoop loading path while the results from the cold HCl exposed tubes are well spread out.

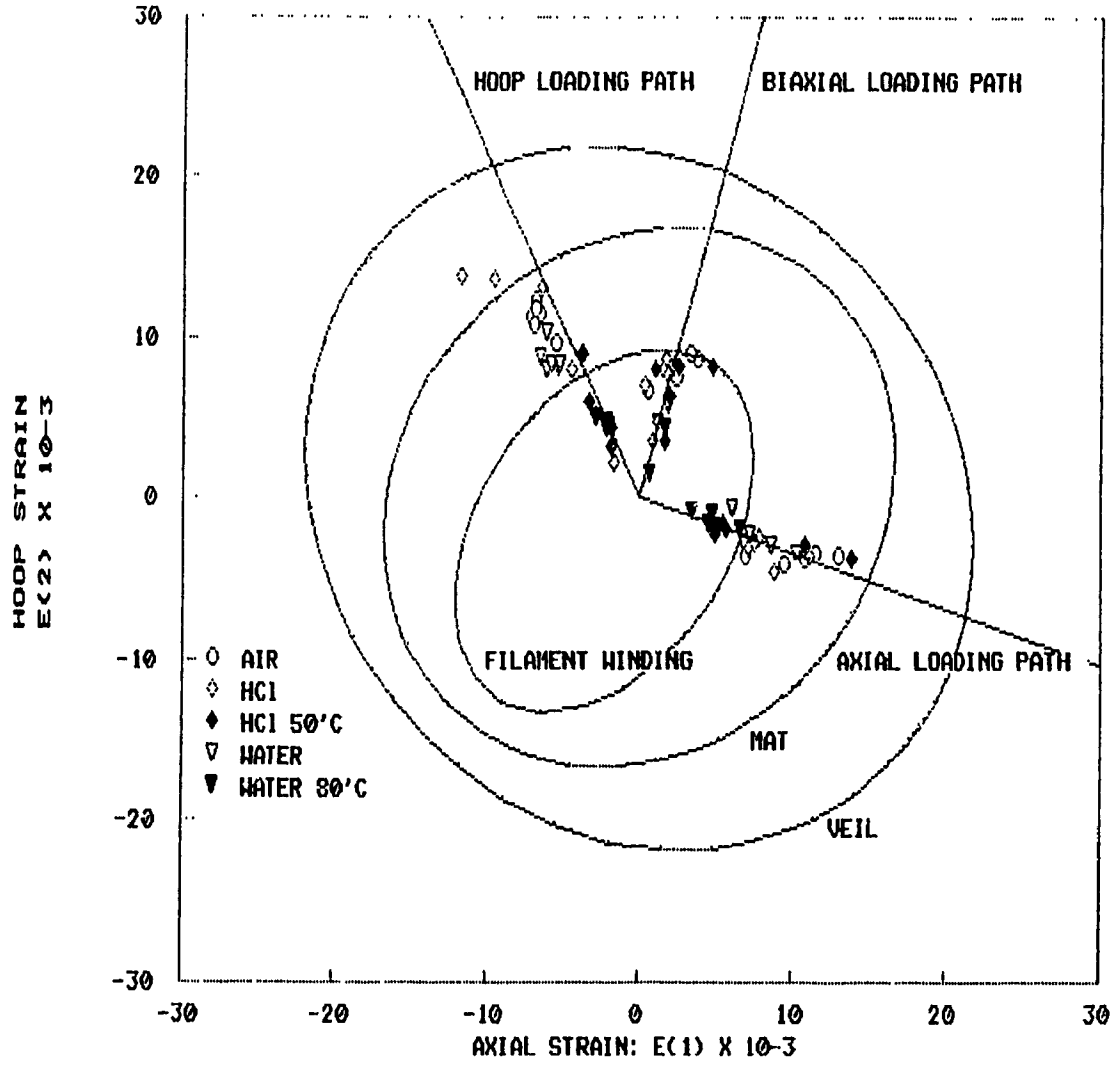

Fig. 7-25: Experimental results plotted onto the theoretical failure envelopes and loading paths in strain space, veil lined tubes.

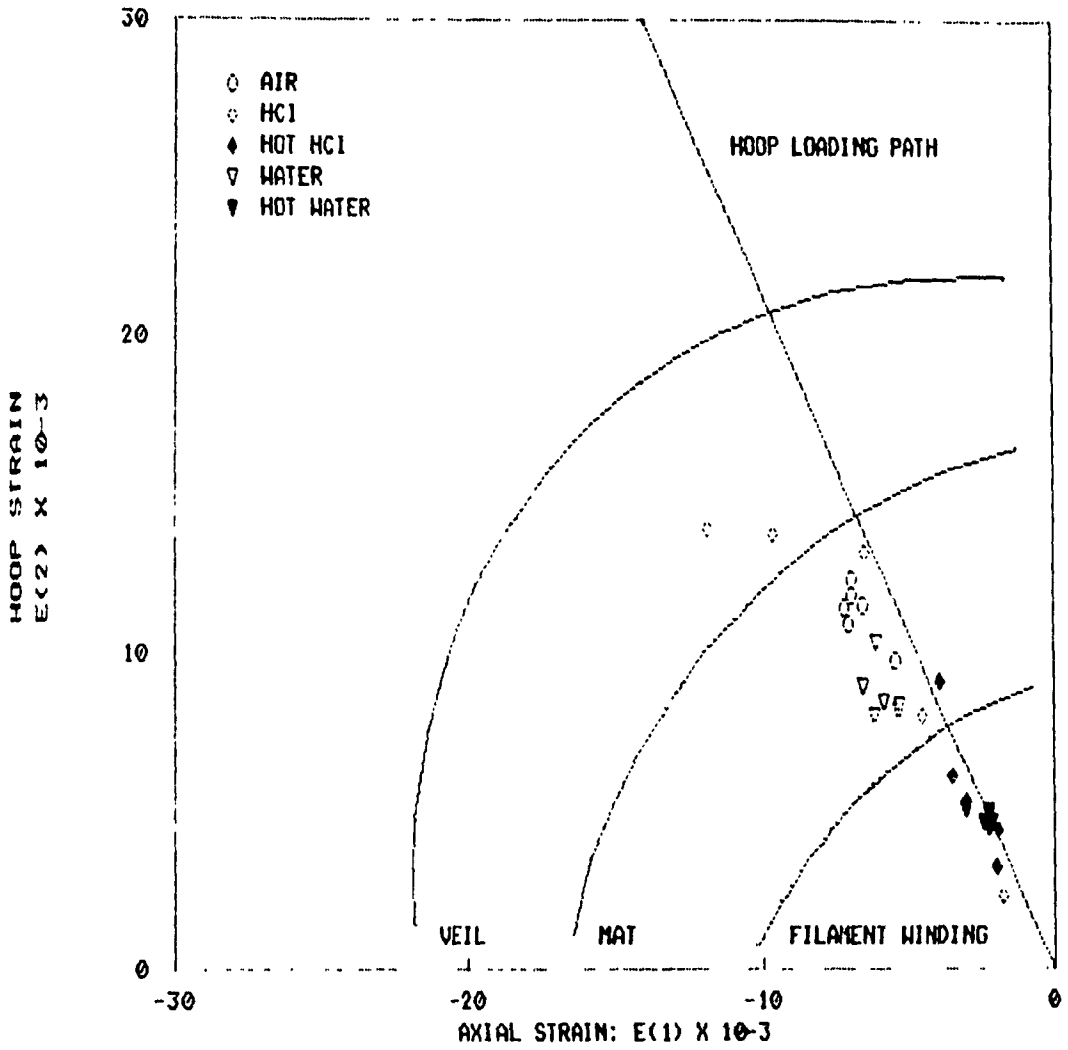

Fig. 7-26: Experimental results plotted onto the theoretical failure envelopes and loading paths in strain space, veil lined tubes, hoop test.

The lowest failure strain is generally shown by those tubes exposed to hot HCl and hot water. The next highest was the water aged tube results followed by the air aged tube results. The tubes exposed to room temperature HCl produced the highest and lowest failure strains recorded. The results from the hot HCl exposed tubes were also spread out along the loading path direction, but to a much lesser degree than the room temperature HCl results. From lowest to highest strain at failure the ranking would be hot water, hot HCl, water, then air.

Fig. 7-27 shows a close-up of the results for the veil lined tubes under biaxial loading. The results for all environments are spread out along the loading path direction and due to the limited results and scatter, no firm trends can be established.

Figure 7-28 shows the results for the veil lined tubes under axial loading. As a group, the lowest failure strain is shown by those tubes exposed to hot water. The results for other the environments are scattered along the loading path.

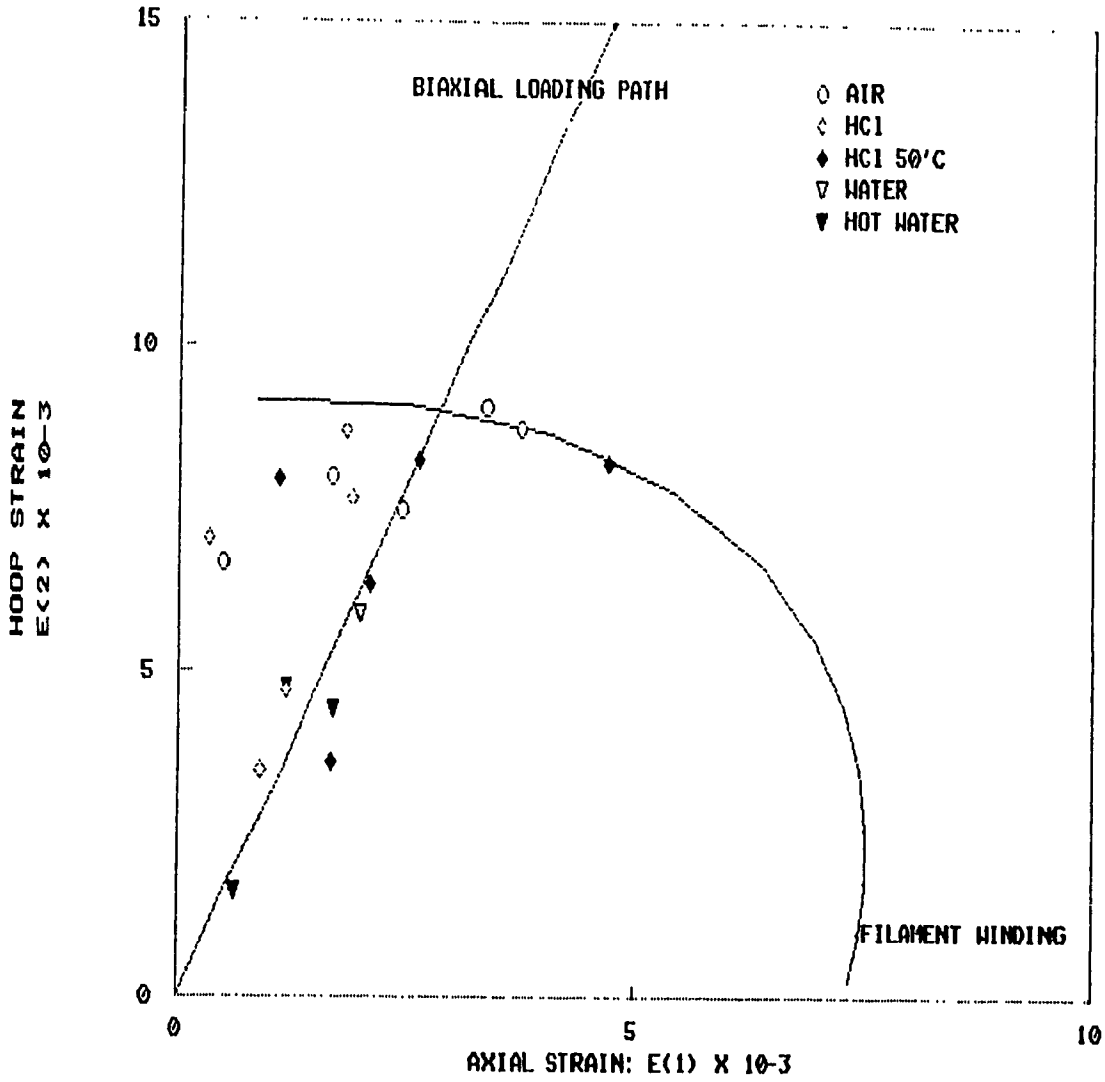

Fig. 7-27: Experimental results plotted onto the theoretical failure envelopes and loading paths in strain space, veil lined tubes, biaxial test.

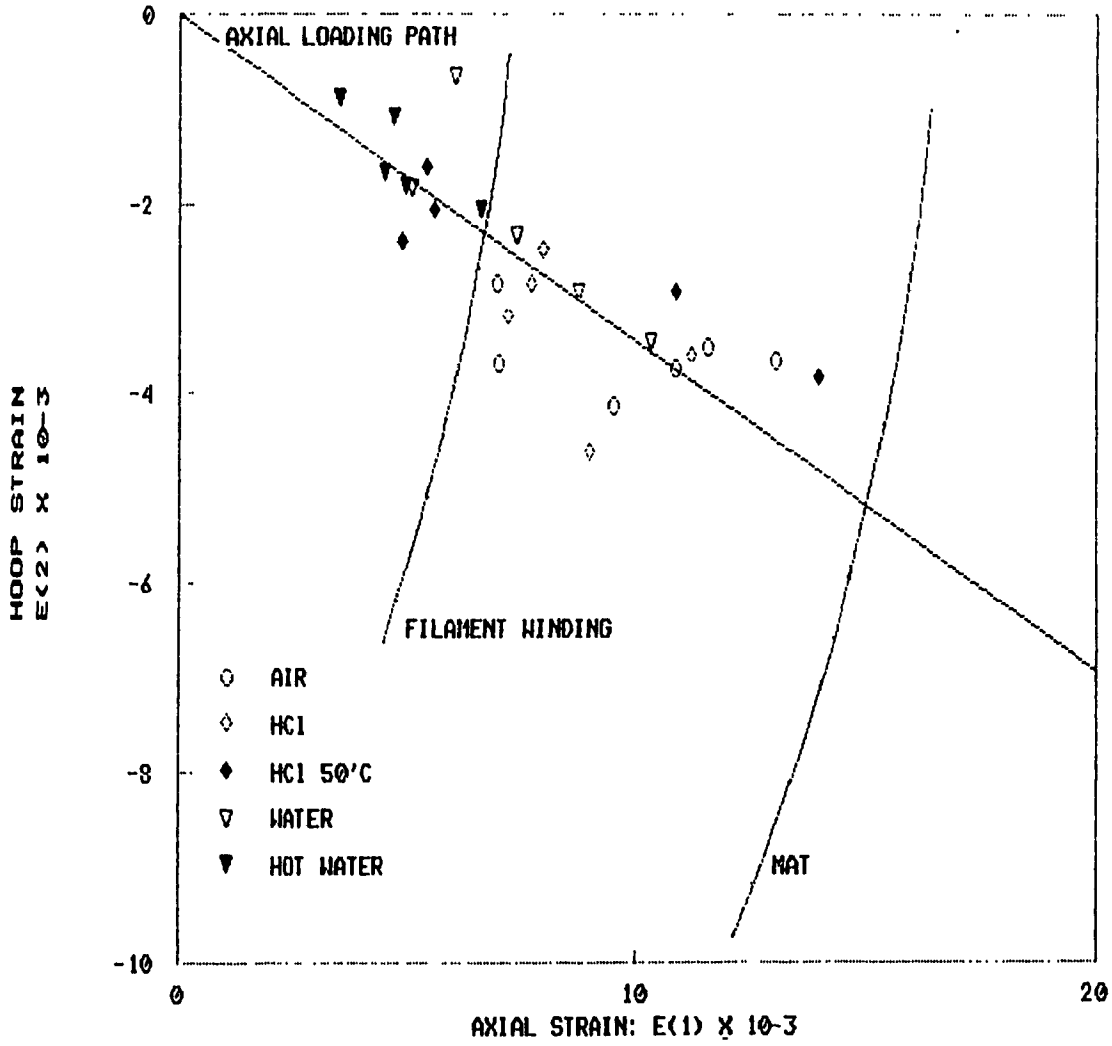

Fig. 7-28: Experimental results plotted onto the theoretical failure envelopes and loading paths in strain space, veil lined tubes, axial test.

7.3.2 PVC Lined Tubes

Fig. 7-29 shows the experimental axial and hoop strain results from the hoop, axial and biaxial tests plotted in strain space along with the theoretical failure envelopes for the PVC lined tubes.

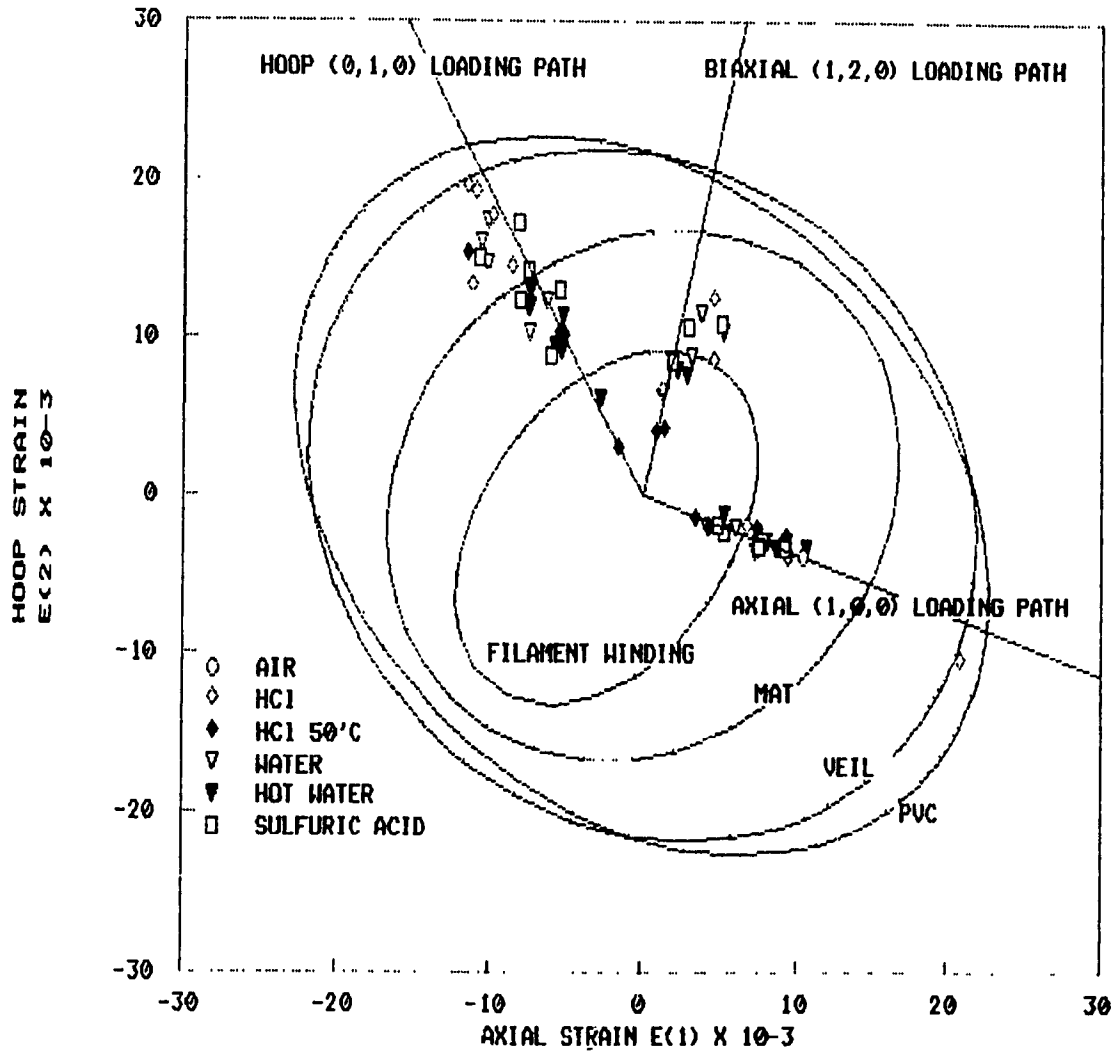

Fig. 7-29: Experimental results plotted onto the theoretical failure envelopes and loading paths in strain space, PVC lined tubes.

The results for all tests are clustered along their respective loading paths. The experimental results for the axial test form a tight cluster centered near the theoretical first ply failure point, with the exception of one point. The experimental results for the biaxial test form a cluster that is centered near the theoretical first ply failure point for biaxial loading. However, this cluster shows a lower Poisson's ratio than the theoretical value. The experimental results from the hoop test form a cluster nearly centered on the theoretical hoop loading path. This cluster starts well inside the filament winding failure envelope and extends to the edge veil layer failure envelope.

This graph also has a few interesting points. The lowest strain at failure for all tests was from those tubes aged in hot HCl (solid diamond). The highest strain at failure was from those tubes exposed to room temperature HCl.

Fig. 7-30 is a close-up of the results from the hoop test on the PVC lined tubes. With the exception of one point, the lowest failure strains tended to be from those tubes exposed to hot HCl or hot water. The highest strains at failure were from those tubes exposed to cold HCl. Results from the other environments were scattered between the two extremes.

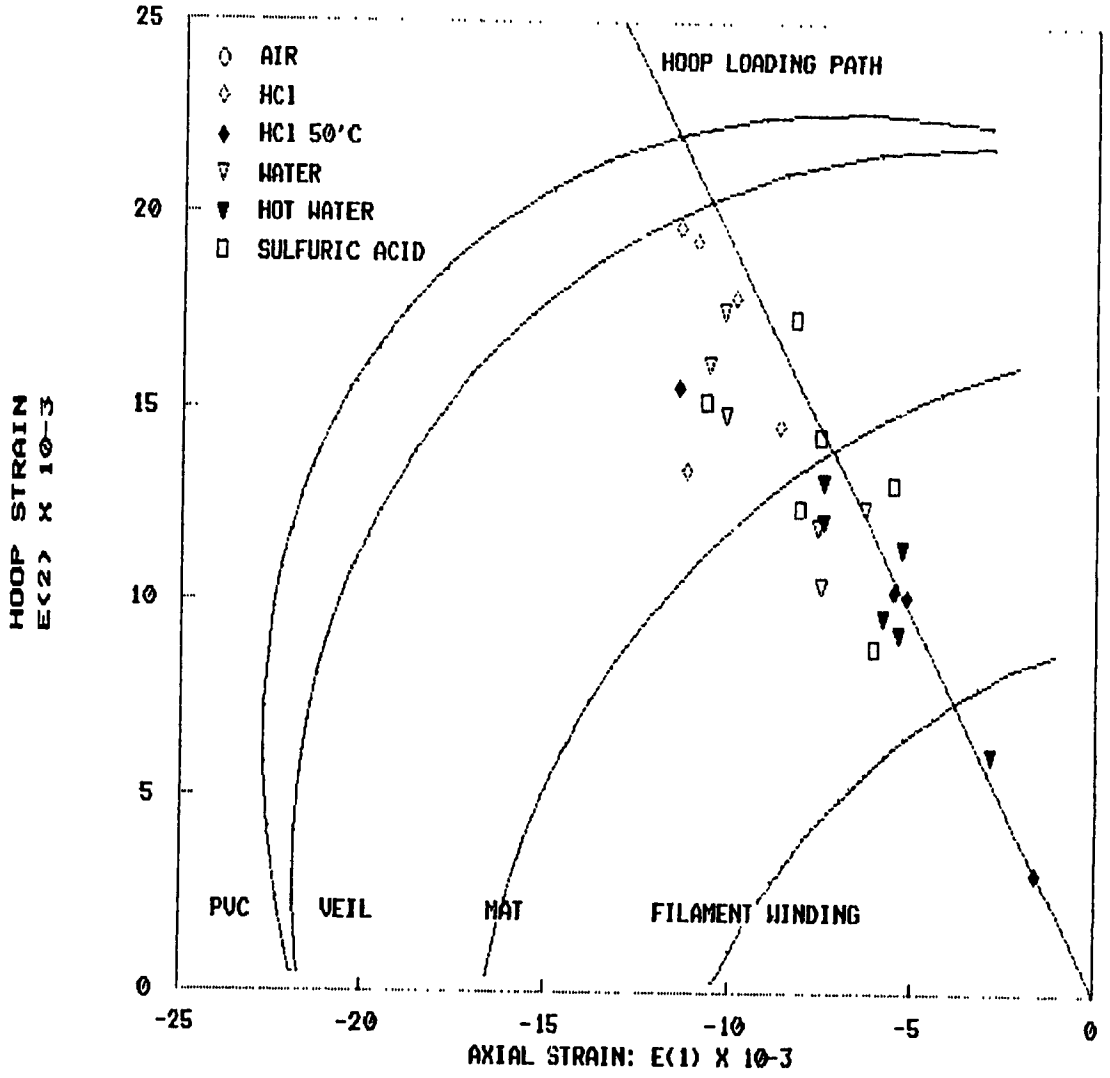

Fig. 7-30: Experimental results plotted onto the theoretical failure envelopes and loading paths in strain space. PVC lined tubes, hoop test.

Fig. 7-31 is a close-up of the results from the biaxial test on the PVC lined tubes. Due to the limited results and scatter no clear trends could be determined. However, the lowest failure strains were shown by those tubes exposed to hot HCl.

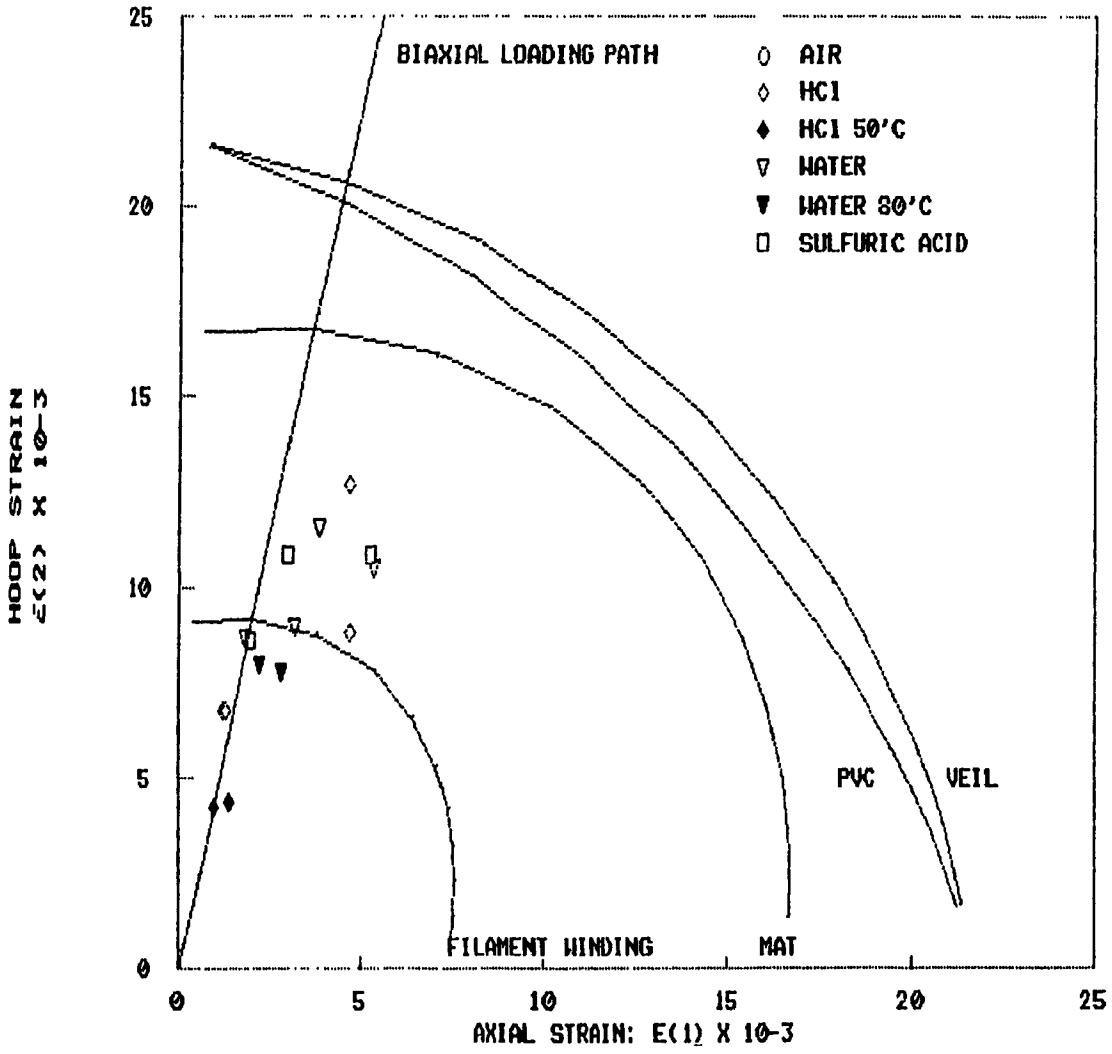

Fig. 7-31: Experimental results plotted onto the theoretical failure envelopes and loading paths in strain space. PVC lined tubes, biaxial test.

Fig. 7-32 is a close-up of the results from the axial test on the PVC lined tubes. For all environments except room temperature water, the failure strains are spread out along the loading path direction. For room temperature water, 4 of the 5 results run parallel to edge of the filament winding failure envelope.

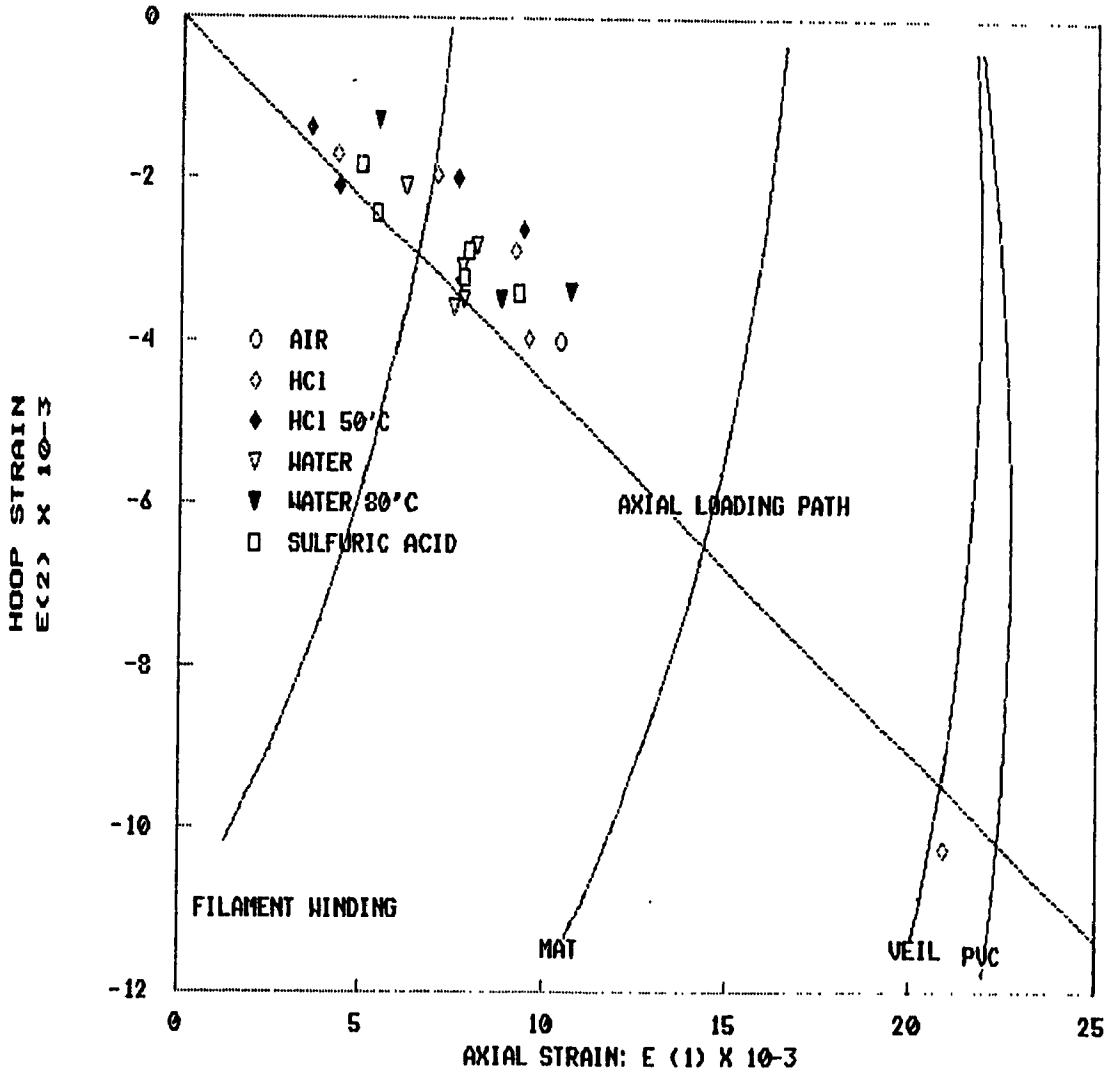

Fig. 7-32: Experimental results plotted onto the theoretical failure envelopes and loading paths in strain space. PVC lined tubes, axial test.

One obvious question with the results in this section is why the trends seen in section 7-1 are not apparent here? One explanation is that the failure pressure (or load) can be thought of as a global result for the whole tube, while the results from strain gauges are the highly localized results from the area where the strain gage is mounted.

7.4 Comparison of Experimental and Theoretical Modulus

Comparison of the experimental and theoretical modulus is done by plotting experimental and theoretical results on the same stress-strain graph. The theoretical stress-strain graphs were presented in Section 4.5. The experimental results come directly from the measured values recorded during testing.

Fig. 7-33 shows the experimental results from tube 15E-1K and the theoretical results for the hoop test on veil lined tubes plotted together. Initially both the hoop and axial strains match, but by 500 psi the lines start to diverge with the experimental results showing a lower modulus. The Poisson's ratio of the experimental and theoretical results are quite different. The experimental result starts lower than the theoretical results and rises steadily as pressure is increased. At roughly 5 MPa they match and at failure the experimental Poisson's ratio is well above the theoretical value.

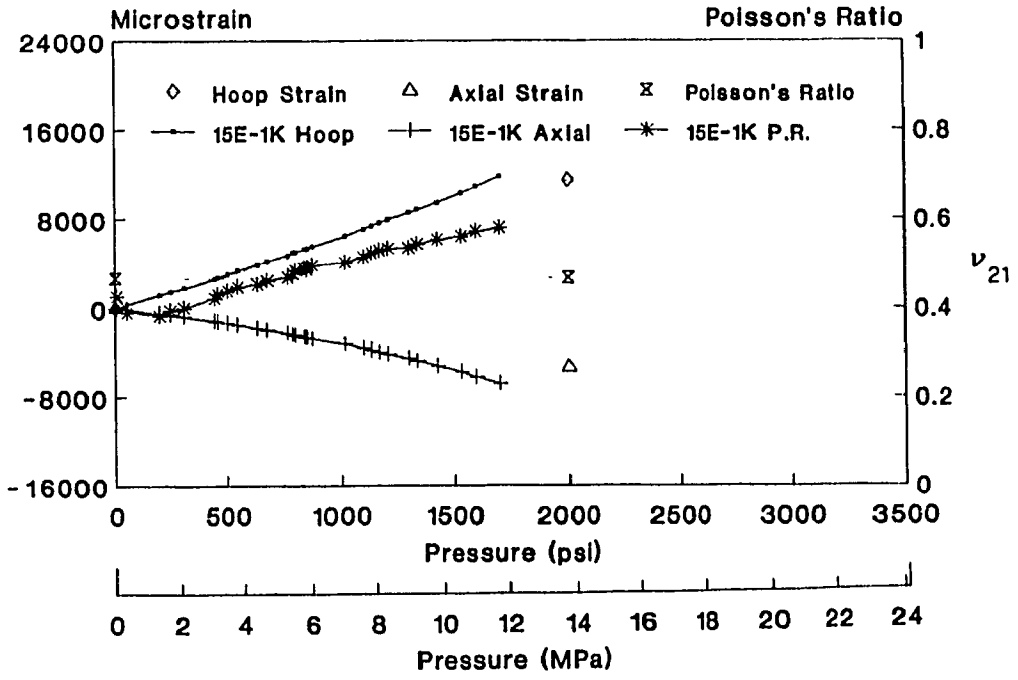

Fig. 7-33: Stress-strain graph, 15E-1K and theory (Hoop stress, veil lined tube).

Fig. 7-34 shows the results of tube 2D-2I plotted with the theoretical hoop strain, axial strain and Poisson's ratio for biaxial stress on a veil lined tube. In this case there is a near perfect match in axial strains while the experimental hoop strain is slightly lower than the theoretical one. The Poisson's ratios are also very close.

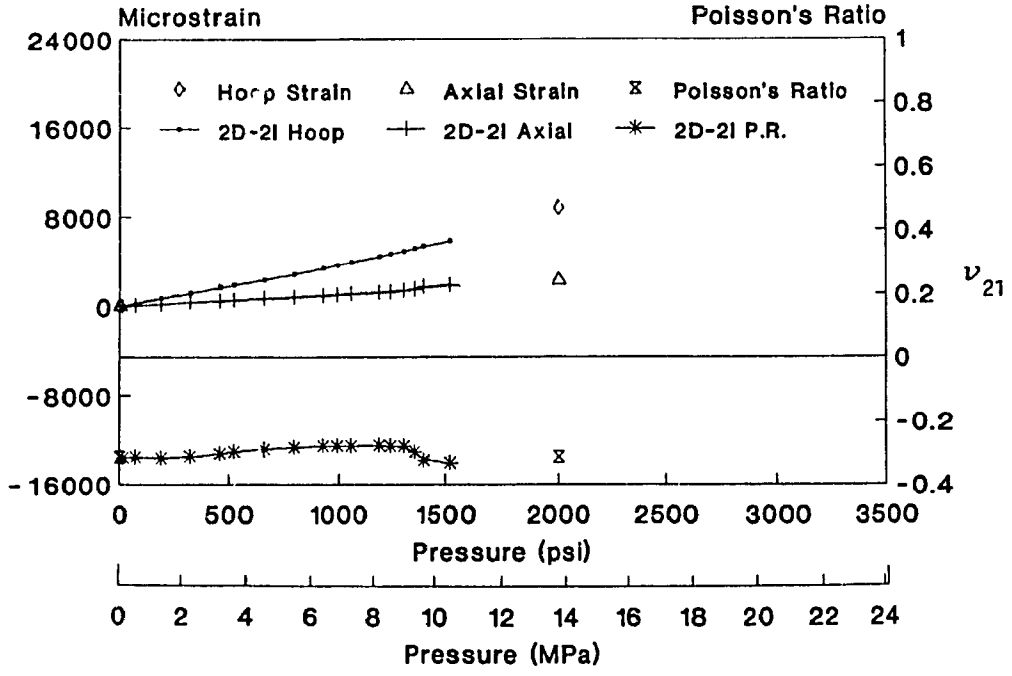

Fig. 7-34: Stress-strain graph, 2D-2I and theory.
(Biaxial stress, veil lined tube)

Fig. 7-35 shows the results of tube 6C-3C plotted with the theoretical hoop strain, axial strain and Poisson's ratio for axial stress on a veil lined tube. The hoop and axial strains are very close and the experimental Poisson's ratio runs nearly parallel to, and slightly higher than the theoretical values.

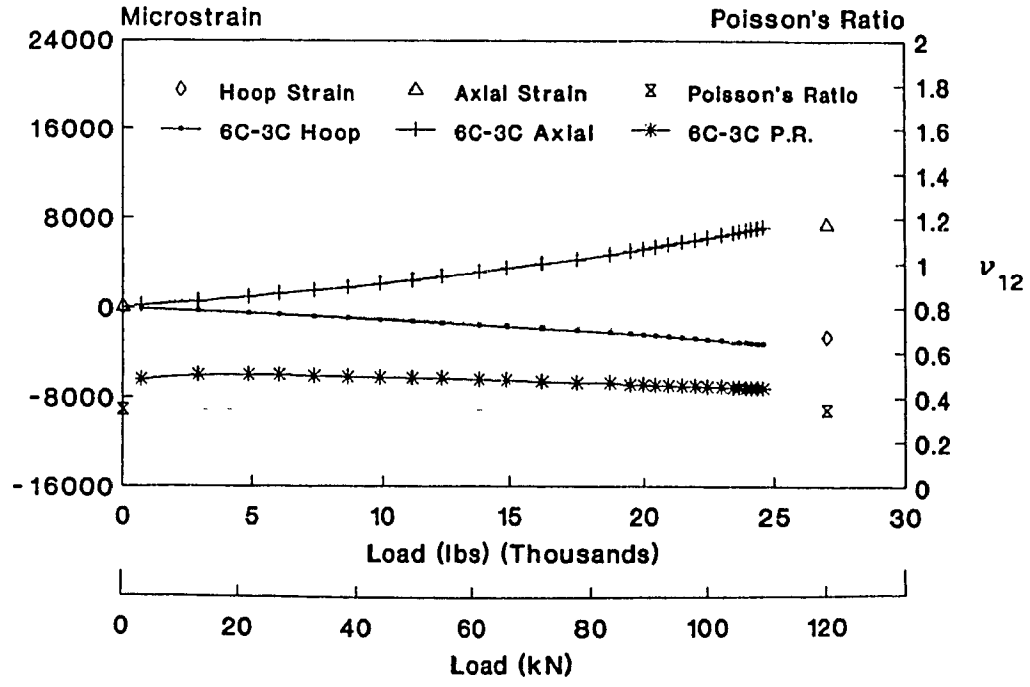

Fig. 7-35: Stress-strain graph, 6C-3C and theory.
(Axial stress, veil lined tube)

In Figure 7-36 tube 23E-1E's experimental results and the theoretical hoop, axial strain and Poisson's ratio for a PVC lined tube under hoop loading are plotted together. Fig. 7-36 shows that the experimental and theoretical hoop and axial strains are reasonably close. It also shows that the tube exhibits increasingly lower modulus with increasing pressure. There is a significant difference in Poisson's ratios.

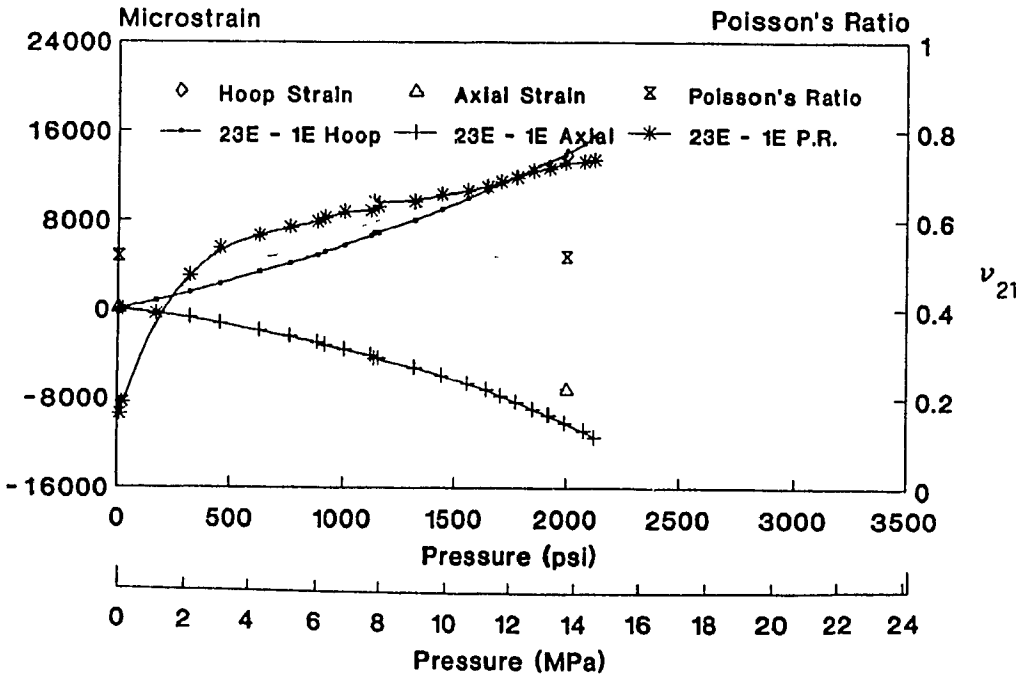

Fig. 7-36: Stress-strain graph, 23E-1E and theory (Hoop stress, PVC lined tube).

Fig. 7-37 shows very close agreement between the results for tube 26E-2G and the theoretical results for biaxial loading on a PVC lined tube.

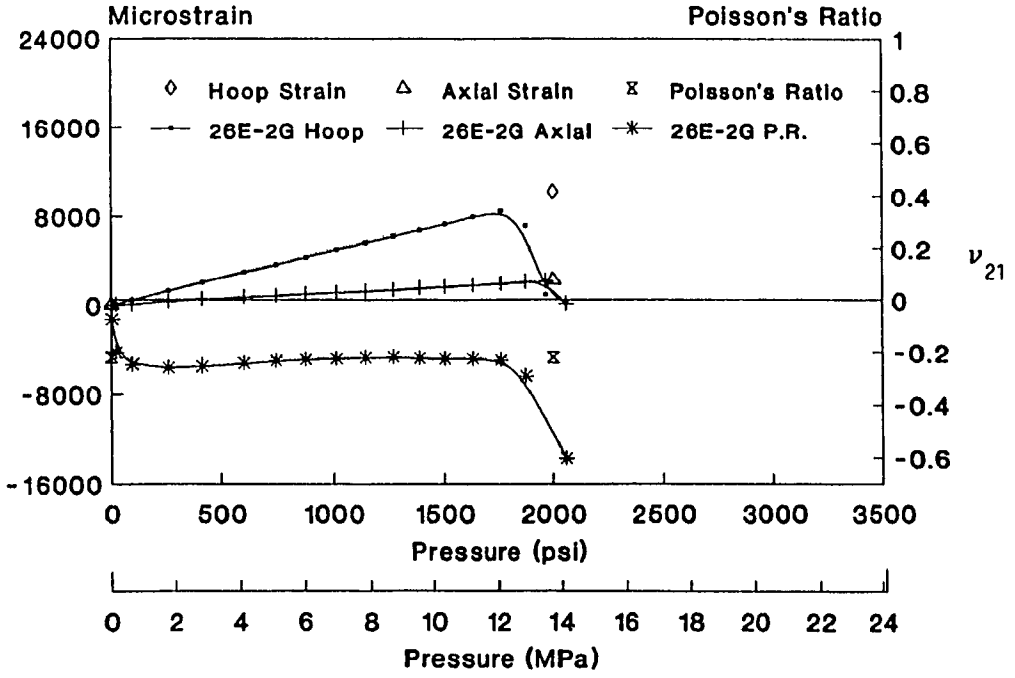

Fig. 7-37: Stress-strain graph, 26E-2G and theory.
(Biaxial stress, PVC lined tube)

Fig. 7-38 shows a close match in experimental and theoretical hoop strain, axial strain and Poisson's ratio for the results of tube 27B-3I and the theoretical results for axial loading on a PVC lined tube.

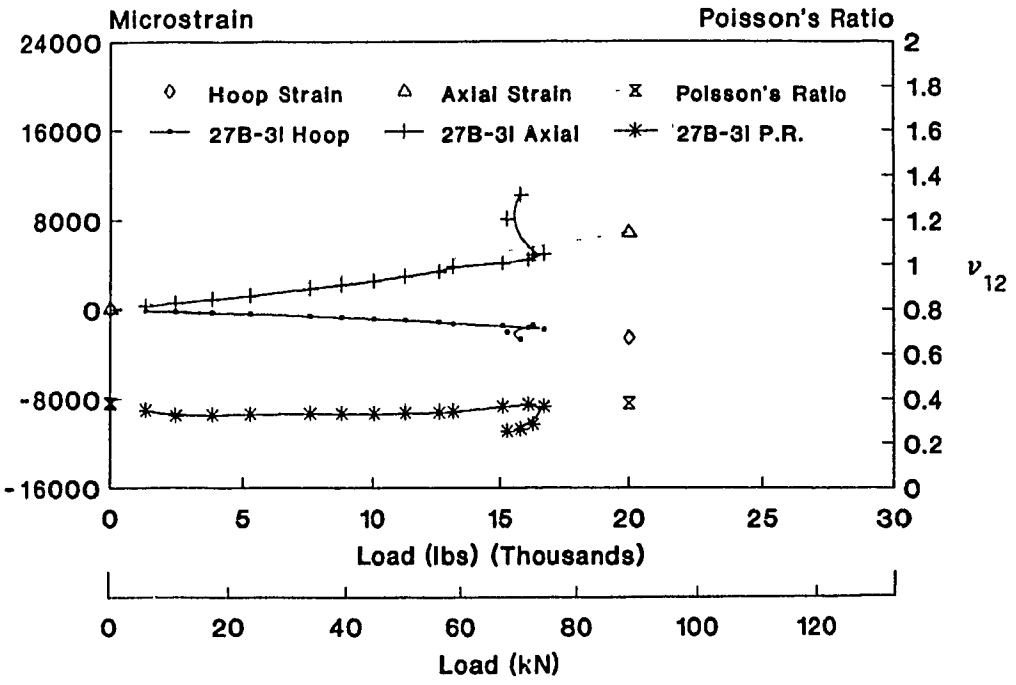

Fig. 7-38: Stress-strain graph, 27B-3I and theory.
(Axial stress, PVC lined tube)

It is interesting to note that no regard to environment was made when selecting an experimental graph. For the veil tube results air, 20°C water and 20°C HCl are covered and for the PVC tube results 50°C HCl and sulfuric acid are covered.

7.5 Explanation of Failure Modes

Failure in FRP is a complicated event. Unlike isotropic materials, the behavior of the components and their interactions with each other must be considered when discussing FRP failure. As this project's focus was not the study of failure patterns, the explanations of the observed failure modes presented here will be general. The weakest component of the tubes is the resin and in all the failures seen during testing resin failure was a common feature.

It is known that the resin rich corrosion barrier will crack at low stress. As the highest principle stress is in the hoop direction during the hoop and biaxial test, the development of cracks perpendicular to the applied stress direction can be expected. This explains the first visible signs of failure of the veil lined tubes during the hoop and biaxial test; a band of whitening along the longitudinal direction of the tube.

Once the crack is established it spreads through the matrix. Local conditions dictate its behavior. In the case of type II failure under hoop loading, the crack is limited to the corrosion liner. Weakened by exposure to 50°C HCl or 80°C water,the liner splits easily as the crack propagates along the length of the tube. Once the crack passes the O-ring, a path for the test fluid to leak out is established.

In the case of the type I failure under hoop loading and the biaxial test, where the end caps prevent type II failure, failure of the corrosion liner allows the high pressure test fluid to reach the filament winding layer. At the filament winding layer the crack propagates by delamination and transverse cracking. This process may be helped by the localized damage of the crack in the corrosion barrier, the in-plane shear stress produced by opposing filament winding layers and any interlaminar shear stresses due to free edge effects. Once a continuous path through the tube is established a jet of test fluid is seen.

In the case of a PVC lined tube, the PVC layer acts like a liner. In the case of the nonexplosive failure under hoop stress the liner, veil and mat layers develop a common split down the length of the tube. The starting point of this failure is believed to be the mat layer as it reaches its tensile strength first. As the remaining intact layers take up the wall stress, the veil and PVC layer exceed their tensile strengths and fail and the liner crack develops. When the high pressure fluid reaches the filament winding layer it burrows through by delamination and transverse cracks assisted by the mechanisms mentioned above for the veil lined tubes.

Under biaxial stress, the PVC lined tubes had multiple cracks. In this case the PVC liner acts like a ruptured balloon, a small crack spreads through the liner in a pattern similar to a balloon tearing itself apart when punctured.

The explosive failure mode of the PVC lined tubes is centered on the PVC liner. In this case the PVC acts as a flexible liner. At first there is a small area of resin failure, it cracks and breaks up producing a spot of whitening. The filament winding strands are now free to move and realign themselves to support the load. As the internal pressure increases so does the pressure on this weak spot causing it to grow. At some point, without the load distribution effect of the matrix, filaments of the filament winding start to break causing a cascade effect of fibers breaking in rapid succession.

Without the support of the filament winding layers the PVC liner ruptures and is ejected violently from the tube. The contribution of the veil and mat layers is negligible.

When a veil lined tube is loaded axially in tension there is a tendency for the filament winding layer to rotate to align with the load. This has two effects, the development of in-plane shear stresses and a compressive effect where the tube wants to collapse into itself.

With the axial tension test, the principle tensile stress is in the longitudinal direction so a crack perpendicular to this would be expected. At some point during loading the weakest part of the tube fails. This highly localized failure is seen as a small patch of

whitening oriented in the hoop direction. Several things happen at this site. The corrosion liner cracks and the resin of the filament winding layer breaks up. This results in a sudden localized elongation and, free of the resin, the filament winding fibers rotate towards the longitudinal direction and unload slightly. This would allow the tube to bend slightly, assisting the spread of damage around the tube. Once the damage encircles the tube, the load in this area is completely supported by the glass fibers of the filament winding layer. In some cases these events occur so rapidly that the whitening band appears to develop around the tube in one step.

As loading continues the events would be repeated over again at another location and the external damage would vary from tube to tube. Rotation of the fibers also means that they must move radially inward. This compressive and inward pulling action of the glass fibers would also influence failure.

With the PVC lined tubes the PVC liner has a stabilizing effect, by preventing collapse inward and delaying the initial localized failure seen with the veil lined tubes. Again, it is not clear which layer of the corrosion liner fails first. Once the PVC liner cracks the FRP above it follows resulting in the sudden appearance of a band of whitening around the tube. In this area the corrosion liner splits and the resin in the filament winding layer breaks up. The glass filaments now rotate to align themselves with the load and loading can continue.

Final failure of both the veil lined and PVC lined tubes occurs when the tensile strength of the filament winding is reached, and the glass fibers fail.

CHAPTER 8. Conclusions

There are several conclusions that can be drawn from the results of this project.

Perhaps the most obvious conclusion that can be drawn from the results of the project is that a given class of chemical solution will give a characteristic type of appearance change in a laminate. The appearance change can be defined by four main points: colour, opacity, blisters and time.

The fuming and production of highly acidic droplets by both veil lined and PVC lined tubes exposed to 50°C HCl demonstrated the absorption of fluids by vinyl ester resins and PVC.

The chemical resistance of Derakane™ 411-45 resin to 21°C air, 21°C water and 80°C water, as indicated in Dow's Chemical Resistance and Engineering Guide, was confirmed by the performance of the veil lined tubes. The results also showed chemical resistance to HCl (35%) at 21°C and 50°C, and lack of chemical resistance to 21°C sulfuric acid (98%).

The chemical resistance of CPF Dualam's Dual laminate design was found to match the veil lined tube's performance with one notable exception. The use of a PVC corrosion liner allowed the use of Derakane™ 411-45 in a 21°C sulfuric acid (98%) environment.

In general, the average performance of the PVC lined tubes was better than the veil lined tubes under hydrostatic loading. This increase in performance was due to the fact that at low pressure the veil liner developed cracks that lead to failure. At the same pressure the PVC would remain intact. The trade off for this is that there was a lack of visual clues indicating impending failure with the PVC lined tubes.

Plotting the failure pressure or load versus time showed that failure pressure or load of a given tube/environment combination was generally constant with respect to time. There were no obvious trends other than the drop in failure pressure or load of the tubes exposed to the elevated temperature environments compared to their room temperature counterparts. This drop occurred by the first test point, and was most obvious with the hoop and biaxial test results and less so with the axial test results. The drop in failure pressure or load was more evident with the veil lined tubes.

The stress-strain behavior of both types of tubes under hoop stress was found to be nonlinear and closely resembled the typical stress-strain behavior of E-glass/epoxy tubes. Under biaxial stress and axial stress the veil lined and PVC lined tubes had a linear or very nearly linear stress-strain behavior. Compared to E-glass/epoxy under biaxial stress, the hoop strain responses of the veil and PVC lined tubes type were similar to the E-glass/epoxy tube's response, while the axial strain responses were different. The appearance of

some veil lined tubes after final failure by fracture under tensile axial load was similar to that seen with E-glass/epoxy tubes.

Comparing the stress-strain behaviors of tubes subjected to different environments indicated that there were no dramatic changes in behavior.

It was found that the stress-strain relations gave accurate predictions of behavior. The theoretical stress-strain behavior of the tubes under hoop stress can be considered to be good linear approximations of the hoop test results for both tube types. For the biaxial and axial stress tests the theoretical results were very close to the experimental results.

The limitations of failure envelopes based upon uniaxial laminate properties was also shown. The theoretical failure envelopes predicted FPF of the filament winding layer. This was not reflected in the failure patterns observed during the internal pressure tests which seem to indicate that failure commences with the loss of integrity of the corrosion liner.

Comparing the experimental results for strain at failure and the failure envelopes in strain space showed that the failure envelopes were only successful in predicting the loading path for both tube types and the three loading conditions. The scatter and highly local nature of the experimental strain results limited analysis for trends.

Rating the aggressiveness of the environments based on the visual changes and the reduction in performance during testing from most to least aggressive: room temperature sulfuric acid (veil lined tubes), HCL 50°C, water 80°C, room temperature HCL, room temperature water, air (veil lined tubes) and room temperature sulfuric acid (PVC lined tubes).

This project and its results also gives rise to certain questions:

- Why do the tube's appearances change the way that the do ?
- What are the mechanisms of strength reduction ?
- How would tubes exposed to 50°C or 80°C air perform ?
- Were there any effects on the results that can be explained by tube lineage and how they were distributed for aging ?
- Are the results from this project repeatable, especially in the field under working conditions ?
- How would aged tubes behave under cyclic loading ?
- What relation does strength reduction have to temperature ?
- Are there any elements being leached out of the tubes by their contents ?

With the use of case studies to guide FRP design, it is hoped that the results from this thesis demonstrates the suitability and potential performance of CPF Dualams' dual laminate design when exposed to 20°C water, 80°C water, 20°C HCl (35%), 50°C HCl (35%) and 20°C H_2SO_4(98%).

References

1. Van Vlack, L. H., *Elements of Materials Science and Engineering*, Fifth ed., (Don Mills, Ontario: Addison-Wesley Publishing Company, 1985) p. 491.

2. DeGarmo, E. P., J. T. Black, and R. N. Kohser, *Materials and Processes in Manufacturing*, Sixth ed. (New York: Macmillan Publishing Company, 1984), p. 228.

3. Mallick, P.K., *Fiber-Reinforced Composites*, (New York: Marcel Dekker, Inc., 1988), p. 1.

4. *Fabricating Tips, Derakane Vinyl Ester Resins*, Form No. 296-00315-791, (U.S.A., The Dow Chemical Company), p. 1.

5. Van Vlack, L. H., *Elements of Materials Science and Engineering*, Fifth ed., (Don Mills, Ontario: Addison-Wesley Publishing Company, 1985) p. 498.

6. *Composites in Pressure Vessels and Piping*, (U.S.A., The American Society of Mechanical Engineers, 1977) p iii.

7. Renoud, W.J., O.H. Fenner and R.J. Lewandowski, "Design for Reliability in Large Fiber Reinforced Plastic Structures", *33rd Annual Conference, Reinforced Plastics/Composites Institute, The Society of the Plastics Industry, Inc.*, February 1978, Section 1-B.

8. *Fabricating Tips, Derakane Vinyl Ester Resins*, Form No. 296-00315-791, (U.S.A., The Dow Chemical Company), p. 31.

9. Short, R.J. and A. Kozloff, "Patented Design Will Enable 5.28 Million Gallon RP Tank to be Air, Highway. Rail and Ship Transportable", *36th Annual Conference, Reinforced Plastics/Composites Institute, The Society of the Plastics Industry, Inc.*, February 1981, Session 3-D.

10. Rohrauer, G., S.V. Hoa, and N. Dudley, *Effect of Environments on the Mechanical Behavior of Filament Wound Tubes* ,(Montreal, Composite Materials Research Group, Department of Mechanical Engineering, Concordia University, 1989), p. 4.

11. Szymanski, W.A., S.J. Scott and M.J. Duffy, "Testing and Evaluation of RTR for Corrosion Control Applications", *36th Annual Conference, Reinforced Plastics/Composites Institute, The Society of the Plastics Industry, Inc.*, February 1981, Session 8-D.

12. Mallick, P.K., *Fiber-Reinforced Composites*, (New York: Marcel Dekker, Inc., 1988), p. 55.

13. Mallick, P.K., *Fiber-Reinforced Composites*, (New York: Marcel Dekker, Inc., 1988), p. 359.

14. Mallick, P.K., *Fiber-Reinforced Composites*, (New York: Marcel Dekker, Inc., 1988), p. 56

15. Breitigam, W.V., "Mechanical Properties and Cure Variables Affecting Appearance of Corrosion Resistant Vinyl Ester *Plastics/Composites Institute, The Society of the Plastics Industry, Inc.*, February 1978, Section 6-E.

16. Mallick, P.K., *Fiber-Reinforced Composites*, (New York: Marcel Dekker, Inc., 1988), p. 23.

17. Mallick, P.K., *Fiber-Reinforced Composites*, (New York: Marcel Dekker, Inc., 1988), p. 25.

18. Soden, P.D. *et al*, "The Strength of a Filament Wound Composite Under Biaxial Loading", *Composites*, October 1978, pp. 247 - 250.

19. Schweitzer, P.A. *Handbook of Corrosion Resistant Piping*, (New York: Industrial Press Inc., 1969), p. 83.

20. Schweitzer, P.A. *Handbook of Corrosion Resistant Piping*, (New York: Industrial Press Inc., 1969), p. 97.

21. Ishii, T. and S. Narisawa, "Fiberglass Reinforced PVC - Characteristics, New Fabrication Methods and Applications", *33rd Annual Conference, Reinforced Plastics/Composites Institute, The Society of the Plastics Industry, Inc.*, February 1978, Section 11-F.

22. *Fabricating Tips, Derakane Vinyl Ester Resins*, Form No. 296-00315-791, (U.S.A., The Dow Chemical Company), p. 2.

23. Duffy, M.J., "An Evaluation of Surfacing Veils", *41st Annual Conference, Reinforced Plastics/Composites Institute, The Society of the Plastics Industry, Inc*, January, 1986, Session 20-D,

24. Lark, R.F., "Recent Advances in Lightweight, Filament-Wound Composite Pressure Vessel Technology", *Composites in Pressure Vessels and Piping* (U.S.A., The American Society of Mechanical Engineers, 1977), pp 10 - 14.

25. Norwood, L.S., and A.F. Millman, "Strain Limited Design Criteria for Reinforced Plastic Process Equipment" *34th Annual Conference, Reinforced Plastics/Composites Institute, The Society of the Plastics Industry, Inc.*, January 1979, Section 3-D.

26. Kober, J.F., "The Filament Winding Market - A Modern Day Review", *36th Annual Conference, Reinforced Plastics/Composites Institute, The Society of the Plastics Industry, Inc.*, February 1981, Session 5-C.

27. Conlisk, P.J., and T.M. Fowler, "Design of Glass Fiber Reinforced Tanks and Vessels", *Composites in Pressure Vessels and Piping*, (U.S.A., The American Society of Mechanical Engineers, 1977), pp 3 - 15,

28. Soden, P.D., R. Kitching and P.C. Tse, "Experimental Failure Stresses for $\pm 55^{\circ}$ Filament Wound Glass Fiber Reinforced Plastic Tubes Under Biaxial Loads", *Composites*, Vol. 20, no. 2, March 1989, pp. 125 - 135.

29. DeGarmo, E. P., J. T. Black, and R. N. Kohser, *Materials and Processes in Manufacturing*, Sixth ed. (New York: Macmillan Publishing Company, 1984), p. 216.

30. Goldsworthy, W.B. and D.E. Beck, "A Continuous Process for Internally Pressurized Tubular Products", *36th Annual Conference, Reinforced Plastics/Composites Institute, The Society of the Plastics Industry*, February 1981, Session 15-F.

31. Hull, D., M. J. Legg and B. Spencer, "Failure of Glass/Polyester Filament Wound Pipe", *Composites*, January 1978, pp. 17 - 24.

32. McDermott, J., "Codes, Standards, and Design Data on Reinforced Plastics", *36th Annual Conference, Reinforced Plastics/Composites Institute, The Society of the Plastics Industry, Inc.*, February 1981, Session 14-A.

33. Peterson, R.W., "Practical Aspects of Specifying RP Vessels and Pipe Systems", *34th Annual Conference, Reinforced Plastics/Composites Institute, The Society of the Plastics Industry, Inc.*, January 1979, Section 8-G.

34. Scott, S.J., "Factors Affecting the Cure of Polyester Laminates", *36th Annual Conference, Reinforced Plastics/Composites Institute, The Society of the Plastics Industry*, January 1982, Session 9-B.

35. *Fabricating Tips, Derakane Vinyl Ester Resins*, Form No. 296-00315-791, (U.S.A., The Dow Chemical Company),, p. 12.

36. *Fabricating Tips, Derakane Vinyl Ester Resins*, Form No. 296-00315-791, (U.S.A., The Dow Chemical Company), p. 3.

37. *Fabricating Tips, Derakane Vinyl Ester Resins*, Form No. 296-00315-791, (U.S.A., The Dow Chemical Company), pp. 26 - 29.

38. Tsai, S.W., H.T. Hahn, *Introduction to Composite Materials*, (Lancaster, Pennsylvania, Technomic Publishing Company, Inc., 1980), p. 280.

39. Tsai, S.W., H.T. Hahn, *Introduction to Composite Materials*, (Lancaster, Pennsylvania, Technomic Publishing Company, Inc., 1980), p. 342.

40. Marshall, J.M., *et al*, "The Diffusion of Liquids into Resins and Composites", *37th Annual Conference, Reinforced Plastics/Composites Institute, The Society of the Plastics Industry, Inc.*, January 1982, Session 9-C.

41. Pritchard, G. and G.J. Swampillai, "Screening Methods for Assessing the Chemical Resistance of FRP", *34th Annual Conference, Reinforced Plastics/Composites Institute, The Society of the Plastics Industry, Inc.*, January 1979, Section 13-A.

42. Vinson, J.R., and R.L. Sierakowski, *The Behavior of Structures Composed of Composite Materials*, (Martinus Nijhoff Publishers) p. 42.

43. Mallick, P.K., *Fiber-Reinforced Composites*, (New York: Marcel Dekker, Inc., 1988),, p. 273.

44. Tsai, S.W., H.T. Hahn, *Introduction to Composite Materials*, (Lancaster, Pennsylvania, Technomic Publishing Company, Inc., 1980), p. 329.

45. Tsai, S.W., H.T. Hahn, *Introduction to Composite Materials*, (Lancaster, Pennsylvania, Technomic Publishing Company, Inc., 1980), p. 362.

46. Mallick, P.K., *Fiber-Reinforced Composites*, (New York: Marcel Dekker, Inc., 1988),, p. 280.

47. Allen, R.C., "Corrosion Mechanisms in Attack of Resin and Resin Glass Laminates", *33rd Annual Conference, Reinforced Plastics/Composites Institute, The Society of the Plastics Industry, Inc.*, February 1978, Section 6-D.

48. Haarsma, J.C., "Evaluation of Resin-Glass Fiber Interface Under Environmental Stress", *33rd Annual Conference, Reinforced Plastics/Composites Institute, The Society of the Plastics Industry, Inc.*, February 1978, Section 22-E.

49. Daughtry, J.L., "Continuity of Appearance Property Evaluation", *36th Annual Conference, Reinforced Plastics/Composites Institute, The Society of the Plastics Industry, Inc.*, February 1981, Session 8-A.

50. *Derakane Resins, Chemical Resistance and Engineering Guide*, Form No. 296-320-1290X SMG (U.S.A., The Dow Chemical Company)

51. Jones, M.L.C. and D. Hull, "Microscopy of Failure Mechanisms in Filament Wound Pipe", *Journal of Materials Science 14*, 1979, pp. 165 - 174.

52. Gottenburg, W.G., *et al*, "Mode of Failure of Hydrostatically Overstressed Reinforced Plastic Pipe", *34th Annual Conference, Reinforced Plastics/Composites Institute, The Society of the Plastics Industry, Inc.*, January 1979, Section 13-C.

53. Mallick, P.K., *Fiber-Reinforced Composites*, (New York: Marcel Dekker, Inc., 1988), p. 190.

54. Seymore, R.B., *Plastics vs. Corrosives*, (New York: John Wiley & Sons, 1982) p. 267.

55. Rohrauer, G., S.V. Hoa, *The Experimental Set-up and Testing of Fiber Reinforced Laminates in Different Chemical Environments*, Concordia Composites CRD Report No.2, Version 1.0, Department of Mechanical Engineering, Concordia University, December 1987, p. 15.

56. Rohrauer, G., S.V. Hoa, *The Experimental Set-up and Testing of Fiber Reinforced Laminates in Different Chemical Environments*, Concordia Composites CRD Report No.2, Version 1.0, Department of Mechanical Engineering, Concordia University, December 1987, p. 4

57. Rohrauer, G., S.V. Hoa, *The Experimental Set-up and Testing of Fiber Reinforced Laminates in Different Chemical Environments*, Concordia Composites CRD Report No.2, Version 1.0, Department of Mechanical Engineering, Concordia University, December 1987, p. 16

58. Toombes, G.R., S.R. Swanson and D.S. Cairns, "Biaxial Testing of Composite Tubes", *Experimental Mechanics*, June 1985, pp. 186 - 192.

59. Tsai, S.W., H.T. Hahn, *Introduction to Composite Materials*, (Lancaster, Pennsylvania, Technomic Publishing Company, Inc., 1980), p. 229.

60. Hoa, S.V., *et al*, Preliminary Results for the Project " *Effect of Degradation due to Fluid Content on the Reliability of Fiber Reinforced Plastic vessels and Pipes*", Department of Mechanical Engineering, Concordia University, Montreal, 1989, pp 29-31.

61. Gross, R.E. and P.D. Lyle, "Failure Analysis of Thin Walled Filament Wound Pipe During Application of Internal Pressure", *36th Annual Conference, Reinforced Plastics/Composites Institute, The Society of the Plastics Industry, Inc.*, February 1981, Session 3-A.

61. Tsai, S.W., H.T. Hahn, *Introduction to Composite Materials*, (Lancaster, Pennsylvania, Technomic Publishing Company, Inc., 1980), p 279.

APPENDIX 1

A computer program to calculate the failure envelope of a given layer of a given laminate using unidirectional strength values and the quadratic interaction failure criterion.

```
10   PRINT"COMPOSITE MATERIAL FAILURE ENVELOPE PROGRAM"
20   PRINT"COPYWRITE 1991" : INPUT"WHAT LAY-UP";E$
30   DEFDBL A-E,G-H,M-Y :DEFINT I-L,Z :DEFSNG N
40   DIM EAA(21,4), EBB (21,4)
50   '
60   ' ENTER LAMINATE'S NORMALIZED COMPLIANCE
70   '
80   INPUT "a11h (TPa)-1 =";A(1,1)
90   INPUT "a22h (TPa)-1 =";A(2,2)
100  INPUT "a66h (TPa)-1 =";A(3,3)
110  INPUT "a12h (TPA)-1 =";A(1,2):A(2,1)=A(1,2)
120  INPUT "a16h (TPa)-1 =";A(1,3):A(3,1)=A(1,3)
130  INPUT "a26h (TPa)-1 =";A(2,3):A(3,2)=A(2,3)
140  '
150  ' ENTER LAYER INFORMATION
160  '
170  INPUT "SPECIFY LAYER ie: PVC,VEIL,...";D$
180  INPUT "LONGITUDINAL TENSILE X (MPa)";X(1)
190  INPUT "LONGITUDINAL COMPRESSIVE X' (MPa)"; X(2)
200  INPUT "TRANSVERSE TENSILE Y (MPa)";Y(1)
210  INPUT "TRANSVERSE COMPRESSIVE Y' (MPa)";Y(2)
220  INPUT "LONGITUDINAL SHEAR S (MPa)"; S(1)
230  INPUT LAYER THICKNESS (M) ";S:S=1!
240  '
250  INPUT "QXX (GPa) = ";QXX
260  INPUT "QYY (GPa) = ";QYY
270  INPUT "QXY (GPa) = ";QXY
280  INPUT "QSS (GPa) = ";QSS
290  '
300  ' CONVERT EVERYTHING TO GPa
310  FOR I=1 TO 3
320       FOR J=1 TO 3
330            AA(I,J)= A(I,J)/1000
340       NEXT
350  X(I) = X(I)/1000
360  Y(I) = Y(I)/1000
370  NEXT
380  S(1) = S(1)/1000
390  Z=0#
400  '
410  ' CALCULATION OF STRENGTH PARAMETERS IN STRESS SPACE
420  '
430  '
440  FXX = 1/(X(1)*X(2)): PRINT "FXX = ";FXX
450  FX  = 1/X(1) - 1/X(2) : PRINT "FX = ";FX
460  FYY = 1/(Y(1)*Y(2)) : PRINT FYY = ";FYY
470  FY  = 1/Y(1) - 1/Y(2): PRINT "FY = ";FY
480  FSS = 1/S(1)^2 : PRINT "FSS = ";FSS
```

```
490  FXY = (SQR(FXX*FYY))*(-.5) : PRINT "FXY = ";FXY : PRINT ""
500  '
510  GXX = (FXX*QXX*QXX)+(2*FXY*QXX*QXY)+(FYY*QXY*QXY):PRINT"GXX=";GXX
520  GYY = (FXX*QXY*QXY)+(2*FXY*QXY*QYY)+(FYY*QYY*QYY):PRINT"GYY=";GYY
530  GXY = (FXX*QXX*QXY)+(FXY*(QXX*QYY+QXY*QXY))+(FYY*QXY*QYY)
     :PRINT"GXY=";GXY
540  GSS = FSS*QSS*QSS :PRINT"GSS=";GSS
550  GX =  (FX*QXX)+(FY*QXY): PRINT "GX = ";GX
560  GY = (FX*QXY)+(FY*QYY): PRINT "GY = ";GY
570  INPUT "WHAT IS THE LAYER'S ANGLE ?";T
580  U = T * 3.141592654#/180.
590  N = SIN(U): IF ABS (N) < .000001# THEN N=0
600  M = COS(U): IF ABS (M) < .000001# THEN M=0
610  G(1,1) = (GXX*M^4)+(GYY*N^4)+(GXY*2*M^2*N^2)+(GSS*4*M*M*N*N)
620  G(2,2) = (GYY*M^4)+(GXX*N^4)+(GXY*2*M^2*N^2)+(GSS*4*M*M*N*N)
630  G(1,2) = (GXX*M^2*N^2)+(GYY*M^2*N^2)+(GXY*(M^4+N^4)
               +(GSS*(-4*M*M*N*N))
640  G(3,3) = (GXX*M*M*N*N)+(GYY*M*M*N*N)+(GXY*(-2*M*M*N*N))
               +(GSS*(M*M-N*N)^2)
650  G(1,3) = (GXX*M*M*N*N)+(GYY*(-M*N*N*N))
               + (GXY*((M*N*N*N)-(M*M*M*N)))
               + (GSS*2*((M*N*N*N)-(M*M*M*N)))
660  G(2,3) = (GXX*M*N*N*N)+(GYY*(-M*M*M*N))
               + (GXY*((M*M*M*N)-(M*N*N*N)))
               + (GSS*2*((M*M*M*N)-(M*N*N*N)))
670  G(3,1) = G(1,3)
680  G(2,1) = G(1,2)
690  G(3,2) = G(2,3)
700  GG(1) = (GX*M*M)+(GY*N*N)
710  GG(2) = (GX*N*N)+(GY*M*M)
720  GG(3) = (GX*M*N)-(GY*M*N)
730  W=0!
740  FOR K=1 TO 3
750      FOR F=1 TO 3
760          FOR I=1 TO 3
770              FOR J=1 TO 3
780              W = W+G(I,J)*AA(I,K)*AA(J,F)
790              NEXT
800          NEXT
810          H(K,F) = W
820          W=0!
830      NEXT
840  NEXT
850  '
860  '
870  FOR J=1 TO 3
880      V=0!
890      FOR I=1 TO 3
```

```
900       V = V + GG(I)*AA(I,J)
910       NEXT
920   HH(J) = V
930   NEXT
940   '
950   'PRINT COMMANDS
960   LPRINT " COMPOSITE MATERIAL FAILURE ENVELOPE PROGRAM"
970   LPRINT " COPYWRITE 1991": PRINT E$:
980   LPRINT " E$
990   INPUT "DO YOU WNT ALL THE PARAMETRS PRINTED ";F$
1000  IF F$ = "N" GOTO 1340
1010  LPRINT
1020  LPRINT "a(I,J)h =          GPa-1
1030  FOR I=1 TO 3
1040  LPRINT USING "###########.######"; AA(I,1);AA(1,2);AA(I,3)
1050  NEXT
1060  LPRINT
1070  '
1080  LPRINT "FXX = ";FXX
1090  LPRINT "FX = ";FX
1100  LPRINT "FYY = ";FYY
1110  LPRINT "FY = ";FY
1120  LPRINT "FSS = ";FSS
1130  LPRINT "FXY = ";FXY:LPRINT ""
1140  LPRINT
1150  LPRINT "GXX =";GXX
1160  LPRINT "GYY =";GYY
1170  LPRINT "GXY =";GXY
1180  LPRINT "GSS = ";GSS
1190  LPRINT "GX =";GX
1200  LPRINT "GY =";GY:PRINT ""
1210  LPRINT "":LPRINT "":LPRINT "G(X,Y) : ","AT"T"DEGREES":LPRINT""
1220  FOR I=1 TO 3
1230  LPRINT USING"########.######";G(I,1),G(I,2),G(I,3), GG(I)
1240  NEXT
1250  LPRINT ""
1260  LPRINT "STRENGTH PAPRAMETERS OF THE "D$" PLY OF THE LAMINATE"
1270  LPRINT ""
1280  LPRINT "H(I,J) =        GPa-2"
1290  LPRINT
1300  FOR K=1 TO 3
1310  LPRINT USING "######.##";H(K,1),H(K,2),H(K,3)
1320  NEXT
1330  LPRINT
1340  ' NOW TO CALACULATE THE DESIRED VALUES FOR THE
        FAILURE ENVELOPES IN STRESS AND STRAIN SPACE
1350  '
1360  '
```

```
1370 LPRINT "CALCULATING THE "D$" FAILURE ENVELOPE IN STRESS SPACE
1380 LPRINT
1390 LPRINT "FOR THE RANGE (0,-1) TO (1,-1)
1400 LPRINT
1410 LPRINT USING "\       \";"N(1)";"N(2)";"N(6)","S=","S'=","X="
     ,"Y=","X'+","Y'="
1420 '
1430 ' FOR THE RANGE OF (0,-1) TO (1,-1)
1440 '
1450 N(1)=0#:N(2)=0#:N(3)=0#
1460 FOR Z=0# TO 10# STEP 1#
1470 N(1)= Z/10#; N(2) = -1#: N(3)= 0#
1480 X=0#
1490      FOR K=1 TO 3
1500          FOR F=1 TO 3
1510          X=X+H(K,F)*N(K)*N(F)
1520          NEXT
1530      NEXT
1540 Y=0#
1550      FOR J=1 TO 3
1560      Y=Y+HH(J)*N(J)
1570      NEXT
1580 Q=(Y/(2*X))^2
1590 RP = (SQR(Q+91/X)))-(Y/(2*X))
1600 RM = 0# - (SQR(Q+(1/X)))-(Y/(2*X))
1610 '
1620 NA(1) = (RP*N(1))
1630 NA(2) = (RP*N(2))
1640 NB(1) = (RM*N(1))
1650 NB(2) = (RM*N(2))
1660 LPRINT USING "######.#";N(1);N(2);N(3);INT(RP*1000#)
          ,INT(RM*1000#),NA(1)*1000#,NA(2)*1000#,NB(1)*1000#
          ,NB(2)*1000#
1670 '
1680 EA(1)=0:EA(2)=0:EA(3)=0:EB(1)=0:EB(2)=0:EB(3)=0
1690 '
1700      FOR I=1 TO 3
1710          FOR J=1 TO 3
1720          EA(I) = EA(I)+A(I,J)*NA(J)
1730          EB(I) = EB(I)+A(I,J)*NB(J)
1740          NEXT
1750      EAA(Z,I) = EA(I): EBB(Z,I) = EB(I)
1760      NEXT
1770 NEXT
1780 LPRINT ""
1790 LPRINT USING "\       \";"N(1)";"N(2)";"N(6)";"E(1)";"E(2)"
          ;"E(6)","E'(1)";"E'(2)","E'(6)"
1800 FOR Z=0# TO 10# STEP 1#
```

```
1810 N(1)=Z/10#: N(2)=-1#: N(3)=0#
1820 LPRINT USING "######.#";N(1);N(2);N(3),EAA(Z,1),EAA(Z,2),EAA(Z,3)
       ,EBB(Z,1),EBB(Z,2),EBB(Z,3)
1830 NEXT
1840 '
1850 LPRINT ""
1860 LPRINT "FOR THE RANGE (1,-1) TO (1,1)"
1870 LPRINT
1880 LPRINT USING "\         \";"N(1)";"N(2)";"N(6)";"S=";"S'=";"X="
       ,"Y=","X'=";"Y'="
1890 LPRINT ""
1900 FOR Z=-10# TO 10 STEP 1#
1910 ZC = (Z+10)
1920 '
1930 ' FOR THE POINTS (1,-1) TO (1,1)
1940 '
1950 N(1)=1#: N(2)= Z/10# ; N(6) = 0#
1960 X=0#
1970     FOR K=1 TO 3
1980         FOR F= 1 TO 3
1990         X=X+H(K,F)*N(K)*N(F)
2000         NEXT
2010     NEXT
2020 Y=0#
2030     FOR J=1 TO 3
2040     Y=Y=HH(J)*N(J)
2050     NEXT
2060 Q=(Y/(2*X))^2
2070 RP = (SQR(Q+(1/X))) - (Y/(2*X))
2080 RM = 0# - (SQR(Q+(1/X))) - (Y/(2*X))
2090 NA(1) = (RP*N(1))
2100 NA(2) = (RP*N(2))
2110 NB(1) = (RM*N(1))
2120 NB(2) = (RM*N(2))
2130 LPRINT USING "######.#";N(1);N(2);N(3);INT(RP*1000#)
       ,INT(RM*1000#),NA(1)*1000#,NA(2)*1000#,NB(1)*1000#
       ,NB(2)*1000#
2140 '
2150 EA(1)=0:EA(2)=0:EA(3)=0:EB(1)=0:EB(2)=0:EB(3)=0
2160     FOR I=1 TO 3
2170         FOR J=1 TO 3
2180         EA(I) = EA(I)+A(I,J)*NA(J)
2190         EB(I) = EB(I)+A(I,J)*NB(J)
2200         NEXT
2210     EAA(ZC,I) = EA(I): EBB(ZC,I) = EB(I)
2220     NEXT:NEXT
2230 LPRINT USING "\       \";"N(1)";"N(2)";"N(6)";"E(1)";"E(2)"
       ;"E(6)","E'(1)";"E'(2)","E'(6)"
```

```
2240 FOR Z= -10# TO 10 STEP 1#
2250 ZC = Z+10
2260 N(1)=1#: N(2)=Z/10#: N(3)=0#
2270 LPRINT USING "#####.#";N(1);N(2);N(3),EAA(ZC,1),EAA(ZC,2)
       ,EAA(ZC,3),EBB(ZC,1),EBB(ZC,2),EBB(ZC,3)
2280 NEXT
2290 '
2300 '
2310 '
2320 LPRINT ""
2330 LPRINT " FOR THE RANGE (1,1) TO (0,1)
2340 LPRINT ""
2350 LPRINT USING "\      \";"N(1)";"N(2)";"N(6)","S=","S'=","X="
       ,"Y=","X'+","Y'="
2360 LPRINT ""
2370 FOR Z=10# TO 0# STEP -1#
2380 N(1)= Z/10#; N(2) = 1#: N(3)= 0#
2390 X=0#
2400     FOR K=1 TO 3
2410         FOR F=1 TO 3
2420         X=X+H(K,F)*N(K)*N(F)
2430         NEXT
2440     NEXT
2450 Y=0#
2460     FOR J=1 TO 3
2470     Y=Y+HH(J)*N(J)
2480     NEXT
2490 Q=(Y/(2*X))^2
2500 RP = (SQR(Q+91/X)))-(Y/(2*X))
2510 RM = 0# - (SQR(Q+(1/X)))-(Y/(2*X))
2520 NA(1) = (RP*N(1))
2530 NA(2) = (RP*N(2))
2540 NB(1) = (RM*N(1))
2550 NB(2) = (RM*N(2))
2560 LPRINT USING "######.#";N(1);N(2);N(3);INT(RP*1000#)
       ,INT(RM*1000#),NA(1)*1000#,NA(2)*1000#,NB(1)*1000#
       ,NB(2)*1000#
2570 EA(1)=0:EA(2)=0:EA(3)=0:EB(1)=0:EB(2)=0:EB(3)=0
2580 '
2590     FOR I=1 TO 3
2600         FOR J=1 TO 3
2610         EA(I) = EA(I)+A(I,J)*NA(J)
2620         EB(I) = EB(I)+A(I,J)*NB(J)
2630         NEXT
2640     EAA(Z,I) = EA(I): EBB(Z,I) = EB(I)
2650     NEXT:NEXT
2660 LPRINT ""
2670 LPRINT USING "\      \";"N(1)";"N(2)";"N(6)";"E(1)";"E(2)"
       ;"E(6)","E'(1)";"E'(2)","E'(6)"
```

```
2680 LPRINT ""
2690 FOR Z=10# TO 0# STEP -1#
2700 N(1)=Z/10#: N(2)=1#: N(3)=0#
2710 LPRINT USING "######.#";N(1);N(2);N(3),EAA(Z,1),EAA(Z,2),EAA(Z,3)
          ,EBB(Z,1),EBB(Z,2),EBB(Z,3)
2720 NEXT
2730 INPUT "ANOTHER LAYER ANGLE  (Y OR N)";B$
2740 IF B$="Y" GOTO 570
2750 INPUT "ANOTHER LAYER (Y OR N) N TO EXIT";C$
2760 IF C$=Y GOTO 170
2770 IF C$=N GOTO 2790
2780 GOTO 2750
2790 END
```